https://doi.org/10.15388/vu.thesis.634
https://orcid.org/0000-0003-1257-0396

VILNIUS UNIVERSITY
CENTER FOR PHYSICAL SCIENCES AND TECHNOLOGY

Maryia Drobysh

Electrochemical Biosensors for COVID- 19 Diagnosis

DOCTORAL DISSERTATION

Natural Sciences,
Chemistry (N 003)

VILNIUS 2024

This dissertation was prepared between 2020 and 2024 (State Research Institute Center for Physical Sciences and Technology). The research was supported by the Research Council of Lithuania with scholarships that were granted for academic accomplishment for the year 2022.

Academic supervisor – Prof. Habil. Dr. Arūnas Ramanavičius (Center for Physical Sciences and Technology, Natural Sciences, Chemistry – N 003).

This doctoral dissertation will be defended in a public meeting of the Dissertation Defence Panel:

Chairman – Prof. Habil. Dr. Rimantas Ramanauskas (State Research Institute Center for Physical Sciences and Technology, Natural Sciences, Chemistry – N 003).

Members:

Assoc. Prof. Dr. Renata Butkutė (State Research Institute Center for Physical Sciences and Technology, Technological Sciences, Material Engineering – T 008),

Prof. Dr. Igor Iatsunskyi (NanoBioMedical Centre, Adam Mickiewicz University in Poznan, Poznan, Poland, Natural Sciences, Chemistry – N 003),

Assoc. Prof. Dr Tatjana Kochanė (Vilnius University, Natural Sciences, Chemistry – N 003),

Prof. Dr. Vida Vičkačkaitė (Vilnius University, Natural Sciences, Chemistry – N 003).

The dissertation shall be defended in a public meeting of the Dissertation Defence Panel at 14:00 on the 23rd of September 2024 in meeting room D401 of the State Research Institute Center for Physical Sciences and Technology. Address: Sauletekio av. 3, Vilnius, Lithuania. Tel. +370 5 264 8884; e-mail: office@ftmc.lt.

The text of this dissertation can be accessed at the libraries of the State Research Institute Center for Physical Sciences and Technology, Vilnius University, as well as on the website of Vilnius University: *www.vu.lt/naujienos.ivykiu-kalendorius.*

https://doi.org/10.15388/vu.thesis.634
https://orcid.org/0000-0003-1257-0396

VILNIAUS UNIVERSITETAS
FIZINIŲ IR TECHNOLOGIJOS MOKSLŲ CENTRAS

Maryia Drobysh

Elektrocheminiai biojutikliai COVID- 19 diagnostikai

DAKTARO DISERTACIJA

Gamtos mokslai,
Chemija (N 003)

VILNIUS 2024

Disertacija rengta 2020–2024 metais Fizinių ir technologijos mokslų centre. Mokslinius tyrimus rėmė Lietuvos mokslo taryba skirdama stipendijas 2022 metais už akademinius pasiekimus.

Mokslinis vadovas – Prof. habil. dr. Arūnas Ramanavičius (Fizinių ir technologijos mokslų centras, gamtos mokslai, chemija – N 003).

Gynimo taryba:

Pirmininkas – Prof. habil. dr. Rimantas Ramanauskas (Valstybinis mokslinių tyrimų institutas Fizinių ir technologijos mokslų centras, gamtos mokslai, chemija – N 003).
Nariai:
Dr. Renata Butkutė (Valstybinis mokslinių tyrimų institutas Fizinių ir technologijos mokslų centras, technologijos mokslai, medžiagų inžinerija – T 008),
Prof. dr. Igor Iatsunskyi (NanoBioMedical centras (NBMC) Adomo Mickevičiaus universitete Poznanėje, Lenkija, gamtos mokslai, chemija – N 003),
Doc. dr. Tatjana Kochanė (Vilniaus universitetas, gamtos mokslai, chemija N 003),
Prof. dr. Vida Vičkačkaitė (Vilniaus universitetas, gamtos mokslai, chemija N 003).

Disertacija ginama viešame Gynimo tarybos posėdyje 2024 m. rugsėjo mėn. 23 d. 14:00 val. Nacionalinio fizinių ir technologijos mokslų centro D401 konferencijų salėje. Adresas: Saulėtekio al. 3, Vilnius, Lietuva, tel. +370 5 264 8884; el. paštas office@ftmc.lt.

Disertaciją galima peržiūrėti Fizinių ir technologijos mokslų centro, Vilniaus universiteto bibliotekose ir VU interneto svetainėje adresu: *https://www.vu.lt/naujienos/ivykiu-kalendorius.*

ABBREVIATIONS

aa – amino acids
Ab – antibody
AC – alternating current
ACE2 – angiotensin-converting enzyme 2
anti-rS – antibodies against SARS-CoV-2 spike protein
AuNS – gold nanostructures
BAU – binding antibody unit
CA – chronoamperometry
CE – counter electrode
CHO – Chinese hamster ovary
CLIA – chemiluminescence immunoassay
COVID-19 – coronavirus disease 2019
CPE – constant phase element
CV – cyclic voltammetry
DPV – differential pulse voltammetry
E-protein – SARS-CoV-2 envelope protein
EA – ethanolamine
EASA – electrochemically active surface area
EDC – N - (3-dimethylaminopropyl)-N'-ethyl-carbodiimide hydrochloride
EIS – electrochemical impedance spectroscopy
ELISA – enzyme-linked immunosorbent assay
ER – endoplasmic reticulum
ET – exposition time
EtOH – ethanol
FIA – fluorescent immunoassay
GA – glutaraldehyde
IgG – immunoglobulin G
IgM – immunoglobulin M
LFIA – lateral flow immunoassay
LOD – limit of detection
LOQ – limit of quantification
M-protein – SARS-CoV-2 membrane protein
MIP – molecularly imprinted polymer
N-protein – SARS-CoV-2 nucleocapsid protein
NHS – N-hydroxysuccinimide
NIP – non-imprinted polymer
PA – phytic acid
PAD – pulsed amperometric detection
PANI – polyaniline
PB – phosphate buffer
PBS – phosphate-buffered saline
POC – point-of-care
Ppy – polypyrrole
PtNS – platinum nanostructures
Py – pyrrole
RE – reference electrode
rN – recombinant SARS-CoV-2 nucleocapsid protein
RNA – ribonucleic acid
RPA – recombinase polymerase amplification
rS – recombinant SARS-CoV-2 spike protein
RT – room temperature
RT-LAMP – reverse transcription loop-mediated Isothermal amplification
RT-PCR – reverse transcription-polymerase chain reaction
S-protein – SARS-CoV-2 spike protein
Saccharomyces cerevisiae – *S. cerevisiae*
SAM – self-assembled monolayer
SARS-CoV-2 – severe acute respiratory syndrome coronavirus 2
SDS – sodium dodecyl sulfate
SEM – scanning electron microscope
SPCE – screen-printed carbon electrode
SPE – screen-printed electrode
ssRNA – single-stranded RNA
SWV – square-wave voltammetry
WE – working electrode
peptone dextrose

TABLE OF CONTENTS

INTRODUCTION

Chemical sensors, an integral part of numerous scientific and industrial projects, play a vital role in converting chemical information into readable signals. These devices, consisting of a chemical sensing system and a physicochemical converter, are used in various applications. Among them, biosensors represent a significant subgroup that uses biochemical recognition mechanisms [1]. A biological sensing system works by translating biochemical information, usually the concentration of an analyte, into a specific chemical or physical output signal characterized by a certain sensitivity. An electrochemical biosensor is defined by its utilization of an electrochemical transducer. This type of biosensor is classified as a chemically modified electrode – this designation is associated with the use of an electrically conductive, semiconducting, or ionically conductive material coated with a biochemical film [2,3]. Biological receptors, including tissues, cells, enzymes, antibodies, and other highly active proteins, can be effectively immobilized in a thin layer on the surface of the transducer using various methods. These methods include the use of bilayer lipid membranes, polymeric matrices, self-assembled monolayers (SAMs), bifunctional groups or spacers and others [4]. Biosensors can be classified according to the mechanism conferring biological specificity, encompassing biocatalytic or bioaffinity sensing components. The latter type includes the registration of specific interactions between antibodies and antigens or detection using molecularly imprinted polymer (MIP)-based methods.

Recent years have seen a surge in the development of electrochemical biosensors aimed at detecting pathogens [5]. This trend has become particularly pronounced with the advent of the coronavirus disease 2019 (COVID-19) pandemic, where the need for rapid and accurate diagnosis has led to extensive research into biosensor technologies. These biosensors designed to detect COVID-19 have been extensively studied, focusing on their transduction elements, biorecognition components, and electrochemical methodologies [6,7]. Three primary approaches are employed to detect severe acute respiratory syndrome coronavirus 2 (SARS-CoV-2) and diagnose COVID-19. These approaches encompass molecular tests, which detect viral ribonucleic acid (RNA); antigen tests, which identify viral proteins; and antibody tests, which target specific antibodies against viral proteins. The first two methods enable the detection of an ongoing infection within the organism, whereas the third method facilitates the assessment of the immune status post-recovery or vaccination [6,7]. Electrochemical biosensors can be used for all

three strategies, offering a number of advantages such as rapidity, simplicity, cost-effectiveness, and portability in the diagnosis of COVID-19 [8].

Major goal

Explore the application of biosensing strategies, including SAM, conductive polymers, and MIP-based techniques, for the electrochemical detection of SARS-CoV-2-related biomolecules. The specific aim is to select the most promising approach based on the rate and sensitivity of detection, as well as the necessity of employing additional redox labels.

Tasks

1. Evaluate the effectiveness of biosensor design strategies using SAM, conductive polymers, and MIP for COVID-19 diagnosis.

2. Determine the applicability of cyclic voltammetry (CV), differential pulse voltammetry (DPV), electrochemical impedance spectroscopy (EIS), and pulsed amperometric detection (PAD) for the detection of SARS-CoV-2-related biomolecules.

3. Assess the suitability of SARS-CoV-2 spike (S), nucleocapsid (N) proteins, and antibodies against SARS-CoV-2 for electrochemical biosensor applications.

4. Choose the most promising approach for COVID-19 diagnosis based on the rate and sensitivity of detection, as well as the necessity of employing additional redox mediators.

Statements of defense

1. The modification of screen-printed carbon electrode (SPCE) with gold nanostructures (AuNS) increases electrochemically active surface area (EASA) and heterogeneous electron transfer rate constant (k^0) of working electrode.

2. The SPCE modified with SAM accompanied by CV and DPV methods can be used for the detection of antibodies against SARS-CoV-2 from real serum samples with limits of detection (LODs) of 0.27 and 0.14 nM correspondingly.

3. The SPCE modified with polyaniline (PANI) film accompanied by EIS method can be used for the detection of antibodies against SARS-CoV-2 from real serum samples with LOD of 0.42 nM.

4. The SPCE modified by molecularly imprinted polypyrrole (Ppy) can be used for the detection of SARS-CoV-2 N-protein with LOD of 1.02 pM.

5. The MIP applied on the SPCE pretreated with AuNS shows a lower contribution of non-specific binding compared to the SPCE pretreated with platinum nanostructures (PtNS) or without pretreatment.

Novelty and relevance

The SPCE modified with conductive PANI film was used for the detection of antibodies against SARS-CoV-2 from real serum samples by EIS. The combination of disposable, compact, and affordable SPCE with a conductive PANI film eliminates the need for extra redox mediators. This advancement makes it suitable for point-of-care (POC) assessment of immune status post-COVID-19 recovery or vaccination.

The SPCE modified by the implementation of Ppy for molecular imprinting was used for the detection of SARS-CoV-2 N-protein by PAD. The combination of used SPCE working electrode, PAD method, and MIP technique was used for the first time for SARS-CoV-2 N-protein detection and allowed the avoidance not only additional redox mediators but also minimizing the usage of expensive biomolecules as biorecognition elements. The developed biosensing system can be used for POC detection of COVID-19.

1. LITERATURE OVERVIEW

1.1 Electrochemical biosensors

Biosensors are analytical tools designed to convert biological reactions into measurable signals. The development of biosensors, including the selection of materials, transducing devices, and immobilization methods, requires interdisciplinary research spanning chemistry, biology, physics, and engineering. Materials used in biosensors are divided into three groups depending on their mechanism of action: a biocatalytic group, including enzymes; a bioaffinity group consisting of antibodies and nucleic acids; and a microbial-based group which contains microorganisms. Biosensors find applications in various fields such as food and medicine industries, offering superior stability and sensitivity compared to traditional methods [9].

An electrochemical biosensor is an analytical device that converts biochemical events, such as enzyme-substrate reactions and antigen-antibody interactions, into electrical signals such as current, voltage, or impedance [10,11]. Electrochemical biosensors offer numerous advantages, including simplicity, low cost, rapid measurement, the need to use small volumes of analyte and reagents, and high selectivity and sensitivity [12]. In this type of biosensor, the electrode plays a crucial role as a strong support for immobilizing biomolecules such as enzymes, antibodies and nucleic acids, facilitating the movement of electrons [13]. Electrochemical measurements rely on the natural interaction between electrical energy and a chemical reaction, usually a redox reaction, that generates an electrical current, or vice versa. Interactions between immobilized biomaterials and analytes result in the production or consumption of ions or electrons, affecting the electrical current, potential, or other electrical properties of the solution. These reactions occur at the interface between an electrode and an electrolyte [14–16]. Therefore, successful detection depends on reactions occurring in the immediate vicinity of the electrode surface. Therefore, electrodes play a critical role in determining the performance of an electrochemical biosensor. When selecting a suitable electrode, several factors must be considered, including its material, dimensions and suitability for surface modification [12]. Typically, electrochemical cells consist of three electrodes, namely, a reference electrode (RE) providing a stable potential for comparison in electrochemical measurements; a counter electrode (CE) supplying the current required for the electrochemical reaction; and a working electrode (WE). The latter one is the primary electrode where the electrochemical reaction of

interest occurs, serving as the transduction element [12]. The CE and WE must be conductive and chemically stable. Therefore, electrode materials such as gold, silver, platinum, silicon, carbon and graphene are commonly used, depending on the analyte and reaction type.

Some electrochemical biosensors may require additional components such as redox mediators. Redox mediators include compounds that can engage in reversible oxidation and reduction reactions. Their main function is to facilitate electron transfer between the analyte and the electrode surface in electrochemical biosensors [17]. Conversely, in biosensors that use conducting polymers, the use of redox mediators is usually not required. Conducting polymers have intrinsic electrical conductivity, allowing direct exchange of electrons with the analyte without the need for additional redox mediators [17]. The elimination of the need to add additional compounds facilitates the application of biosensors in POC conditions.

1.1.1. Screen-printed electrodes (SPEs)

An innovative approach to conventional electrochemical cells involves screen printing three electrodes onto an insulating substrate, resulting in SPEs. The SPEs have several advantages, such as simplicity, ease of mass production, low manufacturing cost, and minimal usage of analytes/reagents, making them highly appealing for biosensing applications, particularly in the context of POC applications [18–21]. Among the common types of SPEs are the SPCEs, in that chemically inert carbon ink along with organic solvents, additives, and binders are applied to one end of the conductive tracks to create the WE and CE. Typically, silver electroactive paths are used as a RE [22,23].

The SPCEs modified by nanomaterial are widely used to improve the sensitivity of detector devices. For example, the incorporation of AuNS into SPCE can increase the EASA, thereby facilitating electron transfer between the electrode and the analyte. This modification allows the modified electrode to perform rapid, accurate, and reproducible measurements with high sensitivity and selectivity [24].

1.1.2. SAMs in biosensor design

In biosensor design, in addition to improving the electrochemical properties of the WE, it is important to functionalize the electrode to make it a biocompatible sensing platform. The utilization of a SAM offers a

straightforward method for functionalizing electrode surfaces with organic molecules [25]. The SAMs are molecular layers that assemble on a surface through adsorption, typically from a solution. They form due to the interaction of specific functional groups with particular surfaces. Various SAMs have been developed for a wide range of materials, including medically relevant metals like titanium [26]. However, the most extensively studied SAMs involve alkane thiolates and gold [27–29]. When a gold surface is submerged in a solution of alkane thiolates, the sulfur atoms form coordination bonds with the gold surface in a densely packed arrangement. The alkane portion extends outward from the surface, providing opportunities for a wide range of chemical modifications, either before or after assembly, to create surfaces with specific chemistries. The SAMs offer beneficial properties such as optical transparency when applied to thin gold layers and electrical conductivity, making them suitable for electrochemical modulation of surface properties [27].

The SAMs have many attractive properties for biosensor design, making them very advantageous for various reasons [30]. Their minimal resource consumption facilitates easy miniaturization. In addition, the highly ordered and densely packed nature of long-chain alkanethiols in the SAM closely resembles the cellular microenvironment of lipid bilayer structures, providing innovative substrates for immobilized biomolecules or biological systems. Moreover, the simple SAM formation procedure and compatibility with metal substrates for electrochemical measurements offer significant advantages for biosensing applications involving current or potential measurements. Finally, the chemical stability of the monolayer and the associated specificity for transducer-integrated biological sensing make the SAMs highly effective for biosensors [25].

1.1.3. Conducting polymers in biosensor design

Another highly promising avenue in electrode modification for biosensing design involves the utilization of conducting polymers [31]. The enhancement of sensing performance in analytical and bioanalytical systems necessitates conducting polymers possessing key properties such as electrochemical activity, electrical conductivity, mechanical elasticity, biocompatibility, and environmental stability [32]. Among the various conducting polymers Ppy, PANI, polythiophene, and poly(3,4-ethylenedioxythiophene) are predominantly utilized due to their significant technological potential, which has been extensively leveraged in sensor applications [33–37]. Conducting

polymers can be synthesized through various methods, including electrochemical [37,38], chemical [39], and biotechnological approaches [40]. Following synthesis or deposition, conducting polymer-based layers can be readily doped and de-doped using electrochemical techniques. The doping procedure allows for the customization of the properties of the conducting polymer-based sensing layer. Electrochemical deposition, in particular, proves highly advantageous for depositing conducting polymer-based layers directly onto electrodes and other conducting surfaces. By adjusting electrochemical parameters such as potential, current, potential sweep rate, and duration, one can finely tune the analytical characteristics of the resulting polymeric layers [37,41]. Furthermore, the electrical conductivity and certain electrochemical properties of conducting polymers can be precisely tailored and controlled by adjusting parameters such as polymerizable monomer concentrations, pH of the polymerization bulk solution, and employing various dopant concentrations [42,43]. In biosensors, conducting polymers find application as immobilization matrices [37], signal transduction systems [37,44], and even as analyte recognition structures based on molecular imprints formed within deposited layers of conducting polymers [45–48].

Molecularly imprinted polymer (MIP)-based sensors

MIP-based sensors hold significant promise as they primarily rely on polymeric matrices and eliminate the need for costly biological recognition materials [49–51]. MIPs are polymers with artificially engineered specific molecular recognition sites that precisely match the structure of the imprinted target molecule. As a result, MIPs replicate the functionality of receptors and antibodies. Both electrochemical and chemical polymerization methods are viable for creating MIPs using conducting polymers. The oxidative polymerization process is notably straightforward and cost-effective, enabling the production of large quantities of MIPs using this method [52,53]. Electrochemical polymerization offers advantages over oxidative polymerization. This method enables the creation of a MIP layer over electrodes or other conducting surfaces and can be conducted in various solvents depending on the requirements of the polymerizable monomer and/or imprinted analyte. Moreover, electrochemical polymerization allows for the adjustment of the morphology, homogeneity, conductivity, and thickness, of the resulting polymer layer with molecular imprints. While various techniques exist for MIP formation, they typically involve several common stages. Most monomers, featuring functional groups necessary for recognizing the target molecule, are copolymerized with cross-linking monomers lacking

recognition properties in the presence of the target molecule. Following this, the target molecule is extracted from the formed MIP in the subsequent stage [54].

1.1.4. Electrochemical methods for analytical signal registration

Another crucial aspect in the design of electrochemical biosensors is the selection of an appropriate signal registration method. Commonly used electrochemical methods in biosensing design include CV, DPV, EIS, and PAD. The underlying principles of electrochemical detection involve measuring the physicochemical properties of the bioreactor and target analyte to generate a readable signal, such as electrical current, voltage, or resistance. When a chemical reaction occurs between the target analyte and the bioreactors (electrode), it leads to changes in the electrical properties of the solution due to the production of ions or electrons [4,55]. Broadly, electrochemical detection techniques can be categorized as amperometric-based, impedimetric-based, potentiometric-based, and conductometric-based.

Voltammetric methods

Voltammetry encompasses a range of measurement techniques wherein the applied potential undergoes systematic variation across a defined range. The resulting current response typically manifests as a peak or plateau, which correlates with the analyte concentration [4]. Notable voltammetric methods include CV, DPV, square-wave voltammetry (SWV), and linear sweep voltammetry, among others. These techniques are known for their broad dynamic range and are particularly valuable for quantifying analytes at low levels [56].

At its most fundamental level, CV involves sweeping the potential versus the RE in both forward and reverse directions, typically encompassing the electroactive species. This enables the exploration of the resulting electrochemical species generated at the electrode surface. The CV furnishes both qualitative and quantitative insights into electrochemical systems and has become firmly established as a rapid and dependable characterization tool. It is frequently employed to investigate the kinetics of electron transfer reactions, including catalysis, and has been extended for applications in organic and inorganic synthesis, sensor and biological system assessment, as well as the fundamental elucidation of physical mechanics underlying electron transfer reactions, such as reversibility, formal potentials, and diffusion

coefficient determination [57]. The Randles-Sevcik equation describes the relationship between the peak current height observed in CV and experimental parameters such as the scan rate and the concentration of the electroactive species:

$$i_p = 0.4463nFAC\left(\frac{nF\nu D}{RT}\right)^{\frac{1}{2}} \quad (1),$$

where i_p – current maximum; n – number of electrons transferred in the electrochemical reaction; A – electrode area; F – Faraday constant; D – diffusion coefficient; C – concentration of the electroactive species; ν – scan rate; R – gas constant; T – temperature.

The DPV stands out as a technique with distinct advantages over a common CV. In the DPV, the waveform comprises a series of pulses incrementing along a linear baseline. This unique approach to current measurement at each pulse helps minimize the detection of background current [57]. Typically, pulse techniques like DPV exhibit higher sensitivity compared to linear-sweep methods, with CV being the preferred technique for exploratory purposes. Consequently, it is quite common in sensor development to utilize both these methods. CV offers essential insights into aspects like process reversibility and the nature of redox processes occurring at the electrode-solution interface during analysis. On the other hand, potential-pulse-based techniques can sometimes simplify analyte quantification [37]. Under normal conditions, the DPV peak height can be determined using the equations [57]:

$$\delta i = i(\tau) - i(\tau') \quad (2),$$

$$\sigma = \exp\left(\frac{nF}{RT}\frac{\Delta E}{2}\right) \quad (3),$$

$$\delta i_{max} = \frac{nFAD^{\frac{1}{2}}C}{\pi^{\frac{1}{2}}(\tau - \tau')^{\frac{1}{2}}}\left(\frac{1-\sigma}{1+\sigma}\right) \quad (4),$$

where δi – difference in current; τ' – time just before the application of the potential pulse, τ – time at the end of the pulse; ΔE – pulse height.

Amperometric methods

Chronoamperometry (CA) is an amperometric technique, where the variations in current resulting from the electrochemical oxidation or reduction processes are directly observed over time, while a constant, stepped, or pulsed potential is maintained at the working electrode [58]. The changes in current occur due to variations in the diffusion layer around the electrode. Nernst introduced the concept of a diffusion layer, which refers to a stationary, thin layer of solution in direct contact with the electrode surface. Within the diffusion layer, the concentration of electroactive species diminishes to zero at the electrode surface, and the migration of electroactive species from the bulk solution, where the concentration is higher, is regulated by diffusion. As a result, a concentration gradient forms away from the electrode surface, while the concentration in the bulk solution remains constant due to convective transfer [18].

The CA is a method closely linked to the Cottrell equation, which characterizes the current-time relationship for linear diffusion control at a planar electrode [59,60]. According to the Cottrell equation, the current is determined by the rate at which the analyte diffuses to the electrode:

$$i(t) = \frac{nFAD^{\frac{1}{2}}C}{\pi^{\frac{1}{2}}t^{\frac{1}{2}}} \quad (5),$$

where t – time.

Amperometric detection is frequently employed in biocatalytic and affinity sensors due to its simplicity and low LOD [61–63]. Its fixed potential during detection helps minimize background signal, particularly the charging current, which can adversely affect the LOD.

Impedimetric methods

EIS involves assessing the resistive and capacitive characteristics of materials when a system is perturbed by a small sinusoidal alternating current (AC) signal [58,64,65]. The frequency of this signal is adjusted across a broad spectrum to generate an impedance profile. By analyzing the in-phase and out-of-phase current responses, the resistive and capacitive elements of impedance are determined, respectively. The EIS is valuable as it can monitor both electron transfer at high frequencies and mass transfer at low frequencies. The EIS is commonly measured by applying an AC potential to an electrochemical cell and subsequently gauging the current passing through the cell:

$$E(t) = E_0 \sin(\omega t) \quad (6),$$

where $E(t)$ – applied potential; E_0 – potential sine wave amplitude; t – time; ω – angular frequency; ωt –the phase of the waveform.

$$i(t) = i_0 \sin(\omega t + \varphi) \quad (7),$$

where $i(t)$ – output current; i_0 – current sine wave amplitude; φ – phase angle.

The equation describing the amplitude of impedance ($|Z|$) is akin to Ohm's law:

$$|Z| = \frac{E_0(\omega)}{i_0(\omega)} \quad (8),$$

where $E(\omega)$ – frequency-dependent potential; $i(\omega)$ – frequency-dependent current.

A periodic or sinusoidal signal can be represented as a complex number, which can also be expressed in terms of its magnitude:

$$Z(\omega) = |Z|(cos\varphi + jsin\varphi) = Z' + jZ'' \quad (9),$$

where Z' – real part of the impedance; Z'' – imaginary part of the impedance; j – imaginary number $\sqrt{-1}$. In EIS, one method of data representation is the Nyquist plot, where the Z' is plotted on the X-axis and the Z'' is plotted on the Y-axis of a chart.

The EIS is a valuable tool for analyzing complex electrochemical systems by modeling different components with known circuit elements, each characterized by specific impedance properties. The Randles circuit is a widely used equivalent electrical circuit model consisting of a resistor (R), a capacitor (C), and optionally a Warburg impedance (W) representing the diffusion process, often employed in the EIS to characterize electrochemical systems:

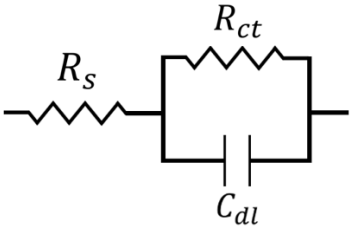

Figure 1. Randles circuit. R_s – solution resistance; R_{ct} – charge transfer resistance; C_{dl} – electrochemical double-layer capacitance [57].

The equations describing the corresponding impedances of equivalent circuit elements:

$$Z_R = R \tag{10},$$

$$Z_C = \frac{-j}{\omega C}, \tag{11}$$

where Z_R – impedance of the resistor; R – resistance; Z_C – impedance of the capacitor; C – capacitance.

After rearrangement and simplification, the impedance of the electrochemical system can be described by the following equation:

$$Z(\omega) = R_s + \frac{R_{ct}}{1 + R_{ct}C_{dl}} \tag{12}$$

Based on equation 12, at high frequencies, the impedance across the capacitor decreases, allowing current to flow through the capacitor (C_{dl}). Conversely, at low frequencies, the impedance of the capacitor increases, causing current to pass through the resistor (R_{ct}).

Impedance techniques are valuable in electrochemical sensing to track alterations in electrical properties stemming from biorecognition events occurring at modified electrode surfaces. This includes measuring shifts in electrode conductance resulting from protein immobilization and antibody-antigen reactions on the electrode surface [66–71].

1.2 Diagnosis of COVID-19

The global pandemic of COVID-19, caused by SARS-CoV-2, was declared in March 2020. Efforts to reduce the transmission rate, particularly through tracking infected individuals and their contacts, were crucial in combating the

spread of the infection. Hence, there was and remains a pressing need for the development of rapid, reliable, and sensitive diagnostic methods for COVID-19. Electrochemical biosensors offer a promising solution, leveraging various detection methods and markers to generate analytical signals tailored to meet these urgent requirements.

1.2.1 SARS-CoV-2 virus

Structure of SARS-CoV-2 virus

The SARS-CoV-2 virus, approximately 130 nm in diameter, features a spike-covered spherical structure resembling the sun's corona, typical of coronaviruses [72–74]. Its genetic material, single-stranded RNA (ssRNA), housed within a helically symmetrical nucleocapsid, shares similarities with other coronaviruses such as SARS-CoV and middle east respiratory syndrome coronavirus [75]. The genome encompasses ten open reading frames, encoding vital structural proteins including S-, N-, envelope (E), and membrane (M) proteins [75]. The S-protein, a trimer composed of S1 and S2 subunits, facilitates viral attachment, fusion, and infection by binding to host cell receptors [76–81]. The E-protein contributes to viral envelope formation and maturation, while the N-protein binds to viral ssRNA, aiding in virion formation [82–86]. The M-protein shapes the viral envelope and collaborates with other proteins for virion assembly and stabilization [87–90].

Life cycle of SARS-CoV-2 virus

The SARS-CoV-2 primarily infects the respiratory system, replicating in the alveoli and potentially spreading to organs expressing high levels of angiotensin-converting enzyme 2 (ACE2) receptors, such as enterocytes, cholangiocytes, myocardial cells, and kidney proximal tubule cells [91–94]. The virus attaches to host cells via the receptor binding domain within the S1 subunit of the S-protein and the ACE2 receptor, leading to membrane fusion and injection of the viral genome into the cytoplasm [75]. Translation of the replicase gene and cleavage of polyproteins by coronavirus-encoded proteases form the replicase-transcriptase complex for RNA synthesis, producing genomic and subgenomic RNAs for structural and accessory genes [95,96]. The S-, E-, and M-proteins are translated and placed into the endoplasmic reticulum (ER) and then transferred through the secretory pathway into the ER-Golgi intermediate compartment [95,96]. There, the N-protein forms the nucleocapsid, which buds into the membrane to form the virus, facilitated by

interactions managed by the M-protein [84]. Vesicles transport virions to the cellular surface for exocytosis [75].

Immune response towards SARS-CoV-2 virus infection

Upon entry into the host, SARS-CoV-2 triggers an immune response, initially involving innate immune cells like macrophages [97]. This response leads to the activation of humoral immunity, resulting in the production of antigen-specific antibodies, primarily immunoglobulin M (IgM) and immunoglobulin G (IgG), that serve as markers for coronavirus presence [98]. The IgM levels peak around 2-5 weeks after onset of symptoms, while the IgG levels peak later, around 3-7 weeks, and remain relatively stable for up to 105 days [99,100]. Structural proteins of SARS-CoV-2, particularly the S- and N-proteins, serve as antigens for specific antibody binding [101]. However, there has been a significant rise in mutations, raising concerns about their potential effects on the virus's infectivity and pathogenicity levels. A noteworthy observation is that most of these mutations are centered around the S-protein [102]. In contrast, the N-protein exhibits a lower incidence of mutations, suggesting its relative conservation throughout the evolutionary process [103].

1.2.2 COVID-19 diagnostic strategies

Three main diagnostic strategies are employed for detecting SARS-CoV-2 and diagnosing COVID-19: molecular tests to detect viral RNA, antigen tests to detect viral proteins, and antibody tests to detect specific antibodies against viral proteins.

Detection of SARS-CoV-2 virus RNA

Molecular-based methods, such as reverse transcription-polymerase chain reaction (RT-PCR) [104–106], reverse transcription loop-mediated isothermal amplification (RT-LAMP) [106–108], and recombinase polymerase amplification (RPA) [109,110] are utilized for detecting SARS-CoV-2 RNA. The RT-PCR, considered the gold standard, offers high sensitivity but requires expensive equipment and skilled personnel. The RT-LAMP offers faster results with simplified protocols, albeit with primer design complexities. The RT-RPA provides rapid detection within 20 min, while clustered regularly interspaced short palindromic repeats-based assays offer promising alternatives with quick detection times and low LODs [111–115]. Despite their advantages, all methods face challenges related to complexity and the need for specialized resources.

Detection of antibodies against SARS-CoV-2 virus proteins

Antibody tests, categorized under serological methods, confirm past SARS-CoV-2 infections, aiding in disease stage monitoring and immunity identification. Common methods include lateral flow immunoassay (LFIA), enzyme-linked immunosorbent assay (ELISA), and chemiluminescence immunoassay (CLIA). The LFIA combines IgG and IgM detection within 15 min [116], while the ELISA requires 2–5 hours for completion [117]. The CLIA offers rapid testing (20 min) with specificity ranging from 92.3% to 97.5% [118]. While serological assays are cost-effective and scalable, challenges include variations in individual immune responses and seroconversion delays, leading to potential false results.

Detection of SARS-CoV-2 proteins

The SARS-CoV-2 structural proteins detection methods, akin to both molecular and antibody tests, identify current viral infections by detecting specific antigen-antibody complexes. The LFIA and fluorescent immunoassay (FIA) techniques are utilized to detect SARS-CoV-2 N-proteins, exemplified by the ‘COVID-19 Ag respi-strip LFIA’ assay and the 'standard F COVID-19 Ag FIA' test. Additional methods such as half-strip lateral flow assay, fluorescence immunochromatography, and the CLIA are also employed for N-protein determination [119–123].

Electrochemical biosensors for the diagnosis of COVID-19

Electrochemical biosensors, encompassing CV [67,124–129], SWV [130–134], CA [124,135–138], EIS [67,127,139–143], DPV [124,144–147], and PAD [62,148,149], offer a promising avenue for COVID-19 diagnosis [6,7]. These biosensors, based on electrochemical reactions, utilize various mechanisms such as nucleic acid hybridization [139,144,150–152], antigen-antibody interactions [67,127,129,131–133,140], and reactive oxygen species [125] level changes. They have demonstrated high sensitivity and specificity, with some achieving LOD and short testing times. Additionally, electrochemical sensors are advantageous due to their simplicity, low cost, and scalability, making them ideal for biomedical applications. While significant progress has been made in utilizing electrochemical biosensors for COVID-19 diagnosis, further research and innovation are needed to optimize their performance and address any remaining challenges.

2. METHODS USED IN THIS RESEARCH WORK

2.1. Materials and reagents

2.1.1. Chemicals

Tetrachloroauric acid trihydrate ($HAuCl_4 \cdot 3H_2O$) (99.0%, CAS# 16961-25-4), hexachloroplatinic acid hexahydrate ($H_2PtCl_6 \cdot 6H_2O$) (≥37.5% Pt basis, CAS# 16941-12-1), KNO_3 (99.0%, CAS# 7757-79-1), KCl (≥99.0%, CAS# 7447-40-7), ethanol (EtOH) (99.9%, CAS# 64-17-5), L-Cysteine (97.0%, CAS# 52-90-4), N-(3-dimethylaminopropyl)-N'-ethyl-carbodiimide hydrochloride (EDC) (99.0%, CAS# 25952-53-8), ethanolamine (EA) (98.0%, CAS# 141-43-5), $K_3[Fe(CN)_6]$ (99.0%, CAS# 13746-66-2), $K_4[Fe(CN)_6] \cdot 3H_2O$ (99.0%, CAS# 14459-95-1), phosphate-buffered saline (PBS) tablets (pH 7.4), aniline (98.0%, CAS# 62-53-3), phytic acid (PA) (50.0% w/w H_2O, CAS# 83-86-3), Na_2HPO_4 (≥99.0%, CAS# 7558-79-4) and NaH_2PO_4 (≥99.0%, CAS# 7558-80-7) for preparing phosphate buffer (PB) solution, glutaraldehyde (GA) (50.0% w/w H_2O, CAS# 111-30-8) were obtained from Sigma–Aldrich (Steinheim, Germany). N-hydroxysuccinimide (NHS) (98.0%, CAS# 6066-82-6) and pyrrole (Py) (>98.0%, CAS# 109-97-7) were purchased from Alfa Aesar (Karlsruhe, Germany). H_2SO_4 (>96.0%, CAS# 7664-93-9) was purchased from Lachner (Neratovice, Czech Republic). All reagents were analytical grade and were used without additional purification. All aqueous solutions were prepared in deionized water.

2.1.2. SARS-CoV-2 virus proteins

The recombinant SARS-CoV-2 spike protein (rS) (1 mg/mL) and recombinant SARS-CoV-2 nucleocapsid protein (rN) (1 mg/mL) were purchased from Baltymas (Vilnius, Lithuania).

Yeast extract peptone dextrose (YEPD): yeast extract 1.0% (CAS# 8013-01-2, Acros), peptone 2.0% (CAS# 91079-46-8, Fluka), dextrose 2.0% (≥99.5%, CAS# 50-99-7, Fisher Scientific), 4 mM formaldehyde (≥37.0%, CAS# 50-00-0, Carl Roth), yeast extract peptone dextrose glucose (YEPG): yeast extract 1.0%, peptone 2.0%, galactose 2.5% (≥98.0%, CAS# 59-23-4, Applichem), 4 mM formaldehyde. Lysis buffer: 50 mM NaH_2PO_4 (≥98.0%, CAS# 13472-35-0, Carl Roth) (pH 8.0), 2 M NaCl (≥99.8%, CAS# 7647-14-5, Carl Roth), 1.0% Tween20 (CAS# 9005-64-5, Carl Roth), 10 mM

imidazole (≥99.0%, CAS# 288-32-4, Acros), 1 mM phenylmethylsulfonyl fluoride (≥99.0%, CAS# 329-98-6, Carl Roth). PBS buffer: 10 mM Na_2HPO_4 (≥98.0%, CAS# 7558-79-4, Carl Roth), 1.8 mM KH_2HPO_4 (≥98.0%, CAS# 7778-77-0, Carl Roth), 137 mM NaCl, 2.7 mM KCl (≥99.0%, CAS# 7447-40-7, Carl Roth), (pH 7.4).

Preparation and purification of the SARS-CoV-2 rS protein

The rS protein was synthesized as a trimeric, secreted protein within mammalian Chinese hamster ovary (CHO) cells. To achieve a native conformation locked in a prefusion state, the gene encoding the SARS-CoV-2 spike ectodomain, spanning amino acids (aa) 1–1208 (UniProtKB sequence accession number: P0DTC2 (SPIKE_SARS2)), underwent chemical synthesis at General Biosystems (USA). Subsequently, the synthetically derived gene was integrated into the mammalian expression vector pCAGGS (Creative Biogene, cat. no. VET1375) via NotI and XhoI restriction sites strategically introduced at the 5′′ and 3′′ ends of the gene, respectively. The comprehensive expression construct encompassed the full-length SARS-CoV-2 spike ectodomain (aa 1–1208), excluding transmembrane and cytoplasmic aa. It featured a furin cleavage site mutation from "RRAR" to "GSAS," a C-terminal GSN4 trimerization motif fused to the protein sequence, succeeded by the thrombin cleavage site, Strep-tag II, and His6-tag. Additionally, two mutations (K986P and V987P) were incorporated into the SARS-CoV-2 spike sequence to enhance trimer stability in the pre-fusion conformation [153].

The expression of the rS protein was conducted in CHO cells using the ExpiCHO Expression System (Thermo Fisher Scientific, cat. no. A29133). Transfection procedures and expression conditions adhered to the Max Titer Protocol provided by Thermo Fisher Scientific. On the 9th day post-transfection, the cultivation media were harvested and subjected to centrifugation at 5,000×g for 30 min in a refrigerated centrifuge, and the resulting supernatant was filtered through a 0.22 μm filter. Subsequent to microfiltration, proteins were concentrated and transferred to a binding buffer (50 mM NaH_2PO_4, (pH 8.0), 300 mM NaCl, 10 mM imidazole) through tangential ultrafiltration, utilizing a tangential flow filtration cassette with 100 kDa cut-off membranes (SartoriusStedim Biotech, cat. no. VF20P). The protein solution was applied to nickel-nitrilotriacetic acid-modified SuperFlow (Qiagen, USA) resin. Non-specifically bound proteins were eliminated through column washing with a lysis buffer containing 75 mM imidazole. Tightly bound proteins were eluted using a 75–250 mM imidazole gradient. Fractions containing the purified rS were consolidated, dialyzed against PBS (10 mM Na_2HPO_4, 1.8 mM KH_2PO_4, 137 mM NaCl, 2.7 mM

KCl, (pH 7.4)), adjusted to a concentration of 1.0 mg/mL, filter-sterilized, aliquoted, and cryopreserved for storage. The purity of the produced rS protein was approximately 90.0%, as determined by sodium dodecyl sulfate (SDS) polyacrylamide gel electrophoresis.

Preparation and purification of the SARS-CoV-2 rN protein

The rN expressed in the yeast *Saccharomyces cerevisiae (S. cerevisiae)* was produced following a systematic protocol. The gene encoding the SARS-CoV-2 N-protein (Uniprot accession no. P0DTC9) was optimized for yeast expression and chemically synthesized by General Biosystems, Inc. (USA). A C-terminal histidine tag, consisting of six histidine amino acids, was introduced through polymerase chain reaction using specific primers. The resultant SARS-CoV-2N-6HIS gene was then cloned into the *S. cerevisiae* episomal expression vector pFGAL7, under the control of the galactose-inducible yeast GAL7 promoter, resulting in the creation of the pFGAL7-SARS-CoV-2_N-6HIS plasmid. This plasmid was utilized to transform the *S. cerevisiae* AH22 (MATa leu2 his4) (ATCC 38626) strain. Yeast biomass intended for the purification of the rN was generated by cultivating yeast transformants in the YEPD medium and inducing rN synthesis by transferring cells into the YEPG medium. The resulting yeast biomass was suspended in the lysis buffer and subjected to disruption by vortexing with glass beads. Subsequently, the yeast lysate underwent centrifugation for 30 min at 10,000×g. The soluble fraction obtained was filtered through 0.45 μm filter and applied to Ni-NTA SuperFlow resin (Qiagen, USA). Nonspecifically bound proteins were removed by washing the column with a lysis buffer containing 30 mM imidazole. The tightly bound proteins were then eluted using 20–250 mM imidazole gradient. Fractions containing the rN were pooled and dialyzed against PBS buffer (pH 7.4). Following dialysis, the solution underwent centrifugation for 30 min at 10,000×g. The soluble fraction obtained was filtered through 0.45 μm filter and loaded onto SP FastFlow resin (Cytiva, USA). Bound proteins were eluted using 137–500 mM NaCl gradient. Fractions containing pure rN were pooled and subjected to dialysis against PBS.

2.1.3. Serum sample collection

A volunteer inoculated with a single dose of the Vaxzevria vaccine (formerly known as AstraZeneca), was selected for analysis two weeks after contracting COVID-19. Blood was drawn one month post-confirmation of the volunteer's

positive status, as determined by SARS-CoV-2 virus detection through RT-PCR, leading to a COVID-19 diagnosis. Whole blood was collected using a vacuum tube containing 3.5 mL of CAT serum sep clot activator (Greiner Bio-One GmbH, Austria) at the laboratory of Tavo Klinika, LtD. (Vilnius, Lithuania). After centrifugation at 5,000×g for 15 min, the serum was separated. The initial quantification of binding antibodies against SARS-CoV-2 in the serum sample was conducted using a chemiluminescent microparticle immunoassay, yielding a stock concentration of ~5860 binding antibody units (BAU)/mL. The antibody concentration in the sample was then converted from BAU/mL to nM concentration, employing a conversion ratio of 1 BAU/mL:20 ng/mL (considering the molecular weight of immunoglobulin to be approximately 150 kDa) [154–156]. The serum sample was subsequently stored at –20°C until analysis. The collection of the sample adhered to the Lithuanian ethics law and the study was determined not to require approval from the ethics committee, as confirmed by the Vilnius Regional Biomedical Research Ethics Committee.

2.2. Electrochemical biosensing systems

The DRP-110 SPCEs were obtained from Metrohm DropSens (Oviedo, Spain). Metrohm DropSens SPCEs, designed for use with microvolumes or immersion in solutions, serve as optimal platforms for the development of biosensors. The electrochemical cell configuration includes carbon WE (4 mm diameter), carbon CE, and silver RE (Fig. 2) [157]. In the presence of a chloride-containing solution, a reaction occurs on the silver RE, leading to the formation of a layer of silver chloride. This process results in the well-established Ag/AgCl reference system commonly used in electrochemical experiments.

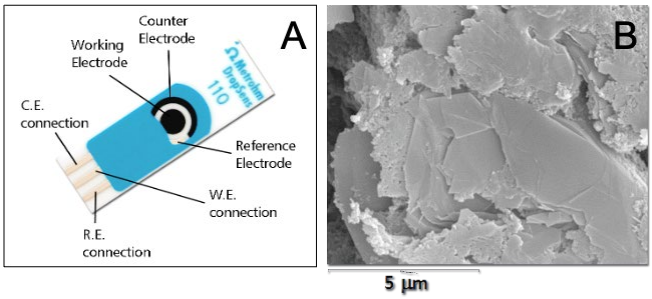

Figure 2. DRP-110 SPCE (A). Scanning electron microscope (SEM) image of carbon working electrode (B) [157].

2.2.1. Working electrode modifications

Electrodeposition of AuNS on SPCE

The SPCE was coated with a 100 µL solution consisting of 0.1 M KNO_3 and 5 mM $HAuCl_4$ (Fig. 3 Step 1). Electrodeposition was executed under a potential of -0.4 V for a duration of 60 s or 120 s. Subsequent to the deposition of AuNS on the SPCE, the electrode underwent rinsing with deionized water and was subsequently dried using a flow of N_2.

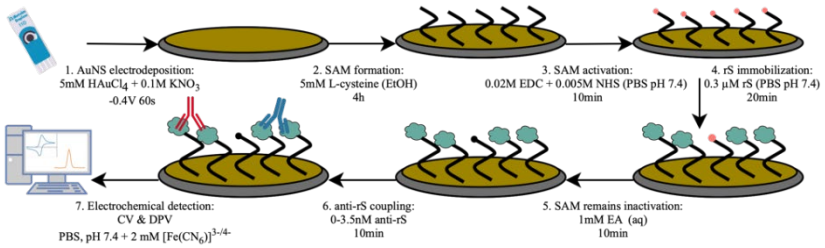

Figure 3. Schematic representations of the SAM-based biosensor design stages.

Electrodeposition of PtNS on SPCE

The protocol involved coating the SPCE with a 100 µL solution containing 5 mM H_2PtCl_6 and 0.1 M KCl, following a methodology similar to that outlined in [148]. Electrodeposition occurred for 120 s at a potential of -0.4 V. After the deposition of PtNS, the electrodes were subjected to thorough rinsing with deionized water and subsequent drying using a flow of N_2.

Deposition of polyaniline (PANI) layer on SPCE surface

To modify the working electrode with a PA-doped PANI film, the electrode surface was coated with a 100 µL aqueous solution composed of 5% aniline and 5% PA, following the method described in [158] (Fig. 4 Step 1). Subsequently, a current of 10 µA was applied for various exposition times (ETs) ranging from 1 to 20 min. Following the electrochemical treatment, the PANI-modified SPCE underwent a thorough rinsing with a substantial amount of deionized water.

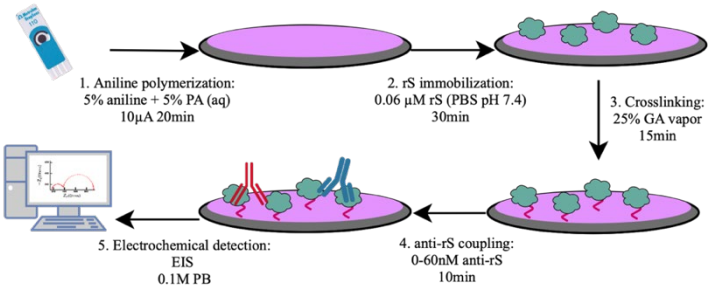

Figure 4. Schematic representations of the PANI-based biosensor design stages.

Deposition of polypyrrole (Ppy) layer on SPCE surface

To achieve this, 100 μL of 0.25 M Py in PBS solution (pH 7.4) was introduced, and the deposition process involved two potential pulses of +0.9 V each for 1 s. During the intervals between these pulses, a potential of 0 V was maintained for 10 s (Fig. 5 Step 1). After SPCE was pre-modified with an underlying polymer layer, 100 μL of PBS solution containing 0.25 M Py and 1 μM of rN was applied atop the electrode. Subsequently, a sequence of four potential pulses, each lasting 1 s at +0.9 V, was applied, with intervals of 0 V potential maintained for 10 s between these pulses (Fig. 5 Step 2).

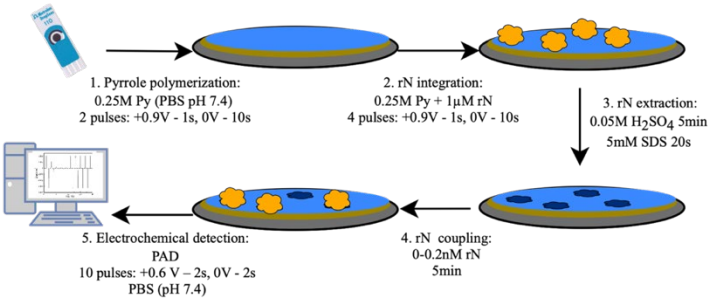

Figure 5. Schematic representations of the MIP-based biosensor design stages.

2.2.2. Sensing element formation

SAM-based immobilization of SARS-CoV-2 virus proteins

The AuNS-modified SPCE underwent an incubation period at room temperature (RT) for 4 hours in a 5 mM L-cysteine EtOH solution, facilitating the formation of a SAM on the working surface (Fig. 3 Step 2). Following the incubation, the electrode underwent a thorough rinsing with deionized water

and subsequent drying under a flow of N_2. The established SAM was activated with 10 µL of a mixture containing 0.02 M EDC and 0.005 M NHS in PBS (pH 7.4) for 10 min (Fig. 3 Step 3). Subsequent to activation, the WE was incubated with 10 µL of 0.3 µM rS in PBS (pH 7.4) atop, at RT for 20 min (Fig. 3 Step 4). The immobilization of rS was accomplished through the covalent coupling of the protein's primary amine functional groups with the activated carboxylic groups of the SAM. Any remaining reactive esters were rendered inactive by incubating the electrode with a 1 mM aqueous solution of EA for 10 min (Fig. 3 Step 5).

Glutaraldehyde-based immobilization of SARS-CoV-2 virus proteins

The SPCE modified with PANI was coated with 6 µL of a 0.06 µM PBS (pH 7.4) solution of rS and incubated for 30 min at RT. Following the complete coverage, the electrode was transferred to a beaker containing a 25% GA solution and incubated in vapor for 15 min. Subsequently, the modified SPCE was immersed in a PB solution and kept overnight at 4°C to get rid of the GA remains.

Formation of molecularly imprinted polymer (MIP)-based layers

The SPCE modified with Ppy film incorporating rN underwent an extraction procedure. Initially, the Ppy-modified SPCE was incubated in a 0.05 M H_2SO_4 solution for 5 min at RT and subsequently rinsed with water and PBS solution (pH 7.4). Subsequent to this, the SPCE was immersed in a 5 mM SDS solution for approximately 20 s and then rinsed with PBS solution (pH 7.4) resulting in the formation of molecularly imprinted polypyrrole-based rN templates (Fig. 5 Step 3):

MIP1 – SPCE/AuNS modified with Ppy/rN;

MIP2 – SPCE/PtNS modified with Ppy/rN;

MIP3 – SPCE modified with Ppy/rN.

Non-imprinted polymer (NIP) systems were also tested in parallel to evaluate the contribution of non-specific binding and assess the affinity sensor's efficiency:

NIP1 – SPCE/AuNS modified with Ppy;

NIP2 – SPCE/PtNS modified with Ppy;

NIP3 – SPCE modified with Ppy.

2.2.3. Determination of SARS-CoV-2 virus related analytes

Detection of antibodies against SARS-CoV-2 spike protein (anti-rS)

The SPCE with immobilized rS was subjected to incubation with 6-10 µL of anti-rS spanning a concentration range for 10 min at RT. After each incubation step, the electrodes were rinsed with either PBS or PB solution (Fig. 3 Step 6, Fig. 4 Step 4).

Detection of SARS-CoV-2 recombinant nucleocapsid protein (rN) with MIP-based sensor

The SPCE modified with MIP was subjected to incubation in PBS (pH 7.4), containing rN at various concentrations. These incubations were performed for 5 min at RT. Between each round of incubation in different concentrations of rN and subsequent measurements, the electrodes were thoroughly rinsed with PBS (pH 7.4) (Fig. 5 Step 4).

2.3. Electrochemical measurements

2.3.1. Electrochemical equipment

A potentiostat controlled by the DStat interface software from Wheeler Microfluidics Lab (University of Toronto, Toronto, ON, Canada). The DRP-110 SPCEs were connected via a specialized 'box-connector' designed for SPEs (DRP-DSC, DropSens, Oviedo, Spain). Metrohm DropSens µStat400 potentiostat (Asturias, Spain) equipped with DropView 8400 software. µAUTOLAB TYPE III potentiostat (Metrohm, Netherlands) controlled by FRA2-EIS software from ECO-Chemie (Utrecht, Netherlands).

2.3.2. Electrochemical methods

Cyclic voltammetry (CV)

The CV was recorded within the potential range of -0.4 to +0.6 V versus Ag/AgCl, employing a scan rate of 0.05 V/s in PBS (pH 7.4) with 2 mM potassium ferricyanide/ferrocyanide ($[Fe(CN)_6]^{3-/4-}$) solution served as the redox probe.

Differential pulse voltammetry (DPV)

The DPV experiments were carried out within the potential range of -0.4 to +0.6 V versus Ag/AgCl, utilizing a scan rate of 0.04 V/s in PBS (pH 7.4) with 2 mM $Fe(CN)_6]^{3-/4-}$ solution served as the redox probe.

Electrochemical impedance spectroscopy (EIS)

The EIS signal was recorded across a frequency range spanning from 0.1 Hz to 100 kHz, utilizing a perturbation amplitude of 0.01 V and a potential of 0.1 V versus an Ag/AgCl reference electrode.

Pulsed amperometric detection (PAD)

The PAD was carried out under the following conditions: 10 potential pulses of +0.6 V versus Ag/AgCl reference electrode for 2 s, with intervals between these pulses set at 0 V for 2 s. The experiment was performed at a sampling rate of 200 datapoints/s in a PBS solution (pH 7.4), as per the methodology outlined by Ratautaite et al [148].

2.4. Calculations

2.4.1. Electrochemical characterization of electrodes

The EASA was determined using the Randles-Sevcik equation at 25 °C:

$$i_p = (2.69 \cdot 10^5) n^{\frac{3}{2}} A D^{\frac{1}{2}} C v^{\frac{1}{2}} \quad (13),$$

where i_p – current maximum; n – number of electrons transferred in the electrochemical reaction (n=1); A – electrode area; D – diffusion coefficient ($6.40 \cdot 10^{-6}$ cm^2/s for $[Fe(CN)_6]^{4-}$); C – concentration of the electroactive species ($2 \cdot 10^{-6}$ mol/cm^3); v – scan rate.

The heterogeneous electron transfer rate constant (k^0) was determined using the improved Nicholson approach [159,160], where the dimensionless kinetic parameter Ψ was calculated based on the empirical equation:

$$\Psi = \frac{\left(-0.6288 + 0.0021 n \Delta E_p\right)}{1 - 0.017 n \Delta E_p} \quad (14),$$

$$\Psi = k^0 \left(\frac{\pi D n \nu F}{RT}\right)^{-\frac{1}{2}} \quad (15),$$

where Ψ – dimensionless kinetic parameter; D – diffusion coefficient ($6.40 \cdot 10^{-6}$ cm^2/s for $[Fe(CN)_6]^{4-}$); n – number of electrons transferred in the electrochemical reaction (n=1); ν – scan rate; F – Faraday constant; R – gas constant; T – temperature.

2.4.2. Signal normalization

For PAD method, calibration curves were plotted using a normalized difference in current density, Δj, (Fig. 6).

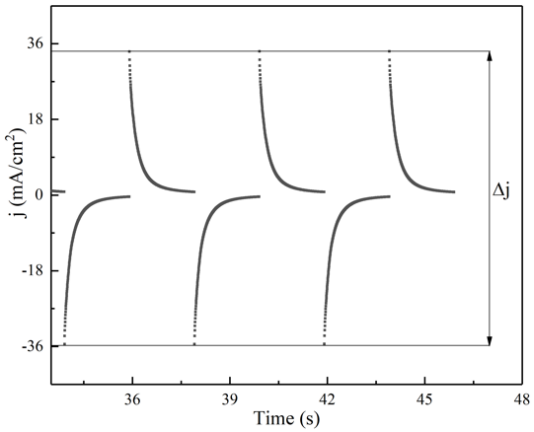

Figure 6. The principle of the analytical signal calculation for the PAD method.

The normalization of the Δj signals was performed by taking Δj at 0 nM of rN as zero:

$$Normalized\ signal = \Delta j_0 - \Delta j \quad (16),$$

where Δj_0 – signal at 0 nM of rN.

2.4.3. Limit of detection (LOD) and limit of quantification (LOQ) calculation

To analyze the performance of the biosensors, the LOD and LOQ were determined:

$$LOD = \frac{3.33\sigma}{Slope} \quad (17),$$

$$LOQ = \frac{10\sigma}{Slope} \quad (18),$$

where σ – is the standard deviation of the blank and *Slope* – the slope of the linear part of the calibration curve.

2.4.4. Evaluation of molecularly imprinted polymer (MIP)-based sensors

The MIP affinity was evaluated by the calculation of the Langmuir constant based on the isotherm equation adapted for the MIP-based electrochemical measurements [161]:

$$Norm.signal = Normal.signal_{max} \frac{K[rN]}{1 + K[rN]} \quad (19),$$

where *K* – adapted Langmuir constant; *[rN]* – concentration of rN.

3. RESULTS AND DISCUSSION

3.1. Detection of anti-rS antibodies with SPCE modified by electrodeposited AuNS

To enhance the surface area for immobilizing the rS and to facilitate better electron transfer kinetics, electrochemical deposition of AuNS was performed on the working electrode of the SPCE.

In addition, the effectiveness of the AuNS deposition was confirmed using CV in 10 mM H_2SO_4 solution (Fig. 7). During the experiment, the reproducibility of the data was ensured by testing three electrodes. The presence of characteristic gold reduction and oxidation peaks within the potential window from 0 to +1.0 V [162] was observed, while no oxidation or reduction peaks were evident on the unmodified SPCE surface (Fig. 7, inset).

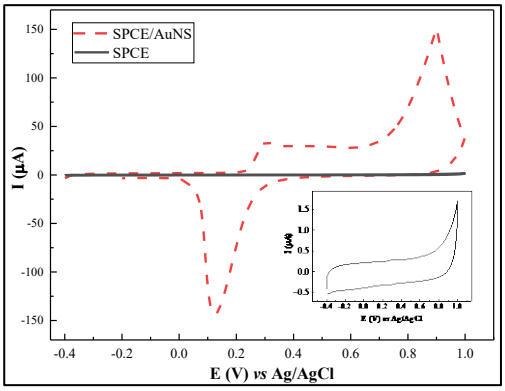

Figure 7. Cyclic voltammogram of SPCE/AuNS in 10 mM H_2SO_4. Inset: cyclic voltammogram of SPCE. Potential scan range was from −0.4 to +1.0 V vs. Ag/AgCl, at a scan rate of 0.1 V/s. The figure presents the average of 3 measurements.

Based on the data obtained from CV at scan rates ranging from 0.01 to 0.15 V/s (Fig. 8), and utilizing the Randles–Sevcik equation (Eq. 13) (Fig. 9A), the EASAs were calculated as $13.80 \pm 0.15 \cdot 10^{-2}$ cm² for SPCE and $23.50 \pm 0.12 \cdot 10^{-2}$ cm² for SPCE/AuNS (Table 1). Since charge transfer in the cathodic region is slower than in the anodic region [67], the values of peak anodic current were used for EASA and further calculations.

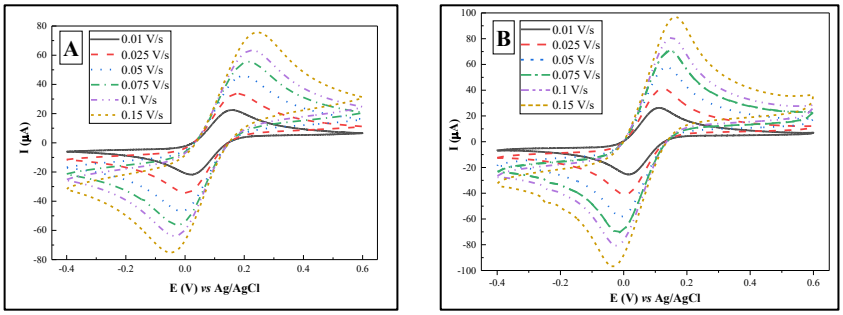

Figure 8. Cyclic voltammograms for SPCE (A) and SPCE/AuNS (B) at scan rates of 0.01, 0.025, 0.05, 0.075, 0.1 and 0.15 V/s vs. Ag/AgCl in PBS (pH 7.4), containing 2 mM $[Fe(CN_6)]^{3-/4-}$. The figure represents the average of 3 measurements.

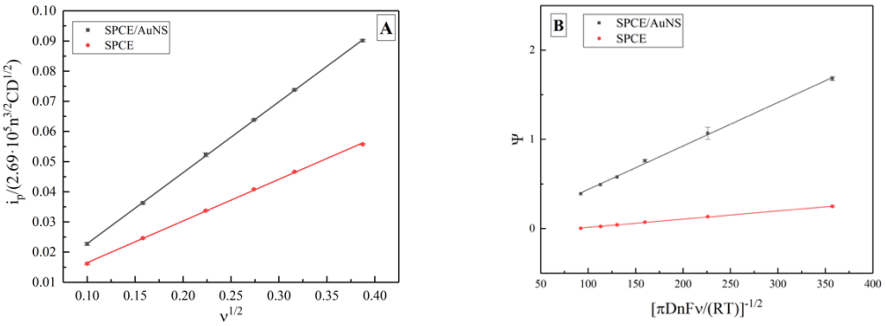

Figure 9. Plot for EASA calculation (A); plot for k_0 calculation (B). Error bars are calculated as a standard deviation (n=3).

Table 1. Calculated EASA and k_0 values for SPCE and SPCE/AuNS. Error bars are calculated as a standard deviation (n=3).

	SPCE	SPCE/AuNS
EASA·10^{-2}, cm^2	13.80±0.15	23.50±0.12
k_0·10^{-4}	9.23±0.16	48.70±0.90

The difference between the values can be explained by the increase in surface roughness (Fig. 10), thus improving the working substrate properties for subsequent immobilization of the biorecognition element.

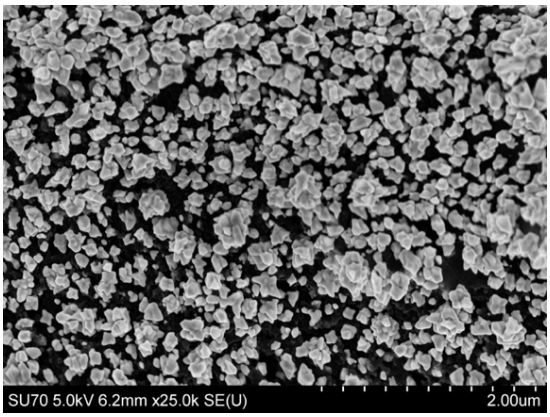

Figure 10. SEM micrograph of SPCE/AuNS.

Furthermore, k_0 was assessed by means of the improved Nicholson's approach for quasi-reversible electrochemical reactions (Eq. 13-14) (Fig. 9B), utilizing data obtained from CV at different scan rates (Fig. 8). The value for SPCE was found to be $9.23\pm0.16\cdot10^{-4}$, while for SPCE/AuNS, it was $48.70\pm0.90\cdot10^{-4}$ (Table 1). Thus, it can be concluded that the electrodeposition of AuNS contributes not only to an increase in the electrode's active area but also to the rate of heterogeneous electron transfer.

The CV and DPV measurements were performed in PBS (pH 7.4), using 2 mM $[Fe(CN_6)]^{3-/4-}$ as a redox probe to evaluate SPCE/AuNS, SPCE/AuNS/SAM, and SPCE/AuNS/SAM/rS (Fig. 11).

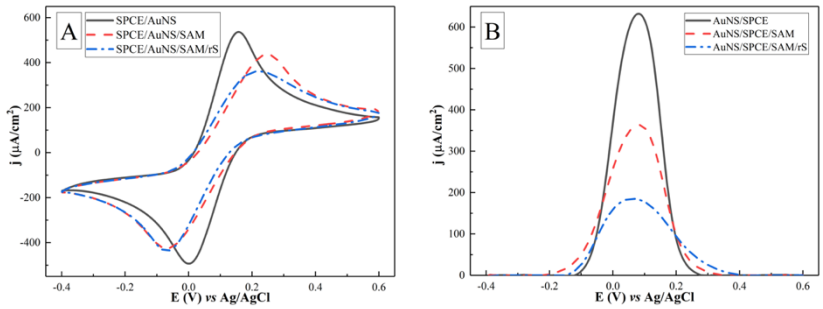

Figure 11. Cyclic voltammograms (A) and differential pulse voltammograms (B) of SPCE/AuNS (—), after SPCE/AuNS/SAM formation (- - -), and for SPCE/AuNS/SAM/rS protein immobilization (-·-). Potential range was from −0.4 to +0.6 V, with a CV scan rate of 0.05 V/s, DPV scan rate of 0.04 V/s in PBS (pH 7.4), containing 2 mM $[Fe(CN_6)]^{3-/4-}$. Signal normalized to the geometrical area of the working electrode (0.126 cm^2).

The CV analysis of SPCE/AuNS revealed voltammograms (Fig. 11A) characterized by sharp oxidative peaks, with a j_{pa} value of 536.30±0.42 μA/cm^2. Subsequent formation of SPCE/AuNS/SAM led to a decrease in j_{pa} to 436.96±0.18 μA/cm^2. CV following antigen immobilization with SPCE/AuNS/SAM/rS formation and blocking revealed a further decrease in current density to 361.83±0.28 μA/cm^2.

The DPV measurements for the aforementioned biosensing element formation stages exhibited a similar trend (Fig. 11B), with a stepwise decrease in current density: 632.53±0.83, 363.52±0.28, and 185.26±1.17 μA/cm^2 for SPCE/AuNS, SPCE/AuNS/SAM, and SPCE/AuNS/SAM/rS, respectively.

The decrease in current density observed through both CV and DPV methods can be attributed to the increasing layer thickness on the working electrode surface, hindering electron transfer. The stepwise broadening of DPV peaks may be associated with a reduced electron exchange rate.

In the CV measurements (Fig. 11A), the potential values for j_{pa} shifted within the +0.1 – +0.2 V window, possibly due to alterations in the electron transfer process and/or changes in the reference Ag/AgCl electrode, which is sensitive to experimental conditions such as the presence of Cl^- in PBS (pH 7.4), during AuNS electrodeposition. Meanwhile, DPV exhibited (Fig. 11B) relatively stable potential values, experiencing only slight changes reflecting differences in the principles of electrochemical signal recording and assessment between CV and DPV techniques.

The subsequent phase of the experiment aimed to evaluate the biosensor's capability to detect anti-rS. CV measurements (Fig. 12A) demonstrate a gradual 'flattening' of the voltammograms in the anodic region, accompanied by a decrease in j_{pa} values. This trend initiates at 361.83±0.28 μA/cm^2 for the solution containing 0 nM of anti-rS and declines to 270.04±0.63 μA/cm^2 for the solution with 3.5 nM of anti-rS (Table 2), within the potential range of +0.2 to +0.4 V. The observed 'flattening' of the voltammograms and the shifts in potential signify increasing insulation of the working surface, which further impedes electron access and alters the redox reaction potential.

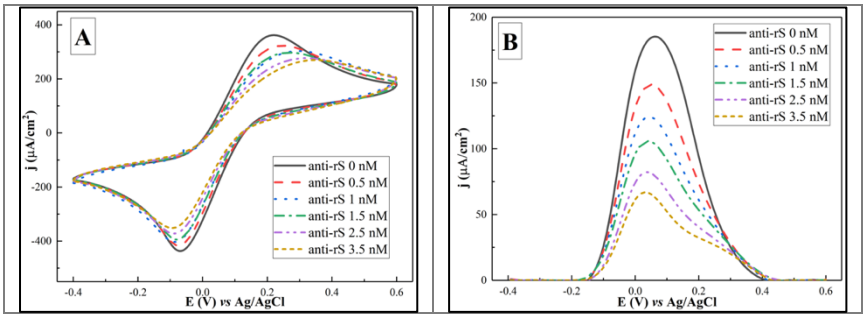

Figure 12. Cyclic voltammograms (A) and differential pulse voltammograms (B) after interaction with anti-rS antibodies of different concentrations (0–3.5 nM). Potential range was from −0.4 to +0.6 V, with a CV scan rate of 0.05 V/s, DPV scan rate of 0.04 V/s in PBS (pH 7.4), containing 2 mM $[Fe(CN_6)]^{3-/4-}$. Signal normalized to the geometrical area of the working electrode (0.126 cm^2).

Table 2. Analytical parameters obtained from CV and DPV. Errors are calculated as a standard deviation (n=3).

Anti-rS, nM	CV	DPV
	j_{pa}, μA/cm^2	j_p, μA/cm^2
0	361.83 ± 1.38	185.26 ± 1.10
0.5	323.11 ± 0.80	148.86 ± 4.60
1.0	303.18 ± 2.90	124.25 ± 3.11
1.5	297.42 ± 3.36	105.86 ± 4.63
2.5	276.91 ± 2.43	82.23 ± 1.53
3.5	270.04 ± 2.86	66.93 ± 3.90

Similarly, DPV experiments corroborate this effect (Fig. 12B), displaying a consecutive decrease in j_p, i.e., 185.26±1.17, 148.86±1.02, 124.25±0.32, 105.86±0.32, 82.23±0.59, and 66.93± 0.2 μA/cm^2 for 0, 0.5, 1.0, 1.5, 2.5, and 3.5 nM anti-rS concentrations, respectively (Table 2). Unlike CV-based experiments, the peaks in the differential pulse voltammograms for solutions with varying concentrations of anti-rS exhibit higher resolution and more consistent potential values, correlating with the applied anti-rS concentrations.

The data obtained from the electrochemical measurements were utilized to assess the LOD and LOQ (Eq. 17-18) for the developed biosensor, employing both CV and DPV methods. Calibration curves are depicted in figure 13.

It was determined that the LOD and LOQ values for the CV-based method were 0.27 nM and 0.81 nM, respectively. In contrast, calculations from DPV data yielded lower values of 0.14 nM for LOD and 0.42 nM for LOQ.

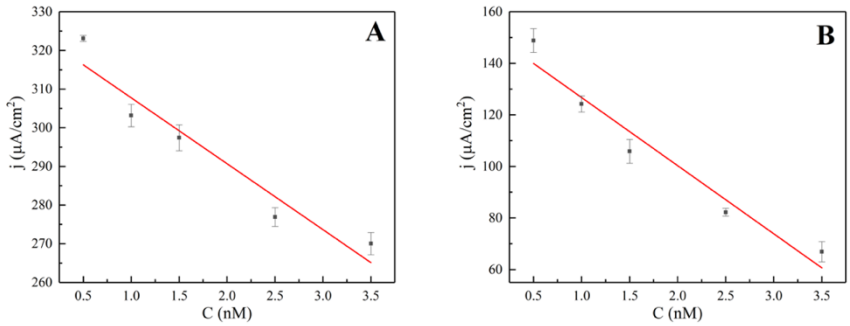

Figure 13. Calibration curves obtained from CV (A) and DPV (B) vs. anti-rS antibody concentration. Error bars are calculated as a standard deviation (n=3).

3.2. Detection of anti-rS antibodies with SPCE modified by PANI film

To achieve the formation of a conductive film atop the SPCE, a mixture of PA and aniline was employed for electropolymerization. The process was conducted at a fixed current (10 μA) while varying the ET, ranging from 1 to 20 min. The ET, selected as a variable, influences the permeability of the polymer for charge transfer, as established by previous studies [163]. This assertion was substantiated by EIS measured immediately after electropolymerization on five SPCEs with varying ET durations (Fig. 14). Notably, the stability of the PANI film doped with PA was evaluated in the previous study [158], which exhibited fluctuations of ≤2% for 7 h, following the initial stabilization period of 30 min.

As it can be seen in figure 14, with the prolonged ET, a noticeable enhancement in the prominence of the semicircles establishment observed on the Nyquist plots was visible, particularly evident from the 5-min mark onward. This observation implies that the effective formation of the PANI film on the WE of the SPCE necessitates a minimum duration of 5 min of electropolymerization.

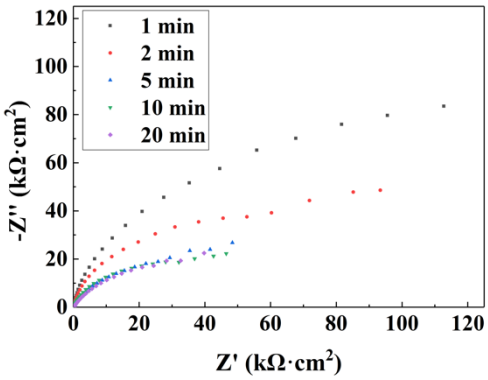

Figure 14. Nyquist plots of the SPCE modified with PANI for the electrodes with ET of polymerization from 1 to 20 min. Measurements were performed in a frequency range from 100 kHz to 0.1 Hz, at 0.01 V amplitude and applied potential 0.1 V vs. Ag/AgCl reference electrode in 0.1 M PB solution, signal normalized to the area of the electrode (0.126 cm^2).

Following the electropolymerization process, the immobilization of rS was performed on the surface of all the SPCEs, accompanied by the use of GA as a cross-linker [158]. Subsequently, EIS measurements were recorded for all five electrodes under identical conditions, serving as blank (0 nM). As depicted in figure 15, alterations in the behavior of the electrochemical system were observed with an increase in ET, evident through the emergence of clearer semicircle shapes in Nyquist plots (Fig. 15). The data obtained for ET durations of 10 and 20 min facilitated data fitting based on the assumptions of the corresponding equivalent circuit (Fig. 15D-E insets). This assumed circuit comprised *Rct*, *Rs*, and a constant phase element (*CPE)*. The *CPE* was selected for the equivalent circuit due to its ability to account for non-ideal capacitive behavior, providing a more accurate representation of the electrode impedance response, especially in the presence of irregularities or discontinuities on the electrode surface. Subsequently, the maximum values of semicircles in the Nyquist plots (Fig. 15D-E) for ET durations of 10 and 20 min were considered, yielding corresponding -Z''max values of 11.34 ± 0.23 kΩ·cm^2 and 9.59±0.22 kΩ·cm^2 (Table 3).

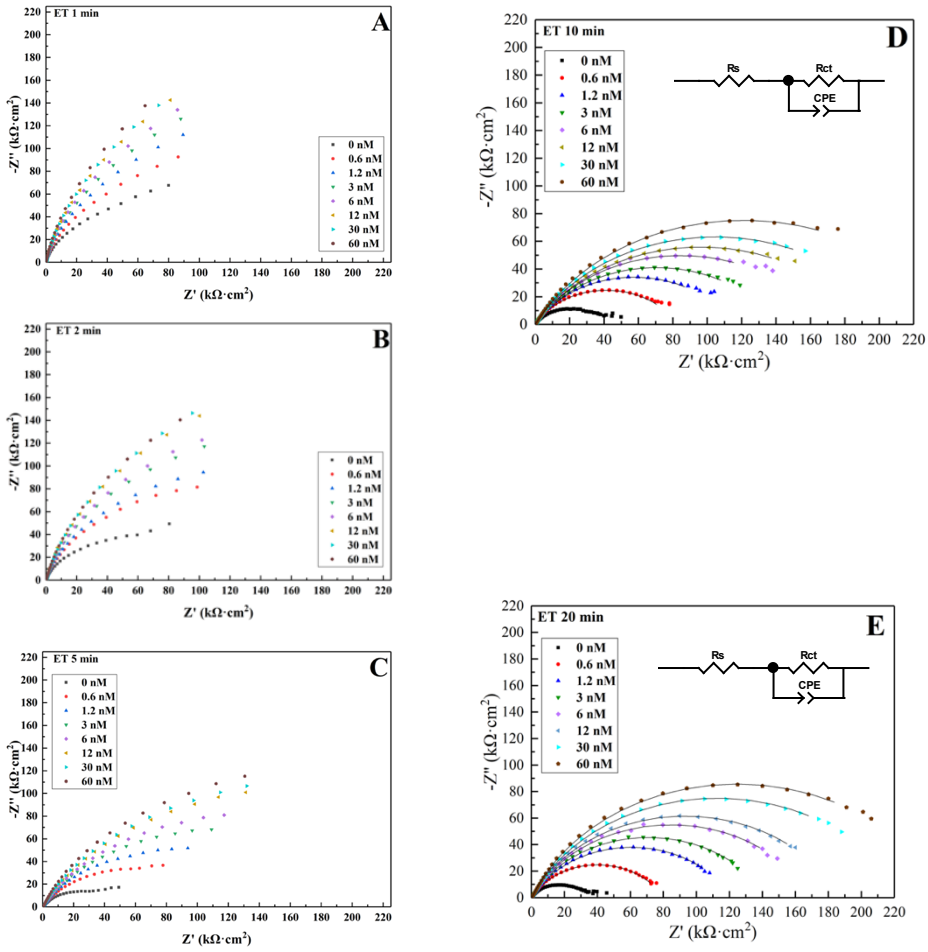

Figure 15. EIS measurements of anti-rS in the range of concentrations from 0 to 60 nM. Nyquist plots for different ET of electropolymerization: A-1 min; B-2 min; C-5 min; D-10 min; E-20 min. Measurements were performed in a frequency range from 100 kHz to 0.1 Hz, at 0.01 V amplitude and applied potential 0.1 V vs. Ag/AgCl reference in 0.1 M PB solution, signal normalized to the area of the electrode (0.126 cm^2).

Table 3. Analytical parameters were obtained from EIS values for the electrodes with ET of 10 and 20 min. Errors are calculated as a standard deviation (n=3).

Anti-rS, nM	ET 10 min	ET 20 min
	Z''max, kΩ·cm^2	Z''max, kΩ·cm^2
0	11.34±0.61	9.59±0.58
0.6	24.82±1.75	24.76±1.80
1.2	34.32±2.28	38.11±2.88
3	41.22±2.80	45.76±2.43
6	49.69±3.04	55.19±4.00
12	55.69±4.37	61.67±3.97
30	62.88±3.70	74.50±5.21
60	74.98±5.74	85.30±6.06

The subsequent step involved electrochemically registering the interaction between immobilized rS and anti-rS across a range of concentrations from 0 to 60 nM on the WE surface. Following incubation with each concentration, EIS signals were recorded (Table 3, Fig. 15).

The models indicate that akin to the blank concentration, Nyquist plots for low ET durations (1-2 min) (Fig. 15A-B) did not form complete semicircles and lacked clear resolutions for signals associated with higher concentrations (3-60 nM), thus impeding data interpretation. Nyquist plots for electrodes subjected to electropolymerization for 5 min (Fig. 15C) still exhibited incomplete semicircles, albeit with noticeable improvements in signal resolutions.

For an ET duration of 10 min, the Nyquist plot (Fig. 15D) displayed relatively well-shaped semicircles with a significant tendency of radii growth, consistent with concentration increase. The corresponding maximum values of -Z'' increased from 11.34±0.23 kΩ·cm^2 to 74.98±2.17 kΩ·cm^2 with the corresponding increase in concentrations from 0.6 to 60 nM.

Subsequently, the electrode subjected to the maximal ET duration of 20 min followed and improved upon the trend established by the electrode with an ET duration of 10 min. The Nyquist plot (Fig. 15E) exhibited quite well-resolved signals with nearly complete semicircles and significant stepwise increases in radii, with -Z''max values ranging from 24.76±0.68 kΩ·cm^2 to 85.30±2.29 kΩ·cm^2.

The clearer and more pronounced semicircles observed in the Nyquist plot with increasing concentration of applied anti-rS for SPCEs coated with PANI film formed for a longer time (10 and 20 min) compared to films formed for 1-5 min can be attributed to several reasons. First, the PANI film formed over a longer ET is expected to be thicker, resulting in more significant changes in the impedance response. This increased thickness provides a greater barrier to charge transport paths, resulting in more visible semicircles in the Nyquist plot. Moreover, longer ET allows the PANI film to be more fully formed and cross-linked, resulting in a denser and more uniform film structure. This improved polymerization increases the film's effectiveness in blocking charge transfer, further contributing to the sharper observed EIS response. In addition, longer ET may also result in a higher density of functional groups on the surface of the PANI film. These additional functional groups provide more binding sites for anti-rS. Consequently, this increased anti-rS binding results in larger impedance changes and more pronounced semicircles in the Nyquist plot.

The LOD and LOQ were calculated for the electrodes with ET from 10 to 20 min to assess and compare the analytical properties of the impedimetric systems. For this purpose, calibration curves, were plotted (Fig. 16). The lowest LOD and LOQ values of 0.42±0.01 and 1.27±0.03 nM correspondingly belonged to the biosensor designed with ET of 20 min.

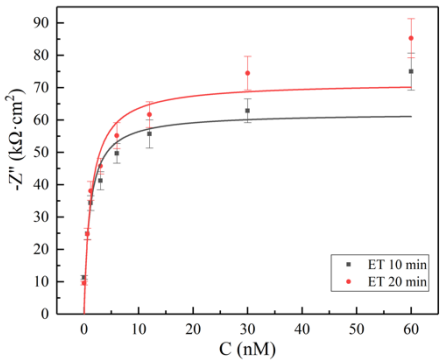

Figure 16. Calibration curves for the electrodes with ET of electropolymerization for 10 and 20 min. The concentration range is from 0 to 60 nM. Error bars are calculated as a standard deviation (n=3).

3.3. Detection of rN protein with SPCE modified by rN imprinted polypyrrole (Ppy)

A pattern was revealed in all tested MIP and NIP systems through the performed PAD measurements. An increase in rN concentration was commonly associated with a decrease in Δj signals (the increase of Normalized signal), a trend that might be linked to changes in charge transfer processes occurring at the surfaces of the working electrodes covered with the conductive Ppy layer. The binding of rN to both the Ppy-imprints and the rest of the polymer surface resulted in a significant decline in the available EASE, consequently leading to a noticeable decrease in the recorded signal.

In figure 17, PAD chronoamperograms for the detection of rN by NIP1 (Fig. 17A-B) and MIP1 (Fig. 17C-D) are displayed. For NIP1, no clear stepwise tendency in signal changes was observed with increasing rN concentration. Initially, the signal exhibited a slight increase, rising from 62.4±0.06 mA/cm^2 at 0 nM of rN to 62.7±0.06 mA/cm^2 at 0.01 nM of rN (Table 4). Subsequently, the Δj value experienced a decline, reaching 61.2±0.1 mA/cm^2 at 0.02 nM. However, it rebounded, reaching 62.3±0.06 mA/cm^2 at 0.2 nM. The values of registered Δj signals can be found in Table 4.

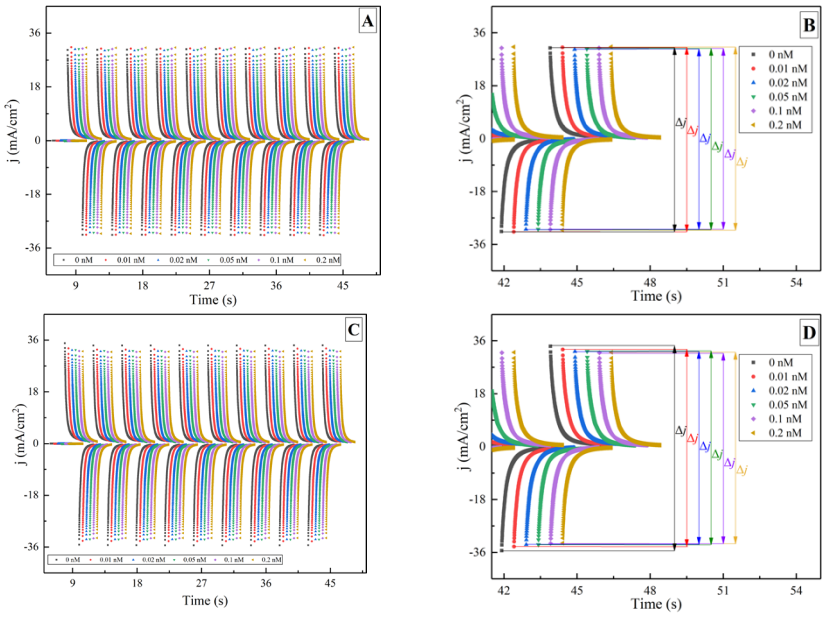

Figure 17. Chronoamperograms registered during the rN detection in the concentration range from 0 to 0.2 nM. By the NIP1: 10 potential pulses (A)

and the last three pulses (B). By the MIP1, there are 10 potential pulses (C) and the last three pulses (D). PAD: 10 potential pulses of +0.6 V vs. Ag/AgCl for 2 s, between these pulses 0 V vs. Ag/AgCl for 2 s. Measurements were performed in PBS solution (pH 7.4). The signal normalized to the geometrical area of the working electrode (0.126 cm^2).

Table 4. Experimental data were obtained from PAD for the detection of rN in the range of concentration. Errors are calculated as a standard deviation (n=3).

rN, nM	NIP1	MIP1	NIP2	MIP2	NIP3	MIP3
	Δj, mA/cm^2	Δj, mA/cm^2	Δj, mA/cm^2	Δj, mA/cm^2	Δj, mA/cm^2	Δj, mA/cm^2
0	62.4±0.06	69.5±0.06	73.3±0.06	71.9±0.01	67.5±0.1	72.2±0.1
0.01	62.7±0.06	67.0±0.06	72.4±0.06	69.9±0.01	66.9±0.06	69.7±0.01
0.02	61.2±0.1	65.6±0.06	71.5±0.06	68.4±0.01	66.4±0.01	69.5±0.01
0.05	61.3±0.01	65.8±0.06	71.5±0.01	68.0±0.06	65.5±0.01	67.6±0.06
0.1	61.8±0.06	64.9±0.01	71.2±0.01	67.8±0.06	65.0±0.01	67.3±0.10
0.2	62.3±0.06	64.9±0.01	71.2±0.01	68.3±0.01	65.2±0.01	67.6±0.01

Moreover, the character of the response can be tracked in the calibration curve plotted using normalized *Δj* vs. concentrations (Fig. 18A). The obtained correlation in figure 18A didn't follow any clear linear or exponential pattern. On the other hand, data obtained from the detection of rN with MIP1 (Fig. 17C-D) showed more significant changes in the signal response from 69.5±0.06 mA/cm^2 to 64.90±0.01 mA/cm^2 with an increase of the concentrations from 0 to 0.2 nM (Table 4, Fig. 18A). When comparing the detection of rN using NIP1 and MIP1, some assumptions can be made. In the case of NIP1, a weak non-specific interaction between the polymer surface and the analyte is observed. The observed response is related to the presence of non-specific binding sites on the polymer. As the concentration of rN increases, the signal decreases. This decrease in the signal can be explained by the non-specific binding sites becoming oversaturated.

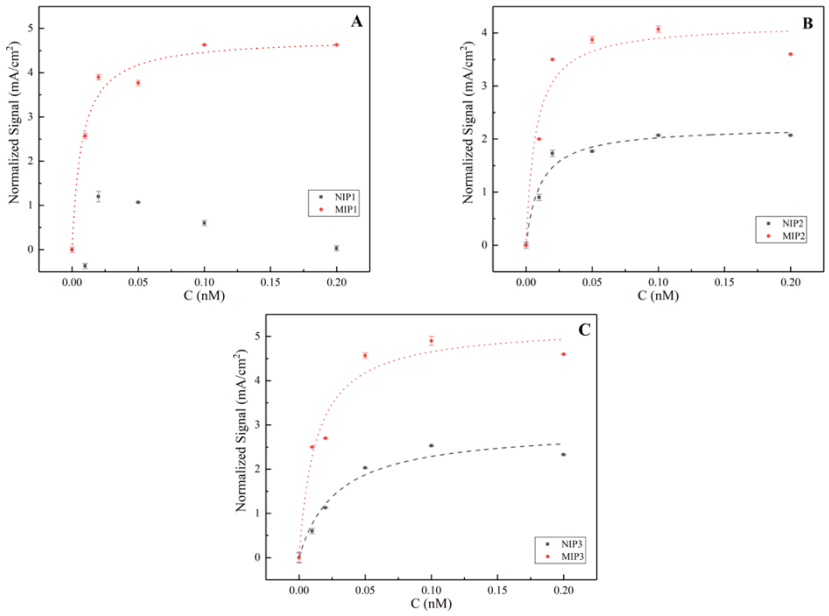

Figure 18. Calibration curves (Normalized signal vs. concentration of rN) obtained using NIP1/MIP1 (A), NIP2/MIP2 (B), and NIP3/MIP3 (C) for the detection of rN in the range of concentration from 0 to 0.2 nM. Error bars were calculated as standard deviations (n=3).

Looking at the results of the NIP2 and MIP2 measurements (Fig. 19), it is observed that both NIP2 and MIP2 show a signal change with the increasing rN concentration (Table 4). The Δj values decreased from 73.3±0.06 mA/cm^2 to 71.20±0.01 mA/cm^2 for NIP2 and from 71.90±0.01 mA/cm^2 68.3±0.01 mA/cm^2 for MIP2, correspondingly. Similar to NIP1, NIP2 also shows a tendency towards non-specific binding. However, when comparing the calibration curves of MIP2 and NIP2, a significant difference in the intensity of the responses is observed (Fig. 18B).

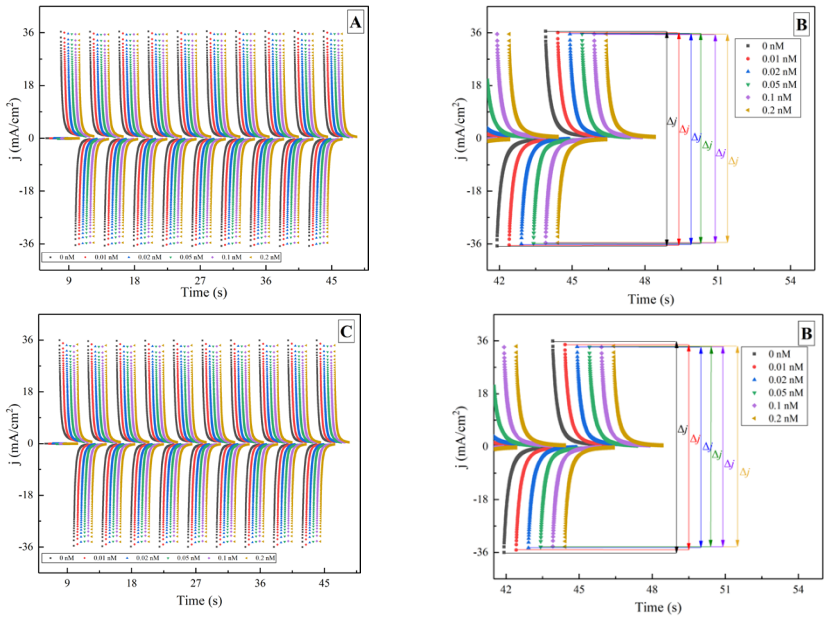

Figure 19. Chronoamperograms registered during the rN detection in the concentration range from 0 to 0.2 nM. By the NIP2: 10 potential pulses (A) and the last three pulses (B). By the MIP2, there are 10 potential pulses (C) and the last three pulses (D). PAD: 10 potential pulses of +0.6 V vs. Ag/AgCl for 2 s, between these pulses 0 V vs. Ag/AgCl for 2 s. Measurements were performed in PBS solution (pH 7.4). The signal normalized to the geometrical area of the working electrode (0.126 cm^2).

Figure 20 displays the chronoamperograms depicting the detection of rN using NIP3 and MIP3. Both systems show a noticeable stepwise change in the signal as the concentration of rN increases from 0 to 0.2 nM. Namely, by NIP3 generated signal decreased from 67.5±0.1 mA/cm^2 to 65.2±0.01 mA/cm^2 while the generated signal decreased from 72.2±0.1 mA/cm^2 to 67.6±0.01 mA/cm^2. This indicates that non-specific interactions between rN and the working surface still play a significant role, as further evidenced by the results presented in figure 18C.

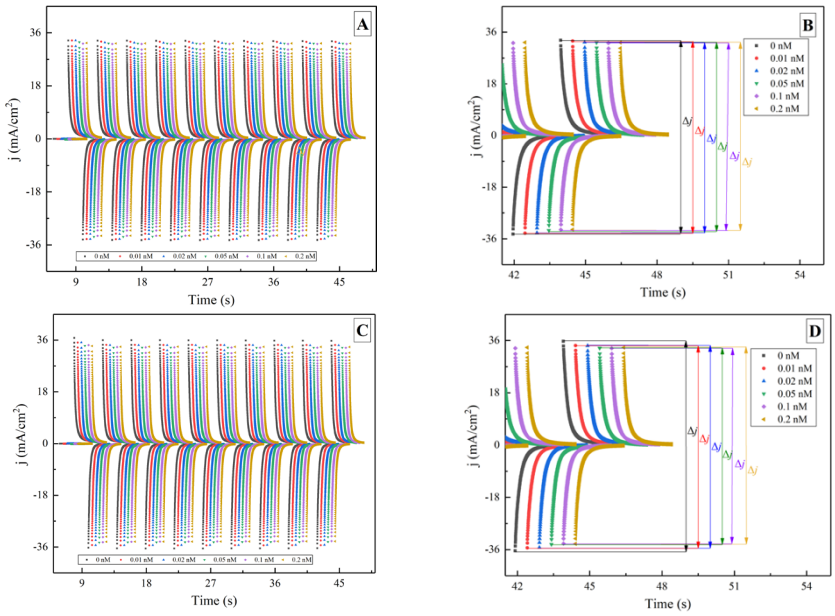

Figure 20. Chronoamperograms registered during the rN detection in the concentration range from 0 to 0.2 nM. By the NIP3: 10 potential pulses (A) and the last three pulses (B). By the MIP3, there are 10 potential pulses (C) and the last three pulses (D). PAD: 10 potential pulses of +0.6 V vs. Ag/AgCl for 2 s, between these pulses 0 V vs. Ag/AgCl for 2 s. Measurements were performed in PBS solution (pH 7.4). The signal normalized to the geometrical area of the working electrode (0.126 cm^2).

Further, biosensor performance was evaluated by the analysis of the calibration curves obtained for all three NIP and MIP systems (Fig. 18). For this purpose, the calibration curves were fitted using the Langmuir isotherm equation adapted for the MIP-based electrochemical measurements by the given equation (Eq. 19). Comparing the values of adapted Langmuir constants (K) allows assessing binding affinity, specificity, efficiency, and imprinting effect of the reported sensing systems. A higher constant value indicates stronger binding affinity, greater specificity of MIPs for the template molecule, higher adsorption capacity, and a more pronounced imprinting effect. As evidenced by the results presented in figure 18A, NIP1 did not show any clear pattern, indicating that it did not exhibit a specific dependence and could not be fitted. On the other hand, MIP1 had a K value of 135±39 nM^{-1}. When comparing NIP/MIP2 and NIP/MIP3, the K values for the non-imprinted systems were approximately 1.4 and 2 times lower, respectively, in comparison with their corresponding imprinted systems (Table 5). This

suggests that the imprinted systems had higher binding affinities. Additionally, the highest R^2 value of 0.97 belonged to MIP1, indicating a relatively good fit for the data.

Table 5. Normalized $signal_{max}$, K, R^2 values for MIPs and NIPs.

Electrode		Normalized $signal_{max}$	K, nM^{-1}	R^2
SPCE/AuNS	MIP1	4.79±0.26	135±39	0.97
	NIP1	-	-	-
SPCE/PtNS	MIP2	4.18±0.33	138±59	0.94
	NIP2	2.23±0.15	96±31	0.96
SPCE	MIP3	5.25±0.37	78±24	0.96
	NIP3	2.94±0.28	35±11	0.96

Figure 18 reveals that non-specific detection made a significant contribution in the SPCE/PtNS-based (Fig. 18B) and SPCE-based (Fig. 18C) systems, while the distinction between NIP1 and MIP1 curves was most noticeable. Considering these observations, MIP1 was selected as the more reliable and specific system for further analysis.

The LOD and LOQ (Eq. 17-18) were calculated for MIP1, resulting in LOD and LOQ values of 1.02±0.01 pM and 3.08±0.03 pM, respectively. Thus, when comparing the responses of MIP and NIP to different concentrations of rN (Fig. 18), it becomes apparent that the MIP1 system using the SPCE/AuNS (Fig. 18A) exhibited less non-specific binding compared to the SPCE/PtNS (Fig. 18B) and the unmodified SPCE (Fig. 18C). This improvement may be attributed to the electrodeposition process, wherein the surface of SPCE is coated with AuNS, resulting in increased surface coverage and a higher density of specific binding sites for the target analyte. Consequently, this reduces the availability of binding sites for non-specific interactions. Additionally, the carried-out analysis of the biosensor based on MIP1 demonstrated its potential for sensitive and specific detection of the target analyte, rN. These findings underscore the advantages of incorporating SPCE/AuNS in MIP design, offering enhanced selectivity and reliability in detecting the target molecules.

Comparative analysis shows that the biosensors reported in previous parts have lower sensitivity compared to some previously published analogs (Table 6). However, it is important to recognize that sensitivity is a multifaceted parameter that is influenced by various experimental factors. Further improvements to the experimental setup, such as optimization of

electrode configurations and assay conditions, could potentially mitigate this limitation. Additionally, performing stringent specificity tests can reveal the selectivity of a biosensor towards target analytes, thereby enhancing its overall performance and applicability.

Table 6. Some of the previously reported SPCE-based electrochemical biosensors for the detection of SARS-CoV-2-related biotargets.

SPCE modification	Sensing element	SARS-CoV-2 target	Method	Redox probe	LOD	
Nickel hydroxide nanoparticles	S-protein	Ab (antibody)	DPV	$[Fe(CN)_6]^{4-/3}$	0.3 aM	[164]
Nitrocellulose membrane	N-protein	Ab	CA		13 pM	[165]
AuNS	Ab	N-protein	SWV	$[Fe(CN)_6]^{4-/3}$	52 fM	[166]
Au/graphene	MIP	N-protein	DPV	$[Fe(CN)_6]^{4-/3}$	3.0 fM	[167]
SiO_2@UiO-66	Ab	S-protein	EIS	$[Fe(CN)_6]^{4-/3}$	18 aM	[168]
Cu_2O nanocubes	Ab	S-protein	EIS	$[Fe(CN)_6]^{4-/3}$	0.25 aM	[169]
AuNS	Aptamer	S-protein	EIS	$[Fe(CN)_6]^{4-/3}$	1.30 pM	[170]
AuNS	Ab	S-protein	EIS	$[Fe(CN)_6]^{4-/3}$	3.16 pM	[171]
Magnetic beads, AuNS	ACE2	S-protein	DPV		2 zM	[172]
-	Ab	S-protein	CA		0.9 pM	[173]
AuNS	Ab	S-protein	PAD		12.5 nM	[129]
Cu_7S_4-Au	MIP	S-protein	DPV	4-Mercaptophenylboronic acid, 3-aminophenyl boronic acid	11 fM	[174]
This work						
AuNS	S-protein	Ab	CV, DPV	$[Fe(CN)_6]^{4-/3}$	0.27 nM, 0.14 nM	
PANI	S-protein	Ab	EIS		0.42 nM	
AuNS	MIP	N-protein	PAD		1.02 pM	

In examining earlier publications within the realm of SPCE-based biosensors for COVID-19 diagnosis, the prevalent utilization of AuNS modification in conjunction with voltammetric methods emerges as a common

trend. Despite adhering to conventional construction and detection methodologies, our biosensor showcases efficacy in directly detecting antibodies against SARS-CoV-2 from real patient serum samples.

The limited utilization of conducting polymers atop SPCEs, as indicated in the revised literature (Table 6), highlights the novelty and potential of our PANI-based impedimetric biosensor. The intrinsic properties of conducting polymers confer several advantages, including the elimination of additional redox mediators and dual functionality as both substrate and mediator for immobilizing biorecognition elements. This unique feature not only simplifies the biosensing process but also enhances sensitivity and signal amplification, thereby positioning our biosensor as a frontrunner in the field.

Another promising application of conducting polymers not particularly represented in other publications lies in the construction of MIP-based detection systems, offering a cost-effective alternative to traditional sensing elements. The absence of expensive biomolecules in MIP systems not only reduces operational costs but also enhances the biosensor's stability and reproducibility. Moreover, the relatively low LOD observed in our developed biosensor underscores its sensitivity and suitability for detecting target biomolecules with precision and reliability.

The implementation of the PAD method represents a unique feature of our biosensor, further enhancing its performance and practical utility. The PAD offers a simple and sensitive approach to detection by minimizing background currents, thereby improving the signal-to-noise ratio and increasing detection limits. This method has great potential for various biosensing applications, especially in scenarios requiring rapid and accurate detection of analytes.

Although this study yielded promising results, there are opportunities for future research and optimization. Continued efforts to improve experimental protocols, explore new surface modification strategies, and integrate advanced signal processing algorithms can further improve the sensitivity, specificity, and practical applicability of our biosensor platform.

CONCLUSIONS

1. The modification of SPCE with AuNS by electrodeposition increases EASA by ~1.7 times and k^0 by ~5.3 times.

2. CV and DPV methods enable detecting antibodies against SARS-CoV-2 from real serum samples. The lowest LOD of 0.14 nM belongs to DPV.

3. SPCE modified with PANI conductive film formed in 20 min of electropolymerization enables redox mediator-free detecting of antibodies against SARS-CoV-2 from real serum samples by EIS with LOD of 0.42 nM.

4. SPCE modified with AuNS can be used as an effective platform for the deposition of molecularly imprinted polypyrrole. The SPCE pretreated with AuNS and modified with MIP enables redox mediator-free detecting of SARS-CoV-2 N-protein by PAD with LOD of 1.02 pM.

BIBLIOGRAPHY

[1] A. Turner, I. Karube, G.S. Wilson, Biosensors: fundamentals and applications, Oxford university press, 1987.

[2] R.A. Durst, A.J. Bäumner, R.W. Murray, R.P. Buck, C.P. Andrieux, Chemically modified electrodes: Recommended terminology and definitions, Pure Appl. Chem. 69 (1997) 1317–1323. https://doi.org/10.1351/pac199769061317.

[3] W. Kutner, J. Wang, M. L'her, R.P. Buck, Analytical aspects of chemically modified electrodes: Classification, critical evaluation and recommendations (IUPAC Recommendations 1998), Pure Appl. Chem. 70 (1998) 1301–1318. https://doi.org/10.1351/pac199870061301.

[4] D.R. Thévenot, K. Toth, R.A. Durst, G.S. Wilson, Electrochemical biosensors: recommended definitions and classification, Biosens. Bioelectron. 16 (2001) 121–131. https://doi.org/10.1016/S0956-5663(01)00115-4.

[5] M. Banakar, M. Hamidi, Z. Khurshid, M.S. Zafar, J. Sapkota, R. Azizian, D. Rokaya, Electrochemical Biosensors for Pathogen Detection: An Updated Review, Biosensors. 12 (2022) 927. https://doi.org/10.3390/bios12110927.

[6] M. Drobysh, A. Ramanaviciene, R. Viter, A. Ramanavicius, Affinity sensors for the diagnosis of covid-19, Micromachines. 12 (2021) 390. https://doi.org/10.3390/mi12040390.

[7] M. Drobysh, A. Ramanaviciene, R. Viter, C.-F. Chen, U. Samukaite-Bubniene, V. Ratautaite, A. Ramanavicius, Biosensors for the Determination of SARS-CoV-2 Virus and Diagnosis of COVID-19 Infection, Int. J. Mol. Sci. 23 (2022) 666. https://doi.org/10.3390/ijms23020666.

[8] F. Cui, H.S. Zhou, Diagnostic methods and potential portable biosensors for coronavirus disease 2019, Biosens. Bioelectron. 165 (2020) 112349. https://doi.org/10.1016/j.bios.2020.112349.

[9] P. Mehrotra, Biosensors and their applications - A review, J. Oral Biol. Craniofacial Res. 6 (2016) 153–159. https://doi.org/10.1016/j.jobcr.2015.12.002.

[10] H. Zheng, X. Ma, L. Chen, Z. Lin, L. Guo, B. Qiu, G. Chen, Label-free electrochemical impedance biosensor for sequence-specific recognition of double-stranded DNA, Anal. Methods. 5 (2013) 5005–5009. https://doi.org/10.1039/c3ay40972d.

[11] H. Li, X. Liu, L. Li, X. Mu, R. Genov, A.J. Mason, CMOS electrochemical instrumentation for biosensor microsystems: A review, Sensors (Switzerland). 17 (2017) 74. https://doi.org/10.3390/s17010074.

[12] S. Damiati, B. Schuster, Electrochemical biosensors based on S-layer proteins, Sensors (Switzerland). 20 (2020) 1721.

https://doi.org/10.3390/s20061721.
[13] I.H. Cho, D.H. Kim, S. Park, Electrochemical biosensors: Perspective on functional nanomaterials for on-site analysis, Biomater. Res. 24 (2020) 6. https://doi.org/10.1186/s40824-019-0181-y.
[14] R. Monošík, M. Streďanský, E. Šturdík, Biosensors - classification, characterization and new trends, Acta Chim. Slovaca. 5 (2012) 109–120. https://doi.org/10.2478/v10188-012-0017-z.
[15] J. Juan Colás, Fabrication and Experimental Techniques, Dual-Mode Electro-Photonic Silicon Biosens. (2017) 37–57. https://doi.org/10.1007/978-3-319-60501-2_3.
[16] A. j. Bard, Fundamentals and Applications Plasmonics : Fundamentals and Applications, John Wiley & Sons, 2004. http://elib.tu-darmstadt.de/tocs/95069577.pdf.
[17] A.G. Tamirat, X. Guan, J. Liu, J. Luo, Y. Xia, Redox mediators as charge agents for changing electrochemical reactions, Chem. Soc. Rev. 49 (2020) 7454–7478. https://doi.org/10.1039/d0cs00489h.
[18] D. Grieshaber, R. MacKenzie, J. Vörös, E. Reimhult, Electrochemical biosensors - Sensor principles and architectures, Sensors. 8 (2008) 1400–1458. https://doi.org/10.3390/s8031400.
[19] T.J. Smith, K.J. Stevenson, Reference electrodes, Academic Press, New York, 2007. https://doi.org/10.1016/B978-044451958-0.50005-7.
[20] R.J. Narayan, Medical Biosensors for Point of Care (POC) Applications, Woodhead Publishing, 2016. https://doi.org/10.1016/c2014-0-01459-1.
[21] D. Rotake, S. Patle, S.G. Singh, Screen-Printed Electrode (SPE)-Based Biosensor for Point-Of-Care (POC) Diagnostic in Medical Applications, Their Scope, and Challenges, in: A. Madhusudhan, S.D. Purohit, R. Prasad, A. Husen (Eds.), Springer Nature Singapore, Singapore, 2024: pp. 331–346. https://doi.org/10.1007/978-981-99-6597-7_12.
[22] M. Tudorache, C. Bala, Biosensors based on screen-printing technology, and their applications in environmental and food analysis, Anal. Bioanal. Chem. 388 (2007) 565–578. https://doi.org/10.1007/s00216-007-1293-0.
[23] M.I. González-Sánchez, B. Gómez-Monedero, J. Agrisuelas, J. Iniesta, E. Valero, Highly activated screen-printed carbon electrodes by electrochemical treatment with hydrogen peroxide, Electrochem. Commun. 91 (2018) 36–40. https://doi.org/10.1016/j.elecom.2018.05.002.
[24] R.A. Farghali, R.A. Ahmed, Gold nanoparticles-modified screen-printed carbon electrode for voltammetric determination of sildenafil citrate (Viagra) in pure form, biological and pharmaceutical formulations, Int. J. Electrochem. Sci. 10 (2015) 1494–1505. https://doi.org/10.1016/s1452-3981(23)05088-5.
[25] N.K. Chaki, K. Vijayamohanan, Self-assembled monolayers as a

tunable platform for biosensor applications, Biosens. Bioelectron. 17 (2002) 1–12. https://doi.org/10.1016/S0956-5663(01)00277-9.
[26] M. Schuier, Q. Trentin, M. Textor, S.G.P. Tosatti, Biomedical interfaces: Titanium surface technology for implants and cell carriers, Nanomedicine. 1 (2006) 449–463. https://doi.org/10.2217/17435889.1.4.449.
[27] J. Robertus, W.R. Browne, B.L. Feringa, Dynamic control over cell adhesive properties using molecular-based surface engineering strategies, Chem. Soc. Rev. 39 (2010) 354–378. https://doi.org/10.1039/b906608j.
[28] M. Mrksich, Using self-assembled monolayers to model the extracellular matrix, Acta Biomater. 5 (2009) 832–841. https://doi.org/10.1016/j.actbio.2009.01.016.
[29] J.C. Love, L.A. Estroff, J.K. Kriebel, R.G. Nuzzo, G.M. Whitesides, Self-assembled monolayers of thiolates on metals as a form of nanotechnology, Chem. Rev. 105 (2005) 1103–1169. https://doi.org/10.1021/cr0300789.
[30] T. Wink, S.J. Van Zuilen, A. Bult, W.P. Van Bennekom, Self-assembled monolayers for biosensors, Analyst. 122 (1997) 43R-50R. https://doi.org/10.1039/a606964i.
[31] S. Ramanavicius, A. Ramanavicius, Conducting polymers in the design of biosensors and biofuel cells, Polymers (Basel). 13 (2021) 1–19. https://doi.org/10.3390/polym13010049.
[32] V. Ratautaite, A. Ramanaviciene, Y. Oztekin, J. Voronovic, Z. Balevicius, L. Mikoliunaite, A. Ramanavicius, Electrochemical stability and repulsion of polypyrrole film, Colloids Surfaces A Physicochem. Eng. Asp. 418 (2013) 16–21. https://doi.org/10.1016/j.colsurfa.2012.10.052.
[33] V. Ratautaite, D. Plausinaitis, I. Baleviciute, L. Mikoliunaite, A. Ramanaviciene, A. Ramanavicius, Characterization of caffeine-imprinted polypyrrole by a quartz crystal microbalance and electrochemical impedance spectroscopy, Sensors Actuators B Chem. 212 (2015) 63–71. https://doi.org/10.1016/J.SNB.2015.01.109.
[34] M. Holguín, O.E. Rojas Álvarez, C.A. Arizabaleta, W. Torres, Molecular dynamics of the interaction of l-tryptophan with polypyrrole oligomers, Comput. Theor. Chem. 1147 (2019) 29–34. https://doi.org/10.1016/J.COMPTC.2018.11.012.
[35] V. Kumar, A. Mirzaei, M. Bonyani, K.H. Kim, H.W. Kim, S.S. Kim, Advances in electrospun nanofiber fabrication for polyaniline (PANI)-based chemoresistive sensors for gaseous ammonia, TrAC Trends Anal. Chem. 129 (2020) 115938. https://doi.org/10.1016/J.TRAC.2020.115938.
[36] T.Y. Tekbaşoğlu, T. Soganci, M. Ak, A. Koca, M.K. Şener, Enhancing biosensor properties of conducting polymers via copolymerization: Synthesis of EDOT-substituted bis(2-pyridylimino)isoindolato-

palladium complex and electrochemical sensing of glucose by its copolymerized film, Biosens. Bioelectron. 87 (2017) 81–88. https://doi.org/10.1016/j.bios.2016.08.020.
[37] A. Ramanavicius, Y. Oztekin, A. Ramanaviciene, Electrochemical formation of polypyrrole-based layer for immunosensor design, Sensors Actuators, B Chem. 197 (2014) 237–243. https://doi.org/10.1016/j.snb.2014.02.072.
[38] V. Syritski, J. Reut, A. Opik, K. Idla, Environmental QCM sensors coated with polypyrrole, Synth. Met. 102 (1999) 1326–1327. https://doi.org/10.1016/S0379-6779(98)01047-9.
[39] K. Leonavicius, A. Ramanaviciene, A. Ramanavicius, Polymerization model for hydrogen peroxide initiated synthesis of polypyrrole nanoparticles, Langmuir. 27 (2011) 10970–10976. https://doi.org/10.1021/la201962a.
[40] A. Ramanavicius, A. Kausaite, A. Ramanaviciene, Self-encapsulation of oxidases as a basic approach to tune the upper detection limit of amperometric biosensors, Analyst. 133 (2008) 1083–1089. https://doi.org/10.1039/b801501e.
[41] Y.Z. Long, M.M. Li, C. Gu, M. Wan, J.L. Duvail, Z. Liu, Z. Fan, Recent advances in synthesis, physical properties and applications of conducting polymer nanotubes and nanofibers, Prog. Polym. Sci. 36 (2011) 1415–1442. https://doi.org/10.1016/j.progpolymsci.2011.04.001.
[42] M.A. Rahman, P. Kumar, D.-S. Park, Y.-B. Shim, Electrochemical Sensors Based on Organic Conjugated Polymers, Sensors. 8 (2008) 118–141. https://doi.org/10.3390/s8010118.
[43] J.L. Bredas, G.B. Street, Polarons, Bipolarons, and Solitons in Conducting Polymers, Acc. Chem. Res. 18 (1985) 309–315. https://doi.org/10.1021/ar00118a005.
[44] Y. Oztekin, A. Ramanaviciene, Z. Yazicigil, A.O. Solak, A. Ramanavicius, Direct electron transfer from glucose oxidase immobilized on polyphenanthroline-modified glassy carbon electrode, Biosens. Bioelectron. 26 (2011) 2541–2546. https://doi.org/10.1016/j.bios.2010.11.001.
[45] V. Ratautaite, S.N. Topkaya, L. Mikoliunaite, M. Ozsoz, Y. Oztekin, A. Ramanaviciene, A. Ramanavicius, Molecularly Imprinted Polypyrrole for DNA Determination, Electroanalysis. 25 (2013) 1169–1177. https://doi.org/10.1002/elan.201300063.
[46] D. Plausinaitis, L. Sinkevicius, U. Samukaite-Bubniene, V. Ratautaite, A. Ramanavicius, Evaluation of electrochemical quartz crystal microbalance based sensor modified by uric acid-imprinted polypyrrole, Talanta. 220 (2020). https://doi.org/10.1016/j.talanta.2020.121414.
[47] N.G. Gurudatt, S. Chung, J.M. Kim, M.H. Kim, D.K. Jung, J.Y. Han, Y.B. Shim, Separation detection of different circulating tumor cells in

the blood using an electrochemical microfluidic channel modified with a lipid-bonded conducting polymer, Biosens. Bioelectron. 146 (2019) 111746. https://doi.org/10.1016/J.BIOS.2019.111746.
[48] P. Rattanarat, A. Suea-Ngam, N. Ruecha, W. Siangproh, C.S. Henry, M. Srisa-Art, O. Chailapakul, Graphene-polyaniline modified electrochemical droplet-based microfluidic sensor for high-throughput determination of 4-aminophenol, Anal. Chim. Acta. 925 (2016) 51–60. https://doi.org/10.1016/J.ACA.2016.03.010.
[49] G. Zhang, Y. Yu, M. Guo, B. Lin, L. Zhang, A sensitive determination of albumin in urine by molecularly imprinted electrochemical biosensor based on dual-signal strategy, Sensors Actuators B Chem. 288 (2019) 564–570. https://doi.org/10.1016/J.SNB.2019.03.042.
[50] A. Tretjakov, V. Syritski, J. Reut, R. Boroznjak, O. Volobujeva, A. Öpik, Surface molecularly imprinted polydopamine films for recognition of immunoglobulin G, Microchim. Acta. 180 (2013) 1433–1442. https://doi.org/10.1007/s00604-013-1039-y.
[51] A. Menaker, V. Syritski, J. Reut, A. Öpik, V. Horváth, R.E. Gyurcsányi, Electrosynthesized Surface-Imprinted Conducting Polymer Microrods for Selective Protein Recognition, Adv. Mater. 21 (2009) 2271–2275. https://doi.org/10.1002/adma.200803597.
[52] L. Ye, K. Mosbach, Molecularly imprinted microspheres as antibody binding mimics, React. Funct. Polym. 48 (2001) 149–157. https://doi.org/10.1016/S1381-5148(01)00050-5.
[53] M. Peeters, S. Kobben, K.L. Jiménez-Monroy, L. Modesto, M. Kraus, T. Vandenryt, A. Gaulke, B. Van Grinsven, S. Ingebrandt, T. Junkers, P. Wagner, Thermal detection of histamine with a graphene oxide based molecularly imprinted polymer platform prepared by reversible addition–fragmentation chain transfer polymerization, Sensors Actuators B Chem. 203 (2014) 527–535. https://doi.org/10.1016/J.SNB.2014.07.013.
[54] X. Zhang, Y. Peng, J. Bai, B. Ning, S. Sun, X. Hong, Y. Liu, Y. Liu, Z. Gao, A novel electrochemical sensor based on electropolymerized molecularly imprinted polymer and gold nanomaterials amplification for estradiol detection, Sensors Actuators B Chem. 200 (2014) 69–75. https://doi.org/10.1016/J.SNB.2014.04.028.
[55] A.T. Lawal, Progress in utilisation of graphene for electrochemical biosensors, Biosens. Bioelectron. 106 (2018) 149–178. https://doi.org/10.1016/j.bios.2018.01.030.
[56] A. Nazare, K. Pal, S. Maji, Electrochemical biosensors, Food, Medical, Environ. Appl. Polysaccharides. 39 (2020) 403–441. https://doi.org/10.1016/B978-0-12-819239-9.00011-7.
[57] A.J. Bard, L.R. Faulkner, H.S. White, Electrochemical methods: fundamentals and applications, John Wiley & Sons, 2022.
[58] P.N. Bartlett, Bioelectrochemistry: Fundamentals, Experimental Techniques and Applications, John Wiley & Sons, 2008.

https://doi.org/10.1002/9780470753842.
[59] B. Eggins, Chemical Sensors and Biosensors, John Wiley & Sons, 2007. https://doi.org/10.1002/9780470511305.
[60] T.M. Nahir, R.P. Buck, Modified Cottrell behavior in thin layers: Applied voltage steps under diffusion control for constant-resistance systems, J. Electroanal. Chem. 341 (1992) 1–14. https://doi.org/10.1016/0022-0728(92)80471-F.
[61] H.B. Halsall, W.R. Heineman, Electrochemical immunoassay: An ultrasensitive method, J. Int. Fed. Clin. Chem. 2 (1990) 179–87. http://www.ncbi.nlm.nih.gov/pubmed/10148952.
[62] V. Ratautaite, R. Boguzaite, E. Brazys, D. Plausinaitis, S. Ramanavicius, U. Samukaite-Bubniene, M. Bechelany, A. Ramanavicius, Evaluation of the interaction between SARS-CoV-2 spike glycoproteins and the molecularly imprinted polypyrrole, Talanta. 253 (2023) 123981. https://doi.org/10.1016/j.talanta.2022.123981.
[63] A. Ramanaviciene, A. Ramanavicius, Molecularly imprinted polypyrrole-based synthetic receptor for direct detection of bovine leukemia virus glycoproteins, Biosens. Bioelectron. 20 (2004) 1076–1082. https://doi.org/10.1016/j.bios.2004.05.014.
[64] I.I. Suni, Impedance methods for electrochemical sensors using nanomaterials, TrAC - Trends Anal. Chem. 27 (2008) 604–611. https://doi.org/10.1016/j.trac.2008.03.012.
[65] N.J. Ronkainen, H.B. Halsall, W.R. Heineman, Electrochemical biosensors, Chem. Soc. Rev. 39 (2010) 1747–1763. https://doi.org/10.1039/b714449k.
[66] A. Ramanavicius, A. Finkelsteinas, H. Cesiulis, A. Ramanaviciene, Electrochemical impedance spectroscopy of polypyrrole based electrochemical immunosensor, Bioelectrochemistry. 79 (2010) 11–16. https://doi.org/10.1016/j.bioelechem.2009.09.013.
[67] V. Liustrovaite, M. Drobysh, A. Rucinskiene, A. Baradoke, A. Ramanaviciene, I. Plikusiene, U. Samukaite-Bubniene, R. Viter, C.-F. Chen, A. Ramanavicius, Towards an Electrochemical Immunosensor for the Detection of Antibodies against SARS-CoV-2 Spike Protein, J. Electrochem. Soc. 169 (2022) 037523. https://doi.org/10.1149/1945-7111/ac5d91.
[68] V. Pinkova Gajdosova, L. Lorencova, A. Blsakova, P. Kasak, T. Bertok, J. Tkac, Challenges for impedimetric affinity sensors targeting protein detection, Curr. Opin. Electrochem. 28 (2021) 100717. https://doi.org/10.1016/j.coelec.2021.100717.
[69] F. Patolsky, M. Zayats, E. Katz, I. Willner, Precipitation of an insoluble product on enzyme monolayer electrodes for biosensor applications: Characterization by Faradaic impedance spectroscopy, cyclic voltammetry, and microgravimetric quartz crystal microbalance analyses, Anal. Chem. 71 (1999) 3171–3180.

https://doi.org/10.1021/ac9901541.
[70] R. Pei, Z. Cheng, E. Wang, X. Yang, Amplification of antigen-antibody interactions based on biotin labeled protein-streptavidin network complex using impedance spectroscopy, Biosens. Bioelectron. 16 (2001) 355–361. https://doi.org/10.1016/S0956-5663(01)00150-6.
[71] E. Katz, I. Willner, Probing biomolecular interactions at conductive and semiconductive surfaces by impedance spectroscopy: Routes to impedimetric immunosensors, DNA-sensors, and enzyme biosensors, Electroanalysis. 15 (2003) 913–947. https://doi.org/10.1002/elan.200390114.
[72] B.W. Neuman, B.D. Adair, C. Yoshioka, J.D. Quispe, G. Orca, P. Kuhn, R.A. Milligan, M. Yeager, M.J. Buchmeier, Supramolecular Architecture of Severe Acute Respiratory Syndrome Coronavirus Revealed by Electron Cryomicroscopy, J. Virol. 80 (2006) 7918–7928. https://doi.org/10.1128/jvi.00645-06.
[73] M. Bárcena, G.T. Oostergetel, W. Bartelink, F.G.A. Faas, A. Verkleij, P.J.M. Rottier, A.J. Koster, B.J. Bosch, Cryo-electron tomography of mouse hepatitis virus: Insights into the structure of the coronavirion, Proc. Natl. Acad. Sci. U. S. A. 106 (2009) 582–587. https://doi.org/10.1073/pnas.0805270106.
[74] L.L. Ren, Y.M. Wang, Z.Q. Wu, Z.C. Xiang, L. Guo, T. Xu, Y.Z. Jiang, Y. Xiong, Y.J. Li, X.W. Li, H. Li, G.H. Fan, X.Y. Gu, Y. Xiao, H. Gao, J.Y. Xu, F. Yang, X.M. Wang, C. Wu, L. Chen, Y.W. Liu, B. Liu, J. Yang, X.R. Wang, J. Dong, L. Li, C.L. Huang, J.P. Zhao, Y. Hu, Z.S. Cheng, L.L. Liu, Z.H. Qian, C. Qin, Q. Jin, B. Cao, J.W. Wang, Identification of a novel coronavirus causing severe pneumonia in human: a descriptive study, Chin. Med. J. (Engl). 133 (2020) 1015–1024. https://doi.org/10.1097/CM9.0000000000000722.
[75] Y.A. Malik, Properties of coronavirus and SARS-CoV-2, Malays. J. Pathol. 42 (2020) 3–11.
[76] H.C. Song, M.-Y. Seo, K. Stadler, B.J. Yoo, Q.-L. Choo, S.R. Coates, Y. Uematsu, T. Harada, C.E. Greer, J.M. Polo, P. Pileri, M. Eickmann, R. Rappuoli, S. Abrignani, M. Houghton, J.H. Han, Synthesis and Characterization of a Native, Oligomeric Form of Recombinant Severe Acute Respiratory Syndrome Coronavirus Spike Glycoprotein, J. Virol. 78 (2004) 10328–10335. https://doi.org/10.1128/jvi.78.19.10328-10335.2004.
[77] R.N. Kirchdoerfer, C.A. Cottrell, N. Wang, J. Pallesen, H.M. Yassine, H.L. Turner, K.S. Corbett, B.S. Graham, J.S. McLellan, A.B. Ward, Pre-fusion structure of a human coronavirus spike protein, Nature. 531 (2016) 118–121. https://doi.org/10.1038/nature17200.
[78] S. Liu, G. Xiao, Y. Chen, Y. He, J. Niu, C.R. Escalante, H. Xiong, J. Farmar, A.K. Debnath, P. Tien, S. Jiang, Interaction between heptad repeat 1 and 2 regions in spike protein of SARS-associated coronavirus: implications for virus fusogenic mechanism and

identification of fusion inhibitors, Lancet. 363 (2004) 938–947. https://doi.org/10.1016/S0140-6736(04)15788-7.
[79] F. Li, W. Li, M. Farzan, S.C. Harrison, Structure of SARS Coronavirus Spike Receptor-Binding Domain Complexed with Receptor, Science (80-.). 309 (2005) 1864 LP – 1868. https://doi.org/10.1126/science.1116480.
[80] G. Lu, Y. Hu, Q. Wang, J. Qi, F. Gao, Y. Li, Y. Zhang, W. Zhang, Y. Yuan, J. Bao, B. Zhang, Y. Shi, J. Yan, G.F. Gao, Molecular basis of binding between novel human coronavirus MERS-CoV and its receptor CD26, Nature. 500 (2013) 227–231. https://doi.org/10.1038/nature12328.
[81] A.C. Walls, Y.J. Park, M.A. Tortorici, A. Wall, A.T. McGuire, D. Veesler, Structure, Function, and Antigenicity of the SARS-CoV-2 Spike Glycoprotein, Cell. 181 (2020) 281–292. https://doi.org/10.1016/j.cell.2020.02.058.
[82] J.L. Nieto-Torres, M.L. DeDiego, E. Álvarez, J.M. Jiménez-Guardeño, J.A. Regla-Nava, M. Llorente, L. Kremer, S. Shuo, L. Enjuanes, Subcellular location and topology of severe acute respiratory syndrome coronavirus envelope protein, Virology. 415 (2011) 69–82. https://doi.org/10.1016/j.virol.2011.03.029.
[83] P. Venkatagopalan, S.M. Daskalova, L.A. Lopez, K.A. Dolezal, B.G. Hogue, Coronavirus envelope (E) protein remains at the site of assembly, Virology. 478 (2015) 75–85. https://doi.org/10.1016/j.virol.2015.02.005.
[84] C.A.M. de Haan, P.J.M. Rottier, Molecular Interactions in the Assembly of Coronaviruses, Adv. Virus Res. 64 (2005) 165–230. https://doi.org/10.1016/S0065-3527(05)64006-7.
[85] C.K. Chang, S.C. Sue, T.H. Yu, C.M. Hsieh, C.K. Tsai, Y.C. Chiang, S.J. Lee, H.H. Hsiao, W.J. Wu, W.L. Chang, C.H. Lin, T.H. Huang, Modular organization of SARS coronavirus nucleocapsid protein, J. Biomed. Sci. 13 (2006) 59–72. https://doi.org/10.1007/s11373-005-9035-9.
[86] Y. Peng, N. Du, Y. Lei, S. Dorje, J. Qi, T. Luo, G.F. Gao, H. Song, Structures of the SARS -CoV-2 nucleocapsid and their perspectives for drug design, EMBO J. 39 (2020). https://doi.org/10.15252/embj.2020105938.
[87] B.W. Neuman, G. Kiss, A.H. Kunding, D. Bhella, M.F. Baksh, S. Connelly, B. Droese, J.P. Klaus, S. Makino, S.G. Sawicki, S.G. Siddell, D.G. Stamou, I.A. Wilson, P. Kuhn, M.J. Buchmeier, A structural analysis of M protein in coronavirus assembly and morphology, J. Struct. Biol. 174 (2011) 11–22. https://doi.org/10.1016/j.jsb.2010.11.021.
[88] A.R. Fehr, S. Perlman, Coronaviruses: An overview of their replication and pathogenesis, in: Coronaviruses Methods Protoc., 2015: pp. 1–23. https://doi.org/10.1007/978-1-4939-2438-7_1.

[89] D. Escors, J. Ortego, H. Laude, L. Enjuanes, The Membrane M Protein Carboxy Terminus Binds to Transmissible Gastroenteritis Coronavirus Core and Contributes to Core Stability, J. Virol. 75 (2001) 1312–1324. https://doi.org/10.1128/jvi.75.3.1312-1324.2001.

[90] H. Vennema, G.J. Godeke, J.W.A. Rossen, W.F. Voorhout, M.C. Horzinek, D.J.E. Opstelten, P.J.M. Rottier, Nucleocapsid-independent assembly of coronavirus-like particles by co-expression of viral envelope protein genes, EMBO J. 15 (1996) 2020–2028. https://doi.org/10.1002/j.1460-2075.1996.tb00553.x.

[91] W. Chen, Y. Lan, X. Yuan, X. Deng, Y. Li, X. Cai, L. Li, R. He, Y. Tan, X. Deng, M. Gao, G. Tang, L. Zhao, J. Wang, Q. Fan, C. Wen, Y. Tong, Y. Tang, F. Hu, F. Li, X. Tang, Detectable 2019-nCoV viral RNA in blood is a strong indicator for the further clinical severity, Emerg. Microbes Infect. 9 (2020) 469–473. https://doi.org/10.1080/22221751.2020.1732837.

[92] H. Zhang, Z. Kang, H. Gong, D. Xu, J. Wang, Z. Li, X. Cui, J. Xiao, T. Meng, W. Zhou, J. Liu, H. Xu, The digestive system is a potential route of 2019-nCov infection: a bioinformatics analysis based on single-cell transcriptomes, BioRxiv. (2020) 2020.01.30.927806. https://doi.org/10.1101/2020.01.30.927806.

[93] X. Chai, L. Hu, Y. Zhang, W. Han, Z. Lu, A. Ke, J. Zhou, G. Shi, N. Fang, J. Fan, J. Cai, J. Fan, F. Lan, Specific ACE2 Expression in Cholangiocytes May Cause Liver Damage After 2019-nCoV Infection, BioRxiv. (2020) 2020.02.03.931766. https://doi.org/10.1101/2020.02.03.931766.

[94] X. Zou, K. Chen, J. Zou, P. Han, J. Hao, Z. Han, Single-cell RNA-seq data analysis on the receptor ACE2 expression reveals the potential risk of different human organs vulnerable to 2019-nCoV infection, Front. Med. 14 (2020) 185–192. https://doi.org/10.1007/s11684-020-0754-0.

[95] J. Tooze, S. Tooze, G. Warren, Replication of coronavirus MHV-A59 in sac- cells: determination of the first site of budding of progeny virions, Eur. J. Cell Biol. 33 (1984) 281–293.

[96] J. Krijnse-Locker, M. Ericsson, P.J.M. Rottier, G. Griffiths, Characterization of the budding compartment of mouse hepatitis virus: Evidence that transport from the RER to the Golgi complex requires only one vesicular transport step, J. Cell Biol. 124 (1994) 55–70. https://doi.org/10.1083/jcb.124.1.55.

[97] G. Li, Y. Fan, Y. Lai, T. Han, Z. Li, P. Zhou, P. Pan, W. Wang, D. Hu, X. Liu, Q. Zhang, J. Wu, Coronavirus infections and immune responses, J. Med. Virol. 92 (2020) 424–432. https://doi.org/10.1002/jmv.25685.

[98] X. Li, M. Geng, Y. Peng, L. Meng, S. Lu, Molecular immune pathogenesis and diagnosis of COVID-19, J. Pharm. Anal. 10 (2020) 102–108. https://doi.org/10.1016/j.jpha.2020.03.001.

[99] N. Post, D. Eddy, C. Huntley, M.C.I. van Schalkwyk, M. Shrotri, D.

Leeman, S. Rigby, S. V Williams, W.H. Bermingham, P. Kellam, J. Maher, A.M. Shields, G. Amirthalingam, S.J. Peacock, S.A. Ismail, Antibody response to SARS-CoV-2 infection in humans: A systematic review, PLoS One. 15 (2020) e0244126. https://doi.org/10.1371/journal.pone.0244126.

[100] B. Isho, K.T. Abe, M. Zuo, A.J. Jamal, B. Rathod, J.H. Wang, Z. Li, G. Chao, O.L. Rojas, Y.M. Bang, A. Pu, N. Christie-Holmes, C. Gervais, D. Ceccarelli, P. Samavarchi-Tehrani, F. Guvenc, P. Budylowski, A. Li, A. Paterson, F.Y. Yue, L.M. Marin, L. Caldwell, J.L. Wrana, K. Colwill, F. Sicheri, S. Mubareka, S.D. Gray-Owen, S.J. Drews, W.L. Siqueira, M. Barrios-Rodiles, M. Ostrowski, J.M. Rini, Y. Durocher, A.J. McGeer, J.L. Gommerman, A.-C. Gingras, Persistence of serum and saliva antibody responses to SARS-CoV-2 spike antigens in COVID-19 patients, Sci. Immunol. 5 (2020) eabe5511. https://doi.org/10.1126/sciimmunol.abe5511.

[101] N.D. Pecora, M.S. Zand, Measuring the Serologic Response to Severe Acute Respiratory Syndrome Coronavirus 2: Methods and Meaning, Clin. Lab. Med. 40 (2020) 603–614. https://doi.org/10.1016/j.cll.2020.08.014.

[102] A.S. Lauring, E.B. Hodcroft, Genetic Variants of SARS-CoV-2—What Do They Mean?, JAMA. 325 (2021) 529. https://doi.org/10.1001/jama.2020.27124.

[103] X. Li, M. Xiong, Q. Deng, X. Guo, Y. Li, The utility of SARS-CoV-2 nucleocapsid protein in laboratory diagnosis, J. Clin. Lab. Anal. 36 (2022) e24534. https://doi.org/10.1002/jcla.24534.

[104] M.C. Smithgall, M. Dowlatshahi, S.L. Spitalnik, E.A. Hod, A.J. Rai, Types of Assays for SARS-CoV-2 Testing: A Review, Lab. Med. 51 (2020) e59–e65. https://doi.org/10.1093/labmed/lmaa039.

[105] S. Pfefferle, S. Reucher, D. Nörz, M. Lütgehetmann, Evaluation of a quantitative RT-PCR assay for the detection of the emerging coronavirus SARS-CoV-2 using a high throughput system, Eurosurveillance. 25 (2020). https://doi.org/10.2807/1560-7917.ES.2020.25.9.2000152.

[106] P. Khan, L.M. Aufdembrink, A.E. Engelhart, Isothermal SARS-CoV-2 diagnostics: Tools for enabling distributed pandemic testing as a means of supporting safe reopenings, ACS Synth. Biol. 9 (2020) 2861–2880. https://doi.org/10.1021/acssynbio.0c00359.

[107] T. Notomi, H. Okayama, H. Masubuchi, T. Yonekawa, K. Watanabe, N. Amino, T. Hase, Loop-mediated isothermal amplification of DNA., Nucleic Acids Res. 28 (2000). https://doi.org/10.1093/nar/28.12.e63.

[108] Y.H. Baek, J. Um, K.J.C. Antigua, J.H. Park, Y. Kim, S. Oh, Y. il Kim, W.S. Choi, S.G. Kim, J.H. Jeong, B.S. Chin, H.D.G. Nicolas, J.Y. Ahn, K.S. Shin, Y.K. Choi, J.S. Park, M.S. Song, Development of a reverse transcription-loop-mediated isothermal amplification as a rapid early-detection method for novel SARS-CoV-2, Emerg. Microbes Infect. 9

(2020) 998–1007. https://doi.org/10.1080/22221751.2020.1756698.
[109] O. Piepenburg, C.H. Williams, D.L. Stemple, N.A. Armes, DNA detection using recombination proteins, PLoS Biol. 4 (2006) 1115–1121. https://doi.org/10.1371/journal.pbio.0040204.
[110] Y.L. Lau, I. binti Ismail, N.I. binti Mustapa, M.Y. Lai, T.S.T. Soh, A.H. Hassan, K.M. Peariasamy, Y.L. Lee, M.K.B.A. Kahar, J. Chong, P.P. Goh, Development of a reverse transcription recombinase polymerase amplification assay for rapid and direct visual detection of Severe Acute Respiratory Syndrome Coronavirus 2 (SARS-CoV-2), PLoS One. 16 (2021) 2–9. https://doi.org/10.1371/journal.pone.0245164.
[111] J.S. Gootenberg, O.O. Abudayyeh, M.J. Kellner, J. Joung, J.J. Collins, F. Zhang, Multiplexed and portable nucleic acid detection platform with Cas13, Cas12a and Csm6, Science (80-.). 360 (2018) 439–444. https://doi.org/10.1126/science.aaq0179.
[112] J.P. Broughton, X. Deng, G. Yu, C.L. Fasching, V. Servellita, J. Singh, X. Miao, J.A. Streithorst, A. Granados, A. Sotomayor-Gonzalez, K. Zorn, A. Gopez, E. Hsu, W. Gu, S. Miller, C.Y. Pan, H. Guevara, D.A. Wadford, J.S. Chen, C.Y. Chiu, CRISPR–Cas12-based detection of SARS-CoV-2, Nat. Biotechnol. 38 (2020) 870–874. https://doi.org/10.1038/s41587-020-0513-4.
[113] J.P. Broughton, X. Deng, G. Yu, C.L. Fasching, J. Singh, J. Streithorst, A. Granados, A. Sotomayor-Gonzalez, K. Zorn, A. Gopez, E. Hsu, W. Gu, S. Miller, C.-Y. Pan, H. Guevara, D.A. Wadford, J.S. Chen, C.Y. Chiu, Rapid Detection of 2019 Novel Coronavirus SARS-CoV-2 Using a CRISPR-based DETECTR Lateral Flow Assay., MedRxiv Prepr. Serv. Heal. Sci. (2020) 1–28. https://doi.org/10.1101/2020.03.06.20032334.
[114] J. Joung, A. Ladha, M. Saito, M. Segel, R. Bruneau, M.W. Huang, N.-G. Kim, X. Yu, J. Li, B.D. Walker, A.L. Greninger, K.R. Jerome, J.S. Gootenberg, O.O. Abudayyeh, F. Zhang, Point-of-care testing for COVID-19 using SHERLOCK diagnostics, MedRxiv. (2020) 2020.05.04.20091231. https://doi.org/10.1101/2020.05.04.20091231.
[115] J. Dronina, U.S. Bubniene, A. Ramanavicius, The application of DNA polymerases and Cas9 as representative of DNA-modifying enzymes group in DNA sensor design (review), Biosens. Bioelectron. 175 (2021) 112867. https://doi.org/10.1016/j.bios.2020.112867.
[116] Z. Li, Y. Yi, X. Luo, N. Xiong, Y. Liu, S. Li, R. Sun, Y. Wang, B. Hu, W. Chen, Y. Zhang, J. Wang, B. Huang, Y. Lin, J. Yang, W. Cai, X. Wang, J. Cheng, Z. Chen, K. Sun, W. Pan, Z. Zhan, L. Chen, F. Ye, Development and clinical application of a rapid IgM-IgG combined antibody test for SARS-CoV-2 infection diagnosis, J. Med. Virol. 92 (2020) 1518–1524. https://doi.org/10.1002/jmv.25727.
[117] F. Xiang, X. Wang, X. He, Z. Peng, B. Yang, J. Zhang, Q. Zhou, H. Ye, Y. Ma, H. Li, X. Wei, P. Cai, W.L. Ma, Antibody Detection and Dynamic Characteristics in Patients with Coronavirus Disease 2019,

Clin. Infect. Dis. 71 (2020) 1930–1934. https://doi.org/10.1093/cid/ciaa461.
[118] D. Lin, L. Liu, M. Zhang, Y. Hu, Q. Yang, J. Guo, Y. Dai, Y. Xu, Y. Cai, X. Chen, K. Huang, Z. Zhang, Evaluations of serological test in the diagnosis of 2019 novel coronavirus (SARS-CoV-2) infections during the COVID-19 outbreak, Eur. J. Clin. Microbiol. Infect. Dis. (2020) 2020.03.27.20045153. https://doi.org/10.1101/2020.03.27.20045153.
[119] A. Scohy, A. Anantharajah, M. Bodéus, B. Kabamba-Mukadi, A. Verroken, H. Rodriguez-Villalobos, Low performance of rapid antigen detection test as frontline testing for COVID-19 diagnosis, J. Clin. Virol. 129 (2020) 104455. https://doi.org/10.1016/j.jcv.2020.104455.
[120] F.M. Liotti, G. Menchinelli, E. Lalle, I. Palucci, S. Marchetti, F. Colavita, M. La Sorda, G. Sberna, L. Bordi, M. Sanguinetti, P. Cattani, M.R. Capobianchi, B. Posteraro, Performance of a novel diagnostic assay for rapid SARS-CoV-2 antigen detection in nasopharynx samples, Clin. Microbiol. Infect. 27 (2021) 487–488. https://doi.org/10.1016/j.cmi.2020.09.030.
[121] B.D. Grant, C.E. Anderson, J.R. Williford, L.F. Alonzo, V.A. Glukhova, D.S. Boyle, B.H. Weigl, K.P. Nichols, SARS-CoV-2 Coronavirus Nucleocapsid Antigen-Detecting Half-Strip Lateral Flow Assay Toward the Development of Point of Care Tests Using Commercially Available Reagents, Anal. Chem. 92 (2020) 11305–11309. https://doi.org/10.1021/acs.analchem.0c01975.
[122] L. Porte, P. Legarraga, V. Vollrath, X. Aguilera, J.M. Munita, R. Araos, G. Pizarro, P. Vial, M. Iruretagoyena, S. Dittrich, T. Weitzel, Evaluation of a novel antigen-based rapid detection test for the diagnosis of SARS-CoV-2 in respiratory samples, Int. J. Infect. Dis. 99 (2020) 328–333. https://doi.org/10.1016/j.ijid.2020.05.098.
[123] Y. Hirotsu, M. Maejima, M. Shibusawa, Y. Nagakubo, K. Hosaka, K. Amemiya, H. Sueki, M. Hayakawa, H. Mochizuki, T. Tsutsui, Y. Kakizaki, Y. Miyashita, S. Yagi, S. Kojima, M. Omata, Comparison of automated SARS-CoV-2 antigen test for COVID-19 infection with quantitative RT-PCR using 313 nasopharyngeal swabs, including from seven serially followed patients, Int. J. Infect. Dis. 99 (2020) 397–402. https://doi.org/10.1016/j.ijid.2020.08.029.
[124] S.A. Hashemi, S. Bahrani, S.M. Mousavi, N. Omidifar, N.G.G. Behbahan, M. Arjmand, S. Ramakrishna, K.B. Lankarani, M. Moghadami, M. Firoozsani, Graphene-Based Femtogram-Level Sensitive Molecularly Imprinted Polymer of SARS-CoV-2, Adv. Mater. Interfaces. 8 (2021) 2101466. https://doi.org/10.1002/admi.202101466.
[125] Z.S. Miripour, R. Sarrami-Forooshani, H. Sanati, J. Makarem, M.S. Taheri, F. Shojaeian, A.H. Eskafi, F. Abbasvandi, N. Namdar, H. Ghafari, P. Aghaee, A. Zandi, M. Faramarzpour, M. Hoseinyazdi, M. Tayebi, M. Abdolahad, Real-time diagnosis of reactive oxygen species

(ROS) in fresh sputum by electrochemical tracing; correlation between COVID-19 and viral-induced ROS in lung/respiratory epithelium during this pandemic, Biosens. Bioelectron. 165 (2020) 112435. https://doi.org/10.1016/j.bios.2020.112435.

[126] W. Sukjee, A. Thitithanyanont, S. Manopwisedjaroen, S. Seetaha, C. Thepparit, C. Sangma, Virus MIP-composites for SARS-CoV-2 detection in the aquatic environment, Mater. Lett. 315 (2022) 131973. https://doi.org/10.1016/j.matlet.2022.131973.

[127] M. Drobysh, V. Liustrovaite, A. Baradoke, A. Rucinskiene, A. Ramanaviciene, V. Ratautaite, R. Viter, C.-F. Chen, I. Plikusiene, U. Samukaite-Bubniene, R. Slibinskas, E. Ciplys, M. Simanavicius, A. Zvirbliene, I. Kucinskaite-Kodze, A. Ramanavicius, Electrochemical Determination of Interaction between SARS-CoV-2 Spike Protein and Specific Antibodies, Int. J. Mol. Sci. 23 (2022) 6768. https://doi.org/10.3390/ijms23126768.

[128] H. Ghaedamini, K. Khalaf, D.S. Kim, Y. Tang, A novel ACE2-Based electrochemical biosensor for sensitive detection of SARS-CoV-2, Anal. Biochem. 689 (2024) 115504. https://doi.org/10.1016/j.ab.2024.115504.

[129] M. Drobysh, V. Liustrovaite, Y. Kanetski, B. Brasiunas, A. Zvirbliene, A. Rimkute, D. Gudas, I. Kucinskaite-Kodze, M. Simanavicius, S. Ramanavicius, R. Slibinskas, E. Ciplys, I. Plikusiene, A. Ramanavicius, Electrochemical biosensing based comparative study of monoclonal antibodies against SARS-CoV-2 nucleocapsid protein, Sci. Total Environ. 908 (2024) 168154. https://doi.org/10.1016/j.scitotenv.2023.168154.

[130] A.G. Ayankojo, R. Boroznjak, J. Reut, A. Öpik, V. Syritski, Molecularly imprinted polymer based electrochemical sensor for quantitative detection of SARS-CoV-2 spike protein, Sensors Actuators B Chem. 353 (2022) 131160. https://doi.org/10.1016/j.snb.2021.131160.

[131] A. Yakoh, U. Pimpitak, S. Rengpipat, N. Hirankarn, O. Chailapakul, S. Chaiyo, Paper-based electrochemical biosensor for diagnosing COVID-19: Detection of SARS-CoV-2 antibodies and antigen, Biosens. Bioelectron. 176 (2021) 112912. https://doi.org/10.1016/j.bios.2020.112912.

[132] S. Eissa, M. Zourob, Development of a low-cost cotton-tipped electrochemical immunosensor for the detection of SARS-CoV-2, Anal. Chem. 93 (2021) 1826–1833. https://doi.org/10.1021/acs.analchem.0c04719.

[133] V. Liustrovaite, M. Drobysh, V. Ratautaite, A. Ramanaviciene, A. Rimkute, M. Simanavicius, I. Dalgediene, I. Kucinskaite-Kodze, I. Plikusiene, C.F. Chen, R. Viter, A. Ramanavicius, Electrochemical biosensor for the evaluation of monoclonal antibodies targeting the N protein of SARS-CoV-2 virus, Sci. Total Environ. 924 (2024) 171042.

https://doi.org/10.1016/j.scitotenv.2024.171042.
[134] D.S. Rocha, T.A. Baldo, H.A. Silva-Neto, G.F. Duarte-Junior, G.S. Bazílio, C.L. Borges, J.A. Parente-Rocha, W.R. de Araujo, A. de Siervo, T.L.R.C. Paixão, W.K.T. Coltro, Disposable and eco-friendly electrochemical immunosensor for rapid detection of SARS-CoV-2, Talanta. 268 (2024) 125337. https://doi.org/10.1016/j.talanta.2023.125337.
[135] H. Yousefi, A. Mahmud, D. Chang, J. Das, S. Gomis, J.B. Chen, H. Wang, T. Been, L. Yip, E. Coomes, Z. Li, S. Mubareka, A. Mcgeer, N. Christie, S. Gray-Owen, A. Cochrane, J.M. Rini, E.H. Sargent, S.O. Kelley, Detection of SARS-CoV-2 Viral Particles Using Direct, Reagent-Free Electrochemical Sensing, J. Am. Chem. Soc. 143 (2021) 1722–1727. https://doi.org/10.1021/jacs.0c10810.
[136] B.S. Vadlamani, T. Uppal, S.C. Verma, M. Misra, Functionalized TiO2 nanotube-based electrochemical biosensor for rapid detection of SARS-CoV-2, Sensors (Switzerland). 20 (2020) 1–10. https://doi.org/10.3390/s20205871.
[137] S.A. Ali, H. Ayalew, B. Gautam, B. Selvaraj, J.W. She, J.A. Janardhanan, H.H. Yu, Detection of SARS-CoV-2 Spike Protein Using Micropatterned 3D Poly(3,4-Ethylenedioxythiophene) Nanorods Decorated with Gold Nanoparticles, ACS Appl. Mater. Interfaces. (2023). https://doi.org/10.1021/acsami.3c12366.
[138] A. Baradoke, A. Jarusaitis, V. Reinikovaite, A. Jafarov, A. Elsakova, M. Franckevicius, M. Skapas, R. Slibinskas, M. Drobysh, V. Liustrovaite, A. Ramanavicius, Detection of antibodies against SARS-CoV-2 Spike protein by screen-printed carbon electrodes modified by colloidal gold nanoparticles, Talanta. 268 (2024) 125279. https://doi.org/10.1016/j.talanta.2023.125279.
[139] Z. Fan, B. Yao, Y. Ding, J. Zhao, M. Xie, K. Zhang, Entropy-driven amplified electrochemiluminescence biosensor for RdRp gene of SARS-CoV-2 detection with self-assembled DNA tetrahedron scaffolds, Biosens. Bioelectron. 178 (2021) 113015. https://doi.org/10.1016/j.bios.2021.113015.
[140] M.A. Ali, C. Hu, S. Jahan, B. Yuan, M.S. Saleh, E. Ju, S.J. Gao, R. Panat, Sensing of COVID-19 Antibodies in Seconds via Aerosol Jet Nanoprinted Reduced-Graphene-Oxide-Coated 3D Electrodes, Adv. Mater. 33 (2021) 2006647. https://doi.org/10.1002/adma.202006647.
[141] H.A. Hussein, A. Kandeil, M. Gomaa, R. Mohamed El Nashar, I.M. El-Sherbiny, R.Y.A. Hassan, SARS-CoV-2-Impedimetric Biosensor: Virus-Imprinted Chips for Early and Rapid Diagnosis, ACS Sensors. 6 (2021) 4098–4107. https://doi.org/10.1021/acssensors.1c01614.
[142] M. Amouzadeh Tabrizi, J.P. Fernández-Blázquez, D.M. Medina, P. Acedo, An ultrasensitive molecularly imprinted polymer-based electrochemical sensor for the determination of SARS-CoV-2-RBD by using macroporous gold screen-printed electrode, Biosens. Bioelectron. 196 (2022) 113729.

https://doi.org/10.1016/j.bios.2021.113729.
[143] A.A. Khorshed, O. Savchenko, J. Liu, L. Shoute, J. Zeng, S. Ren, J. Gu, N. Jha, Z. Yang, J. Wang, L. Jin, J. Chen, Development of an impedance-based biosensor for determination of IgG galactosylation levels, Biosens. Bioelectron. 245 (2024) 115793. https://doi.org/10.1016/j.bios.2023.115793.
[144] H. Zhao, F. Liu, W. Xie, T.-C. Zhou, J. OuYang, L. Jin, H. Li, C.-Y. Zhao, L. Zhang, J. Wei, Y.-P. Zhang, C.-P. Li, Ultrasensitive supersandwich-type electrochemical sensor for SARS-CoV-2 from the infected COVID-19 patients using a smartphone, Sensors Actuators B Chem. 327 (2021) 128899. https://doi.org/10.1016/j.snb.2020.128899.
[145] A. Raziq, A. Kidakova, R. Boroznjak, J. Reut, A. Öpik, V. Syritski, Development of a portable MIP-based electrochemical sensor for detection of SARS-CoV-2 antigen, Biosens. Bioelectron. 178 (2021) 113029. https://doi.org/10.1016/j.bios.2021.113029.
[146] V. Vásquez, J. Orozco, PCR- and label-free SARS-CoV-2 electrochemical immunosensor, Microchem. J. 193 (2023) 109121. https://doi.org/10.1016/j.microc.2023.109121.
[147] Q. Gao, Y. Li, X. Li, H. Wang, L. Tian, H. Gong, C. Ma, C. Shi, Ultrafast Electrochemical Sensor Based on Electrical Potential-Assisted Hybridization for Non-Amplification Determination of Severe Acute Respiratory Syndrome Coronavirus 2 (SARS-CoV-2) by Differential Pulse Voltammetry (DPV), Anal. Lett. (2023) 1–16. https://doi.org/10.1080/00032719.2023.2279242.
[148] V. Ratautaite, R. Boguzaite, E. Brazys, A. Ramanaviciene, E. Ciplys, M. Juozapaitis, R. Slibinskas, M. Bechelany, A. Ramanavicius, Molecularly imprinted polypyrrole based sensor for the detection of SARS-CoV-2 spike glycoprotein, Electrochim. Acta. 403 (2022) 139581. https://doi.org/10.1016/j.electacta.2021.139581.
[149] G. Pilvenyte, V. Ratautaite, R. Boguzaite, U. Samukaite-Bubniene, D. Plausinaitis, A. Ramanaviciene, M. Bechelany, A. Ramanavicius, Molecularly imprinted polymers for the recognition of biomarkers of certain neurodegenerative diseases, J. Pharm. Biomed. Anal. 228 (2023) 115343. https://doi.org/10.1016/j.jpba.2023.115343.
[150] T. Chaibun, J. Puenpa, T. Ngamdee, N. Boonapatcharoen, P. Athamanolap, A.P. O'Mullane, S. Vongpunsawad, Y. Poovorawan, S.Y. Lee, B. Lertanantawong, Rapid electrochemical detection of coronavirus SARS-CoV-2, Nat. Commun. 12 (2021) 1–10. https://doi.org/10.1038/s41467-021-21121-7.
[151] M. Alafeef, K. Dighe, P. Moitra, D. Pan, Rapid, Ultrasensitive, and Quantitative Detection of SARS-CoV-2 Using Antisense Oligonucleotides Directed Electrochemical Biosensor Chip, ACS Nano. 14 (2020) 17028–17045. https://doi.org/10.1021/acsnano.0c06392.
[152] F. Gerstl, M. Loessl, V. Borggraefe, A.J. Baeumner, Multiplexed electrochemical liposomes applied to the detection of nucleic acids for

Influenza A, Influenza B and SARS-CoV-2, Anal. Bioanal. Chem. (2024) 1–14. https://doi.org/10.1007/s00216-024-05145-8.
[153] D. Wrapp, N. Wang, K.S. Corbett, J.A. Goldsmith, C.L. Hsieh, O. Abiona, B.S. Graham, J.S. McLellan, Cryo-EM structure of the 2019-nCoV spike in the prefusion conformation, Science (80-.). 367 (2020) 1260–1263. https://doi.org/10.1126/science.aax0902.
[154] NIBSC, 20/136. First WHO International Standard for anti-SARS-CoV-2 immunoglobulin (human), (2020). https://www.nibsc.org/documents/ifu/20-136.pdf.
[155] Immundiagnostik AG., IDK anti-SARS-CoV-2 IgG ELISA (manual), (2021). https://www.immundiagnostik.com/media/pages/testkits/k-5004/e859ef5a82-1642471281/k5004_2021-08-10_idk_sars-cov-2-igg.pdf.
[156] D.J. Dietzen, Amino acids, peptides, and proteins, in: N. Rifai, A.R. Horvath, C.T.B.T.-P. and A. of M.D. Wittwer (Eds.), Princ. Appl. Mol. Diagnostics, Elsevier, 2018: pp. 345–380. https://doi.org/10.1016/B978-0-12-816061-9.00013-8.
[157] Metrohm, Screen-Printed Carbon Electrodes, (n.d.). https://www.dropsens.com/en/pdfs_productos/new_brochures/110-11l-c110-c11l.pdf.
[158] A. Baradoke, R. Hein, X. Li, J.J. Davis, Reagentless Redox Capacitive Assaying of C-Reactive Protein at a Polyaniline Interface, Anal. Chem. 92 (2020) 3508–3511. https://doi.org/10.1021/acs.analchem.9b05633.
[159] R.S. Nicholson, Theory and Application of Cyclic Voltammetry for Measurement of Electrode Reaction Kinetics, Anal. Chem. 37 (1965) 1351–1355. https://doi.org/10.1021/ac60230a016.
[160] I. Lavagnini, R. Antiochia, F. Magno, An extended method for the practical evaluation of the standard rate constant from cyclic voltammetric data, Electroanalysis. 16 (2004) 505–506. https://doi.org/10.1002/elan.200302851.
[161] Jyoti, C. Gonzato, T. Żołek, D. Maciejewska, A. Kutner, F. Merlier, K. Haupt, P.S. Sharma, K.R. Noworyta, W. Kutner, Molecularly imprinted polymer nanoparticles-based electrochemical chemosensors for selective determination of cilostazol and its pharmacologically active primary metabolite in human plasma, Biosens. Bioelectron. 193 (2021) 113542. https://doi.org/10.1016/j.bios.2021.113542.
[162] I.S. Park, K.S. Lee, D.S. Jung, H.Y. Park, Y.E. Sung, Electrocatalytic activity of carbon-supported Pt-Au nanoparticles for methanol electro-oxidation, Electrochim. Acta. 52 (2007) 5599–5605. https://doi.org/10.1016/j.electacta.2006.12.068.
[163] J. Wang, S.P. Chen, M.S. Lin, Use of different electropolymerization conditions for controlling the size-exclusion selectivity at polyaniline, polypyrrole and polyphenol films, J. Electroanal. Chem. 273 (1989) 231–242. https://doi.org/10.1016/0022-0728(89)87016-0.
[164] Z. Rahmati, M. Roushani, H. Hosseini, H. Choobin, An

electrochemical immunosensor using SARS-CoV-2 spike protein-nickel hydroxide nanoparticles bio-conjugate modified SPCE for ultrasensitive detection of SARS-CoV-2 antibodies, Microchem. J. 170 (2021) 106718. https://doi.org/10.1016/j.microc.2021.106718.

[165] I.C. Samper, A. Sánchez-Cano, W. Khamcharoen, I. Jang, W. Siangproh, E. Baldrich, B.J. Geiss, D.S. Dandy, C.S. Henry, Electrochemical Capillary-Flow Immunoassay for Detecting Anti-SARS-CoV-2 Nucleocapsid Protein Antibodies at the Point of Care, ACS Sensors. 6 (2021) 4067–4075. https://doi.org/10.1021/acssensors.1c01527.

[166] R. Zeng, M. Qiu, Q. Wan, Z. Huang, X. Liu, D. Tang, D. Knopp, Smartphone-Based Electrochemical Immunoassay for Point-of-Care Detection of SARS-CoV-2 Nucleocapsid Protein, Anal. Chem. 94 (2022) 15155–15161. https://doi.org/10.1021/acs.analchem.2c03606.

[167] T. Zhang, L. Sun, Y. Zhang, Highly sensitive electrochemical determination of the SARS-COV-2 antigen based on a gold/graphene imprinted poly-arginine sensor, Anal. Methods. 13 (2021) 5772–5776. https://doi.org/10.1039/d1ay01478a.

[168] M. Mehmandoust, Z.P. Gumus, M. Soylak, N. Erk, Electrochemical immunosensor for rapid and highly sensitive detection of SARS-CoV-2 antigen in the nasal sample, Talanta. 240 (2022) 123211. https://doi.org/10.1016/j.talanta.2022.123211.

[169] Z. Rahmati, M. Roushani, H. Hosseini, H. Choobin, Electrochemical immunosensor with Cu2O nanocube coating for detection of SARS-CoV-2 spike protein, Microchim. Acta. 188 (2021) 105. https://doi.org/10.1007/s00604-021-04762-9.

[170] J.C. Abrego-Martinez, M. Jafari, S. Chergui, C. Pavel, D. Che, M. Siaj, Aptamer-based electrochemical biosensor for rapid detection of SARS-CoV-2: Nanoscale electrode-aptamer-SARS-CoV-2 imaging by photo-induced force microscopy, Biosens. Bioelectron. 195 (2022) 113595. https://doi.org/10.1016/j.bios.2021.113595.

[171] L.C. Brazaca, A.H. Imamura, N.O. Gomes, M.B. Almeida, D.T. Scheidt, P.A. Raymundo-Pereira, O.N. Oliveira, B.C. Janegitz, S.A.S. Machado, E. Carrilho, Electrochemical immunosensors using electrodeposited gold nanostructures for detecting the S proteins from SARS-CoV and SARS-CoV-2, Anal. Bioanal. Chem. 414 (2022) 5507–5517. https://doi.org/10.1007/s00216-022-03956-1.

[172] E.D. Nascimento, W.T. Fonseca, T.R. de Oliveira, C.R.S.T.B. de Correia, V.M. Faça, B.P. de Morais, V.C. Silvestrini, H. Pott-Junior, F.R. Teixeira, R.C. Faria, COVID-19 diagnosis by SARS-CoV-2 Spike protein detection in saliva using an ultrasensitive magneto-assay based on disposable electrochemical sensor, Sensors Actuators B Chem. 353 (2022) 131128. https://doi.org/10.1016/j.snb.2021.131128.

[173] J. Li, R. Lin, Y. Yang, R. Zhao, S. Song, Y. Zhou, J. Shi, L. Wang, H. Song, R. Hao, Multichannel Immunosensor Platform for the Rapid

Detection of SARS-CoV-2 and Influenza A(H1N1) Virus, ACS Appl. Mater. Interfaces. 13 (2021) 22262–22270. https://doi.org/10.1021/acsami.1c05770.

[174] Z.Z. Yin, Z. Liu, M. Zhou, X. Yang, G. Zheng, H. Zhang, Y. Kong, A surface molecularly imprinted electrochemical biosensor for the detection of SARS-CoV-2 spike protein by using Cu7S4-Au as built-in probe, Bioelectrochemistry. 152 (2023) 108462. https://doi.org/10.1016/j.bioelechem.2023.108462.

SANTRAUKA

Įvadas

Cheminiai jutikliai yra neatsiejama daugelio mokslinių ir pramoninių įrenginių dalis, kurie atlieka svarbų vaidmenį paverčiant cheminę informaciją atitinkamais analiziniais signalais. Šie prietaisai, sudaryti iš cheminio jutiklio sistemos ir fizikinio-cheminio keitiklio yra plačiai naudojami įvairiose technologijų srityse. Ypač svarbus šių analiznių sistemų pogrupis yra biologiniai jutikliai, kuriuose yra naudojami biocheminiai analičių atpažinimo mechanizmai [1]. Biologiniais jutikliais matuojamos biocheminiuose procesuose dalyvaujančių medžiagų koncentracijos,. Elektrocheminiose biologiniuose jutikliuose naudojami elektrocheminiai signalo vertekliai. Šiuose jutikliuose dažniausia naudojami biomolekulėmis modifikuoti elektrodai, kurie papildomai gali būti padengti elektrai laidžiais polimerais, puslaidininkinėmis medžiagomis arba įvairiomis jonams laidžiomis membranomis [2,3]. Biologiniai receptoriai, įskaitant audinius, ląsteles, fermentus, antikūnus ir kitas atpažinimo savybėmis pasižyminčias medžiagas, yraimobilizuojami ant keitiklių paviršiaus, taikant įvairius imobilizavimo metodus. Dažniausiai naudojamosdaugiasluoksnės lipidinės membranos, polimerinės matricos, savitvarkiai monosluoksniai (SAM), bifunkcinės medžiagos bei kovalentinio imobilizavimo metodai [4]. Biologiniai jutikliai taip pat yra pagal biologinio specifiškumo mechanizmus, kurie gali būti biokataliziniai arba afinininiai. Pavyzdžiui, afininino jutiklio elemento veikimas gali būti grįstas specifinės antikūnų ir antigenų tarpusavio sąveikos registravimu arba molekulių įspaudais modifikuotų polimerų (MIP) sąveikos su įspaustomis analitės molekulėmis registravimu.

Pastaraisiais metais sparčiai kuriami elektrocheminiai biologiniai jutikliai, skirti įvairiems patogenams aptikti [5]. Ši tendencija ypač išryškėjo kilus COVID-19 pandemijai, kurios metu greitos ir tikslios diagnostikos poreikis paskatino intensyvų biologinių jutiklių technologijų vystymąsį. COVID-19 diagnozei skirti biologiniai jutikliai buvo kuriami ir tirami, daug dėmesio buvo skiriama jų signalo vertiklių tobulinimui, biologinio atpažinimo komponentų paieškai ir elektrocheminių metodikų vystymui [6,7]. SARS-CoV-2 viruso komponentams aptikti ir COVID-19 diagnozuoti yra taikomos trys pagrindinės metodikų kryptys: ą (1) molekulinia tyrimai, kuriais nustatoma viruso RNR, (2) antigenų tyrimai, kuriais nustatomi viruso baltymai, ir (3) antikūnų tyrimai, kuriais nustatomi specifiniai antikūnai prieš viruso baltymus. Pirmieji du metodai leidžia nustatyti infekciją organizme, o trečiasis metodas igalina imuninės būklės įvertinimą ligos metu, po pasveikimo ar vakcinacijos [6,7]. Elektrocheminiai biologiniai jutikliai gali

būti taikomi visoms šioms strategijoms, suteikdami daug privalumų, tokių kaip nustatymo greitumas, paprastumas, ekonomiškumas ir mobilumas diagnozuojant COVID-19[8].

Pagrindinis tikslas

Ištirti biologinių jutiklių kūrimo strategijųtaikymą su SARS-CoV-2 viruso infekcija susijusių biologinių molekulių elektrocheminiam aptikimui. Konkretus tikslas – pasirinkti tinkamiausius metodus, atsižvelgiant į analitės aptikimo greitį ir jautrumą, taip pat į papildomų redokso žymių taikymo aspektus.

Uždaviniai

1. Įvertinti biologinių jutiklių kūrimo strategijų, naudojant SAM, laidžius polimerus ir MIP, efektyvumą COVID-19 diagnostikai

2. Nustatyti ciklinės voltamperometrijos (CV), diferencinės impulsinės voltamperometrijos (DPV), elektrocheminės impedanso spektroskopijos (EIS) ir impulsinės amperometrinės detekcijos (PAD) pritaikomumą su SARS-CoV-2 viruso infekcija susijusioms biomolekulėms nustatyti.

3. Įvertinti SARS-CoV-2 smaigalio (S), nukleokapsidės (N) baltymų ir antikūnų prieš šiuos baltymus tinkamumą taikymui elektrocheminiuose biologiniuose jutikliuose.

4. Pasirinkti perspektyviausią COVID-19 diagnostikos metodą įvertinant analitės aptikimo greitį ir jautrumą, taip pat būtinumą naudoti papildomus redoks žymenis.

Ginamieji teiginiai

1. Spausdinto montažo būdu pagaminto anglies elektrodo (angl.: screen printed electrode (SPCE)) modifikavimas aukso nanostruktūromis (AuNS) padidina elektrochemiškai aktyvaus paviršiaus plotą (EASA) darbiniame elektrode ir heterogeninio elektronų perdavimo greičio konstantą (k0).

2. SPCE elektrodas, modifikuotas savitvarkiais monosluoksniais, taikant ciklinės voltamperometrijos (CV) ir diferencinės pulsinės voltamperoemtrijos (DPV) metodus gali būti naudojamas antikūnams prieš SARS-CoV-2 viruso baltymus realiuose serumo mėginiuose aptikti, nustatytos šių antikūnų aptikimo ribos (LOD) yra atitinkamai 0,27 ir 0,14 nM.

3. SPCE elektrodą, modifikuotą polianilino (PANI) plėvele, taikant elektrocheminio impedanso spektroskopijos (EIS) metodu galima naudoti antikūnams prieš SARS-CoV-2 viruso baltymus realiuose serumo mėginiuose aptikti, nustatyta šių antikūnų aptikimo riba(LOD) yra 0,42 nM.

4. SPCE elektrodas, padengtas molekulių įspaudais modifikuotu polipirolu, gali būti naudojamas SARS-CoV-2 viruso N baltymui aptikti, nustatyta šių antikūnų aptikimo riba (LOD) yra 1,02 pM.

5. SPCE elektrodas modifikuotas AuNS ir MIP sluoksniu pasižymi mažesniu nespecifinio surišimo įtakotu signalu palyginus su nemodifikuotais SPCE elektrodais, bei SPCE elektrodais modifikuotais platinos nanostruktūromis (PtNS).

Darbo naujumas ir aktualumas

PANI sluoksniu modifikuotas SPCE elektrodas buvo naudojamas antikūnams prieš SARS-CoV-2 realiuose serumo mėginiuose aptikti taikant EIS metodą. Vienkartinio, kompaktiško ir nebrangaus SPCE padengto PANI sluoksniu įgalina išvengti papildomų redoks tarpininkų taikymo. Todėl tokie elektrodai tinka vertinti imuninę būklę pasveikus po COVID-19 arba po atitinkamo skiepijimo.

SPCE elektrodas, padengtas polipirolo (Ppy) modifikuoto molekulinias įspaudais sluoksniu, buvo pritaikytas SARS-CoV-2 N-baltymui aptikti PAD metodu. Darbinio SPCE elektrodo, PAD metodo ir MIP technologijos derinys pirmą kartą buvo panaudotas SARS-CoV-2 N-baltymui aptikti ir įgalino ne tik išvengti papildomų redoks tarpininkų taikymo , bet ir iki minimumo sumažinti santykinai brangių biomolekulių (specifinių antikūnų) naudojimą jutiklių biologinio atpažinimo sistemose. Sukurtą biojutiklių sistemą galima naudoti SARS-CoV-2 N-baltymų aptikimui.

Metodika

SARS-CoV-2 baltymų paruošimas: buvo įsigyti ir paruošti rekombinantiniai SARS-CoV-2 smaigalio ir nukleokapsidės (rN) baltymai. Šie baltymai buvo susintetinti ir išgryninti pagal parengtus protokolus. Rekombinantinių baltymų sintezė buvo atlikta įmonėje – UAB "Baltymas" (Vilnius, Lietuva).

Serumo mėginių rinkimas: Surinkti ir apdoroti savanorio, kuriam patvirtinta COVID-19 diagnozė, serumo mėginiai. Antikūnai prieš SARS-CoV-2 serume buvo kiekybiškai ištirti. Antikūnų koncentracija serumo mėginiuose buvo nustatyta chemiliuminescencinės mikrodalelių imunoanalizės metodu, šiuos tyrimus užsakė ir finansavo UAB „Tavo klinika“. (Vilnius, Lietuva).

Elektrocheminės biologinių jutiklių sistemos: kaip biologinių jutiklių kūrimo platforma buvo naudojami spausdinto montažo anglies elektrodai (SPCE). Siekiant sukurti skirtingus biologinio atpažinimo elementus, darbinis elektrodas buvo įvairiai modifikuojamas: aukso nanostruktūromis (AuNS), taikant elektronusodinimą; platinos nanostruktūromis (PtNS), taikant

elektronusodinimą; elektrai laidžiais polimerais, taikant anilino polimerizaciją ir pirolo polimerizaciją.

Biologinio atpažinimo elementų formavimui buvo taikomi: savitvarkiai monosluoksniai (SAM), biomolekulių surišimas glutaro aldehidu (GA) ir molekulių įspaudų technologija.

Tikslinių biologinių junginių aptikimas: sukurti biojutikliai buvo taikomi tiksliniams biologiniams junginiams, tokiems kaip antikūnai prieš smaigalio baltymą (anti-rS) ir rN baltymai, nustatyti.

Elektrocheminiai matavimai: buvo naudojami įvairūs elektrocheminiai metodai, įskaitant ciklinę voltamperometriją (CV), diferencinę impulsinę voltamperometriją (DPV), elektrocheminę impedanso spektroskopiją (EIS) ir impulsinę amperometrinę detekciją (PAD).

Skaičiavimai: buvo atliktas elektrocheminis elektrodų charakterizavimas ir apskaičiuoti tokie parametrai kaip elektrochemiškai aktyvus elektrodo paviršiaus plotas (EASA); buvo apskaičiuojamos heterogeninio elektronų pernašos greičio konstanta (k_0), adaptuota Langmuiro konstanta, aptikimo ribos (LOD), kiekybinio nustatymo ribos (LOQ) ir kitos elektrocheminių sistemų charakteristikos.

Diskusija ir rezultatai

Lyginamoji analizė rodo, kad mūsų biologinių jutiklių jautrumas yra mažesnis, palyginti su kai kuriais anksčiau mokslinėje literatūroje aprašytais analogais (6 lentelė). Tačiau svarbu pripažinti, kad jautrumas yra daugialypis parametras, kuriam įtakos turi įvairūs eksperimentiniai veiksniai. Tolesnis eksperimentinės sąrangos tobulinimas, pavyzdžiui, elektrodų konfigūracijos ir tyrimo sąlygų optimizavimas, potencialiai galėtų pagerinti šių analizinių sistemų charakteristikas. Be to, atliekant specifiškumo bandymus buvo nustatytas biologinių jutiklių selektyvumas tikslinėms analitėms, taip buvo padidinantas jų bendras efektyvumas ir pritaikomumas.

Nagrinėjant ankstesnes publikacijas apie SPCE elektrodų taikymą biologiniuose jutikliuose, skirtuse COVID-19 diagnostikai, išryškėja bendra tendencija –AuNS modifikuoti elektrodai dažniausiai naudojami voltamperinėse analizinėse sistemose. Nepaisant to, kad šiame darbe aprašyti biologiniai jutikliai sukurti laikantis įprastinių konstrukcijos ir aptikimo metodikų, jie yra veiksmingi tiesiogiai nustatant antikūnus prieš SARS-CoV-2 viruso baltymus realiose pacientų serumo mėginiuose.

SPCE elektrodo modifikavimo polianilinu (PANI) privalumai atsiskleidžia lyginant juos su kitais mokslinėje literatūroje (6 lentelė) aprašytais panašiais elektrodais. Būdingos elektrai laidžiųjų polimerų savybės suteikia keletą privalumų, elektrai laidūs polimerai gali atlikti redoks

tarpininko imobilizacinės matricos funkcijas. Šios unikalios savybės ne tik supaprastina biojutiklių nustatymo procesą, bet ir padidina jautrumą bei signalo stiprinimą.

Kita perspektyvi elektrai laidžiųjų polimerų pritaikymo sritis, kuri kol kas dar nėra itin plačiai taikoma, yra MIP pagrindu sukurtos analizinės sistemos, kurios yra ekonomiškai efektyvios ir yra alternatyvios tradiciniams biologiniams jutikliams. Kadangi MIP sistemose galima apsieti be brangių biomolekulių taikymo, todėl ženkliai sumažėja veiklos sąnaudos bei padidėja biologinių jutiklių stabilumas. Be to, mūsų sukurtiems biologiniamsjutikliams buvo nustatytas palyginti mažas LOD, kuris pabrėžia jo jautrumą ir tinkamumą nustatyti tikslines biomolekules.

PAD metodo taikymas įgalina dar labiau padidinanti sukurtų biologinių jutiklių efektyvumą ir praktinio taikymo galimybes. PAD įgalina sumažinant fonines sroves, taip pagerinant signalo ir triukšmo santykį ir padidinant aptikimo ribas. Šis metodas turi didelį potencialą įvairiems biologinių jutiklių taikymams, ypač tais atvejais, kai reikia greitai ir tiksliai aptikti analites.

Pažymėtina, kad tęsiant šiame darbe aprašytus tyrimus, toliau reikalingos nuolatinės pastangos tobulinant eksperimentines sąlygas, tiriant naujas paviršiaus modifikavimo strategijas ir integruojant pažangius signalų apdorojimo algoritmus, kurie gali dar labiau pagerinti mūsų biologinių jutiklių platformos jautrumą, specifiškumą ir praktinį pritaikomumą.

Išvados:

1. SPCE elektrodų modifikavimas AuNS elektrolitiniu būdu padidina elektrochemiškai aktyvaus elektrodo paviršiaus plotą ~1.7 karto, o k0 ~5.3 karto.

2. Taikant modifikuotus SPCE elektrodus ir CV bei DPV metodus galima nustatyti antikūnus prieš SARS-CoV-2 viruso baltymus realiuose serumo mėginiuose. Mažiausias LOD (0.14 nM) buvo nustatytas taikant DPV metodą.

3. SPCE elektrodas, modifikuotas PANI sluoksniu, suformuotu elektrocheminės polimerizacijos metodu, įgalina nustatyti antikūnų prieš SARS-CoV-2 viruso baltymus realiuose serumo mėginiuose be redoks mediatorių taikant EIS metodą, tokios analizės LOD yra 0.42 nM.

4. SPCE elektrodai, modifikuoti AuNS, gali būti naudojami kaip platforma molekulių įspaudais modifikuotų polimerų sluoksnių formavimui. SPCE elektrodai, modifikuoti AuNS, ir modifikuoti MIP, įgalina nustatyti SARS-CoV-2 N-baltymą netaikant redoks tarpininkų PAD metodu, tokios sistemos LOD yra 1.02 pM.

Autoriaus indėlis

Šio tyrimo eksperimentinį darbą atliko doktorantė, atlikdama įvairias mokslines/technologines užduotis, įskaitant tirpalų paruošimą, elektrodų apdorojimą, biomolekulių imobilizavimą, elektrocheminius matavimus, duomenų analizę ir mokslinių straipsnių rengimą.

Kai kuriuose tyrimuose, SEM vizualizacijoje ir duomenų analizėje taip pat dalyvavo doktorantė V. Liustrovaitė,. Straipsnių peržiūroje ir redagavime dalyvavo prof. habil. dr. A. Ramanavičius, prof. (HP) dr. A. Ramanavičienė ir dr. V. Ratautaitė.

Apie autorių

Maryia Drobysh gimė Minske, Baltarusijoje. 2016 m. baigė Baltarusijos valstybinio universiteto Chemijos fakultetą, įgijo chemiko-farmacininko specialybę. Nuo 2016 m. iki 2018 m. ji pradėjo dirbti chemike, specializavosi radiofarmacinių preparatų sintezės ir kokybės kontrolės srityje Baltarusijos Respublikos Pozitronų emisijos tomografijos centre. 2018-2020 m. Marija dirbo kokybės užtikrinimo inžiniere bendrovėje "ACD Labs" Minske. 2020-2024 m. Marija studijavo Lietuvoje Valstybinio mokslinių tyrimų instituto Fizinių ir technologijos mokslų centro doktorantūroje.

LIST OF PUBLICATIONS

This thesis is based on the results that were published in the following peer reviewed scientific papers:

1. Drobysh, M., Ramanaviciene, A., Viter, R., & Ramanavicius, A. (2021). Affinity Sensors for the Diagnosis of COVID-19. Micromachines, 12(4), p.390. https://doi.org/10.3390/mi12040390.

2. Drobysh, M., Liustrovaite, V., Baradoke, A., Viter, R., Chen, C. F., Ramanavicius, A., & Ramanaviciene, A. (2022). Determination of rSpike Protein by Specific Antibodies with Screen-Printed Carbon Electrode Modified by Electrodeposited Gold Nanostructures. Biosensors, 12(8), 593. https://doi.org/10.3390/bios12080593.

3. Drobysh, M., Ramanavicius, A., & Baradoke, A. (2023). Polyaniline-based electrochemical immunosensor for the determination of antibodies against SARS-CoV-2 spike protein. Science of The Total Environment, 862, 160700. https://doi.org/10.1016/j.scitotenv.2022.160700*.

4. Drobysh, M., Ratautaite, V., Brazys, E., Ramanaviciene, A., & Ramanavicius, A. (2024). Molecularly imprinted composite-based biosensor for the determination of SARS-CoV-2 nucleocapsid protein. Biosensors and Bioelectronics, 116043. https://doi.org/10.1016/j.bios.2024.116043*.

**As an Elsevier journal author, I retain the right to Include the article in a thesis or dissertation (provided that this is not to be published commercially) whether in full or in part, subject to proper acknowledgment. As this is a retained right, no written permission from Elsevier is necessary.*

The author contribution

The experimental work for this study was primarily conducted by the PhD candidate, who undertook various tasks including solution preparations, electrode treatment, immobilization of sensing elements, electrochemical measurements, data analysis, and the writing of research papers. PhD student V. Liustrovaite participated in some of the experiments, SEM visualization, and data analysis. Prof. habil. dr. A. Ramanavičius, prof. (HP) dr. A. Ramanaviciene, and dr. V. Ratautaite contributed a lot to the review and editing of the articles. The synthesis and provision of recombinant proteins were outsourced to Baltymas (Vilnius, Lithuania), while serum samples were generously provided by volunteers. The concentration of antibodies in the serum samples was determined through chemiluminescent microparticle immunoassay at Tavo Klinika, LtD. (Vilnius, Lithuania).

Paper 1: Literature review, writing, drafting, and reviewer's questions answering – PhD candidate; editing, revision, reviewer's questions answering – other co-authors.

Paper 2: Experiment, data analysis, writing, drafting, and reviewer's questions answering – PhD candidate; experiment, SEM imaging, writing, drafting, and reviewer's questions answering – PhD student V. Liustrovaite; editing, revision, and reviewer's questions answering – other co-authors.

Paper 3: Experiment, data analysis, writing, drafting, and reviewer's questions answering – PhD candidate; editing, revision, and reviewer's questions answering – other co-authors.

Paper 4: Experiment, data analysis, writing, drafting, and reviewer's questions answering – PhD candidate; editing, revision, and reviewer's questions answering – other co-authors.

Scientific publications that were not included in the thesis

Viter, R., Tepliakova, I., **Drobysh, M.**, Zbolotnii, V., Rackauskas, S., Ramanavicius, S., Grundsteins, K., Liustrovaite, V., Ramanaviciene, A., Ratautaite, V., Brazys, E., Chen, C.F., Prentice, U., Ramanavicius, A. (2024). Photoluminescence-based biosensor for the detection of antibodies against SARS-CoV-2 virus proteins by ZnO tetrapod structure integrated within microfluidic system. Science of The Total Environment, 173333. https://doi.org/10.1016/j.scitotenv.2024.173333.

Liustrovaite, V., **Drobysh, M.**, Ratautaite, V., Ramanaviciene, A., Rimkute, A., Simanavicius, M., Dalgediene, I., Kucinskaite-Kodze, I., Plikusiene, I., Chen, C.F., Viter, R., Ramanavicius, A. (2024). Electrochemical biosensor for the evaluation of monoclonal antibodies targeting the N protein of SARS-CoV-2 virus. Science of The Total Environment, 171042. https://doi.org/10.1016/j.scitotenv.2024.171042.

Baradoke, A., Jarusaitis, A., Reinikovaite, V., Jafarov, A., Elsakova, A., Franckevicius, M., Skapas, M., Slibinskas, R., **Drobysh M.,** Liustrovaite, V., Ramanavicius, A. (2024). Detection of antibodies against SARS-CoV-2 Spike protein by screen-printed carbon electrodes modified by colloidal gold nanoparticles. Talanta, 268, 125279. https://doi.org/10.1016/j.talanta.2023.125279.

Drobysh, M., Liustrovaite, V., Kanetski, Y., Brasiunas, B., Zvirbliene, A., Rimkute, A., Gudas, D., Kucinskaite-Kodze, I., Simanavicius, M., Ramanavicius, S., Slibinskas, R., Ciplys, E., Plikusiene, I., Ramanavicius, A. (2023). Electrochemical biosensing based comparative study of monoclonal antibodies against SARS-CoV-2 nucleocapsid protein. Science of The Total Environment, 168154. https://doi.org/10.1016/j.scitotenv.2023.168154.

Reinikovaite, V., Matulevicius, M., Elsakova, A., **Drobysh, M.,** Liustrovaite, V., Luksa, A., Jafarov, A., Slibinskas, R., Ramanavicius, A., Baradoke, A. (2023). Electrochemical capacitance spectroscopy based determination of antibodies against SARS-CoV-2 virus spike protein. Science of The Total Environment, 166447. https://doi.org/10.1016/j.scitotenv.2023.166447.

Samukaite Bubniene, U., Zukauskas, S., Ratautaite, V., Vilkiene, M., Mockeviciene, I., Liustrovaite, V., **Drobysh, M.,** Lisauskas, A., Ramanavicius, S., Ramanavicius, A. (2022). Assessment of Cytochrome c and Chlorophyll a as Natural Redox Mediators for Enzymatic Biofuel Cells Powered by Glucose. Energies, 15(18), 6838. https://doi.org/10.3390/en15186838.

Drobysh, M., Liustrovaite, V., Baradoke, A., Rucinskiene, A., Ramanaviciene, A., Ratautaite, V., Viter, R., Chen, C.F., Plikusiene, I., Samukaite-Bubniene, U., Slibinskas, R., Ciplys, E., Simanavicius, M., Zvirbliene, A., Kucinskaite-Kodze, I., Ramanavicius, A. (2022). Electrochemical Determination of Interaction between SARS-CoV-2 Spike Protein and Specific Antibodies. International Journal of Molecular Sciences, 23(12), 6768. https://doi.org/10.3390/ijms23126768.

Liustrovaite, V., **Drobysh, M.,** Rucinskiene, A., Baradoke, A., Plikusiene, I., Ramanaviciene, A., Plikusiene, I., Samukaite-Bubniene, U., Viter, R., Chen, C.F., Ramanavicius, A. (2022). Towards an Electrochemical Immunosensor for the Detection of Antibodies against SARS-CoV-2 Spike Protein. Journal of The Electrochemical Society, 169(3), 037523. https://doi.org/10.1149/1945-7111/ac5d91.

Drobysh, M., Ramanaviciene, A., Viter, R., Chen, C.F., Samukaite-Bubniene, U., Ratautaite, V., Ramanavicius, A. (2022). Biosensors for the Determination of SARS-CoV-2 Virus and Diagnosis of COVID-19 Infection. International Journal of Molecular Sciences, 23(2), 666. https://doi.org/10.3390/ijms23020666.

The results of the thesis were presented at the following conferences

"Nanostructured Bioceramic Materials 2020". International Conference, December 1-3, 2020 Vilnius, Lithuania. Poster presentation: "The development of electrochemical-based immunosensor for SARS-CoV-2 detection".

"Open readings 2021". International conference, March 16-19, 2021 Vilnius, Lithuania. Poster presentation: "Modeling of electrochemical-based immunosensors for the detection of specific antibodies".

"Advanced materials and technologies 2021". International conference, August 23-27, 2021 Palanga, Lithuania. Poster presentation: „Towards electrochemical affinity sensors for the COVID-19 diagnosis".

"Chemistry and chemical technology 2021". International conference, September 24, 2021 Vilnius, Lithuania. Poster presentation: "The review of affinity sensors for the diagnosis of COVID-19".

Conference of PhD students and young researchers "FizTech 2021". October 24, 2021 Vilnius, Lithuania. Poster presentation: "Development of electrochemistry-driven biosensing methods for determining antibodies against SARS-CoV-2 protein".

"Open readings 2022". International conference, March 15-18, 2022 Vilnius, Lithuania. Poster presentation: "The detection of antibodies against SARS-CoV-2 by electrochemical methods".

"Advanced materials and technologies 2022". International conference, August 22-26, 2022 Palanga, Lithuania. Poster presentation: "Application of electrochemical techniques for the detection of antibodies against SARS-CoV-2 Spike Protein".

"Chemistry and chemical technology 2022". International conference, October 14, 2022 Kaunas, Lithuania. Oral presentation: "Applying of screen-printed carbon electrode modified with gold nanostructures for the detection of antibodies against SARS-CoV-2".

Conference of PhD students and young researchers "FizTech 2022". October 19-20, 2022 Vilnius, Lithuania. Oral presentation: "Study of electrochemical biosensors for the detection of antibodies against SARS-CoV-2".

"ANAKON 2023". International conference. April 11-14, 2023 Vienna, Austria. Poster presentation: "Application of conductive polymers in the design of electrochemical biosensors for COVID-19 diagnosis".

"Open readings 2023". International conference, April 18-21, 2023 Vilnius, Lithuania. Poster presentation: "Electrochemistry-driven affinity sensor for the detection of antibodies against SARS-CoV-2".

"Advanced materials and technologies 2023". International conference, August 21-25, 2023 Palanga, Lithuania. Poster presentation: "Application of Electrochemical Biosensor for Comparative Detection of Monoclonal Antibodies Targeting SARS-CoV-2 Nucleoprotein".

Conference of PhD students and young researchers "FizTech 2023". October 18-19, 2023 Vilnius, Lithuania. Oral presentation: "Electrochemically-driven molecularly imprinted polymer based biosensor for detecting the nucleocapsid protein of SARS-CoV-2". Awarded as the best Oral Presentation.

About the author

Maryia Drobysh, born in Minsk, Belarus, graduated from the Chemical Faculty of Belarusian State University in 2016, majoring in Chemist-

Pharmacist. She began her career as a Chemist, specializing in radiopharmaceutical synthesis and quality control at the Belarusian Republic Positron-Emission Tomography Center from 2016 to 2018. Further Maryia served as a Quality Assurance Engineer at ACD Labs from 2018 to 2020 in Minsk. She embarked on her PhD studies at the State Research Institute Center for Physical Sciences and Technology in 2020.

COPIES OF PUBLICATIONS

micromachines

MDPI

Review

Affinity Sensors for the Diagnosis of COVID-19

Maryia Drobysh [1,2], Almira Ramanaviciene [2], Roman Viter [3,4,*] and Arunas Ramanavicius [2,*]

[1] State Research Institute Center for Physical and Technological Sciences, Sauletekio ave. 3, LT-10257 Vilnius, Lithuania; mariadrobysh@gmail.com
[2] NanoTechnas–Center of Nanotechnology and Materials Science, Faculty of Chemistry and Geosciences, Vilnius University, Naugarduko str. 24, 03225 Vilnius, Lithuania; almira.ramanaviciene@chf.vu.lt
[3] Center for Collective Use of Scientific Equipment, Sumy State University, 31, Sanatornaya st., 40018 Sumy, Ukraine
[4] Institute of Atomic Physics and Spectroscopy, University of Latvia, Jelgavas Street 3, LV-1004 Riga, Latvia
* Correspondence: roman.viter@lu.lv (R.V.); arunas.ramanavicius@chf.vu.lt (A.R.)

Abstract: The coronavirus disease 2019 (COVID-19) outbreak caused by severe acute respiratory syndrome coronavirus 2 (SARS-CoV-2) was proclaimed a global pandemic in March 2020. Reducing the dissemination rate, in particular by tracking the infected people and their contacts, is the main instrument against infection spreading. Therefore, the creation and implementation of fast, reliable and responsive methods suitable for the diagnosis of COVID-19 are required. These needs can be fulfilled using affinity sensors, which differ in applied detection methods and markers that are generating analytical signals. Recently, nucleic acid hybridization, antigen-antibody interaction, and change of reactive oxygen species (ROS) level are mostly used for the generation of analytical signals, which can be accurately measured by electrochemical, optical, surface plasmon resonance, field-effect transistors, and some other methods and transducers. Electrochemical biosensors are the most consistent with the general trend towards, acceleration, and simplification of the bioanalytical process. These biosensors mostly are based on the determination of antigen-antibody interaction and are robust, sensitive, accurate, and sometimes enable label-free detection of an analyte. Along with the specification of biosensors, we also provide a brief overview of generally used testing techniques, and the description of the structure, life cycle and immune host response to SARS-CoV-2, and some deeper details of analytical signal detection principles.

Keywords: COVID-19; SARS-CoV-2 virus; RNA analysis; bioelectrochemistry; biosensors; electrochemical immunosensors; antigen-antibody interaction; immune complex; molecularly imprinted polymers (MIPs); surface modification by immobilization of biomolecules

Citation: Drobysh, M.; Ramanaviciene, A.; Viter, R.; Ramanavicius, A. Affinity Sensors for the Diagnosis of COVID-19. *Micromachines* **2021**, *12*, 390. https://doi.org/10.3390/mi12040390

Academic Editor: Katsuo Kurabayashi

Received: 28 February 2021
Accepted: 23 March 2021
Published: 2 April 2021

1. Introduction

The spreading of severe acute respiratory syndrome coronavirus 2 (SARS-CoV-2), which is causing coronavirus disease 2019 (COVID-19) was declared as a global pandemic in March 2020. The main threat of the pandemic is the overloading of the health systems. The key tool against infection spreading is decreasing its distribution rate, in particular by monitoring the infected people and their contacts. For the successful control, the primary step is the detection of SARS-CoV-2 in an organism. Hence, the development and introduction of rapid, precise, and sensitive detection methods are required. For a better understanding of the existing detection method principles, it is worth dwelling in more detail on the structure of SARS-CoV-2, its life cycle and the induced host response.

2. The Structure of SARS-CoV-2 Virus

The coronavirus SARS-CoV-2 is a spherical structure with a diameter of about 130 nm [1–3], its surface is riddled by spikes making the viral particle look like the 'Sun's corona', therefore, similarly looking viruses are named as coronaviruses. Inside the viral

structure, a helically symmetrical nucleocapsid containing ssRNA, which is a genetic information carrier of this virus, is located. The SARS-CoV-2 has a typical for the coronaviruses (CoVs) genome, which is by about 80% and 50% similar to that of known SARS-CoV and middle east respiratory syndrome coronavirus (MERS-CoV), respectively [4]. The genome is including no less than ten open reading frames (ORFs). The virus replicase-transcriptase complex, which is formed by two large polyproteins, is encoded on the 5′-terminal two-thirds of the genome ORF1a/b, while the entire part of the genome encodes four key structural proteins, that are, spike (S), envelope (E), nucleocapsid (N) and membrane (M) proteins (Table 1). These proteins play a crucial role, primarily in the formation of viral particles, and are taking part in other stages of the SARS-CoV-2 life cycle [4]. The S-protein, a large transmembrane homo-trimer (∼150 kDa), which consists of two subunits, namely, S1 and S2 [4–6] and is responsible for the virus attaching to a host cell, followed by fusion and infection [7,8]. An attachment to a host receptor performs through the receptor-binding domain (RBD) in the S1 subunit and then fusion of the viral and host membranes takes place through the S2 subunit [9–12]. The E-protein (∼8–12 kDa) is a transmembrane and also the smallest one. The smaller part of the E-protein, which is expressed in the infected host cells, is forming the viral overall envelope, while the larger part of this protein is involved in viral association and maturation [13,14]. The N-protein is bound with viral ssRNA, and it is responsible for virion formation [15]. The N-protein consists of a monomeric N-terminal domain (NTD) with a mass value of about 15.4 kDa, and a dimeric C-terminal domain (CTD) with a mass of ~28.7 kDa, in such a way that both are needed for the ssRNA binding [15–17]. The M-protein (∼25–30 kDa) is responsible for the shaping of the viral envelope [18]. The M-protein is characterized by the cooperation with 3 other main proteins of SARS-CoV-2. The interaction between S- and M-proteins helps to hold the S-protein in the endoplasmic reticulum (ER)-Golgi intermediate compartment (ERGIC)/Golgi complex followed by its integration into novel virions [19]. The interplay of M- and N-proteins leads to the stabilization of the N-protein/ssRNA complex (nucleocapsid) and the internal core of virions [20]. The complex of M- and E-proteins is involved in the process of viral envelope formation, and it is responsible for the creation and extrication of virus-like particles (VLPs) [21].

Table 1. Severe acute respiratory syndrome coronavirus 2 (SARS-CoV-2) structural proteins location, structure, mass and function.

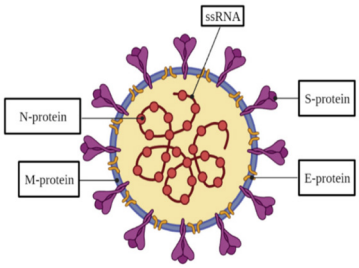

Protein	S-Protein	E-Protein	N-Protein	M-Protein
Subunits	S1 and S2	-	NTD and CTD	-
Mass	∼150 kDa	∼8–12 kDa	∼15.4 kDa (NTD) and ~28.7 kDa (CTD)	∼25–30 kDa
Function	Attachment, fusion and infection of a host cell.	Formation of viral envelope. Association and maturation of the virus.	Virion formation.	Shaping of the viral envelope.

3. Life Cycle of SARS-CoV-2 Virus

Primarily SARS-CoV-2 infects the respiratory system with the following replication of the virus in the alveoli, causing rupture of the alveolar vessels with the sub-sequent virus leakage into the bloodstream [22]. Further SARS-CoV-2 might attack the cells of other organs characterized by high expressing angiotensin-converting enzyme 2 (ACE2) receptors, such as absorptive enterocytes from the ileum and colon [23], cholangiocytes [24], myocardial cells, kidney proximal tubule cells, and bladder urothelial cells [25].

SARS-CoV-2 virus attaches to the host cell by the RBD within the S1 subunit of S-protein and a cellular receptor. In the case of SARS-CoV-2, angiotensin-converting enzyme 2 acts as the host cell receptor [4,26]. Furthermore, the virus is entered into the host cell cytosol through the acid-dependent proteolytic splitting of the S-protein, which leads to the merging of the viral and host membranes with subsequent viral genome injection into the cytoplasm [4]. The translation of the replicase gene from the virion genomic RNA is the next stage. Proteases encoded by CoVs cleave the replicases polyproteins, and then nonstructural proteins (nsps) form the replicase-transcriptase complex (RTC) for RNA synthesis. During the viral RNA synthesis, genomic and subgenomic RNAs are produced, the last one acts as mRNAs for the structural and accessory genes. Afterward, the S, E, and M-proteins are translated and placed into ER, then the proteins are transferred through the secretory pathway into the endoplasmic-reticulum–Golgi intermediate compartment [27,28]. There, N-protein forms the nucleocapsid of the viral genome, which further sprouts into the membrane with subsequent formation of the virus [15], whereas the M-protein manages the protein-protein interactions necessary for the formation of the viral particle. After formation, vesicles transfer the virions to the cellular surface, where exocytosis takes place [4].

4. Humoral Immune Response towards SARS-CoV-2 Virus Infection

The entry of the SARS-CoV-2 into the host triggers an immune response to eliminate the virus, which is initially represented by innate immune system cells, for example, macrophages [29]. Sequential chain stimulation of the different immune cells leads to the inducing of the humoral immune responses by expressing antigen-specific antibodies. The antibodies expressed are mostly immunoglobulins M (IgM) and G (IgG), which are a unique marker for the presence of coronavirus [30]. IgM peak appears approximately after 2–5 weeks, while IgG peak appears later, approximately after 3–7 weeks from post-symptom onset and remains relatively stable up to 105 days [31,32]. Structural proteins of SARS-CoV-2, namely, the S- and N-proteins, act as antigens for specific binding to antibodies [33].

5. Common Diagnostic Types

There are three general strategies currently used to detect SARS-CoV-2 and to diagnose COVID-19, namely, molecular tests based on the determination of viral RNA, antigen tests based on the determination of viral proteins, and antibody tests based on the determination of specific antibodies against viral proteins (Figure 1).

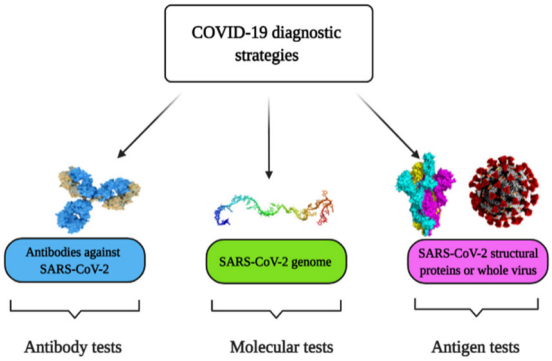

Figure 1. Coronavirus disease 2019 (COVID-19) diagnostic strategies.

5.1. Molecular Methods for the Detection of SARS-CoV-2 Virus

Molecular-based approaches enable determining whether SARS-CoV-2 infection is currently present and active in the host organism. To date, the 'gold standard' is based on the application of Reverse Transcription Polymerase Chain Reaction (RT-PCR) [34], which is aimed at the detection of viral RNA. The method is based on the reverse transcription of the RNA into complementary DNA (cDNA) followed by cDNA amplification and detection by quantitative RT-PCR [35]. Signal registration might be performed by tracking the active and ongoing status of the reaction (real-time) or through post-reaction analysis. Detection time for quantitative RT-PCR is around 1 h with limit of detection (LOD) 0.689 copies/µL [36]. The main limitations of this approach are the requirement for expensive equipment and the need for highly qualified personnel [37]. Another commonly used molecular method is the Reverse Transcription Loop-Mediated Isothermal Amplification (RT-LAMP). LAMP is an improved amplification method by employing DNA polymerase enzyme coupled with several diverse primers, each recognizing dissimilar regions of the target DNA [38]. RT-LAMP assay enables performing transcription and amplification at the same time by blend LAMP-approach based on enzyme–reverse transcriptase [37]. RT-LAMP requires around 30 min per test with LOD 200 copies/reaction [39]. The advantages of RT-LAMP methods are based on the cost reduction of the test by avoiding some steps, which usually are required for the quantitative RT-PCR method and reducing the duration of analysis and the probability of contamination. The disadvantage of this approach is the complicated design of the required primers [37]. One more isothermal amplification method is based on recombinase polymerase amplification (RPA), which involves two primers that bind a double-stranded template using single-stranded binding proteins and recombinase, followed by extension with DNA polymerase [40]. Recently, reverse transcription RPA (RT-RPA) based assay for SARS-CoV-2 detection was reported characterized by test time less than 20 min and LOD 5 copies/µL [41]. Consider also one of the most recent molecular SARS-CoV-2 detection methods, which is based on the Clustered Regularly Interspaced Short Palindromic Repeats (CRISPR)-based approach. The key principle of this approach is the use of Cas12/Cas13 enzymes, which initially were determined as components of the 'bacterial immune system' coupled to RNAs with subsequent specific binding to certain regions of target DNA or RNA [42]. There are two commonly used CRISPR-based SARS-CoV-2 detection techniques: DNA Endonuclease-Targeted CRISPR Trans Reporter (DETECTR) and STOPCovid (SHERLOCK Testing in One Pot COVID). The first technique is targeted to the E-gene and N-gene of SARS-CoV-2 and employs the Cas12a enzyme, while the second one is aimed at the N gene and utilizes the Cas12b enzyme. The essence of the approach is common: the first step is based on the employment of RT-LAMP, followed by utilizing Cas12 enzymes for cleavage of target biomolecules and signal detection by the lateral flow or fluorescent assay [42,43]. Detection times/LODs for DETECTR and SHER-

LOCK for SARS-CoV-2 are ~30 min/10 copies/μL [44] and ~40 min/2 copies/μL [45] correspondingly. A more detailed overview of action DNA-enzyme-based assays, including those based on the action of CRISPR-Cas system, is presented in our previous review article [46]. The simultaneous application of primer-specific amplification and guide RNA-directed detection significantly improved the specificity of the method, however, the limitations of amplification techniques and the activity of the employed Cas enzymes might affect the test results [42].

Hence, based on the description of the listed techniques, it can be concluded that the fastest and at the same time the most sensitive method is RT-RPA. Nevertheless, all of the above mentioned methods have similar limitations that are the laboriousness and time-consuming of the process that requires complex equipment and highly qualified personnel.

5.2. The Determination of Specific Antibodies against SARS-CoV-2

The determination of antibodies belongs to serological methods and in contrast to molecular-based approaches, antibody tests enable confirming that the patient was infected by SARS-CoV-2 in the past, thus allowing for monitoring the stages of the disease, and identifying people who already have immunity to this virus. These tests are based on the detection of a host response, namely, the production of antibodies against the SARS-CoV-2 proteins. Lateral Flow Immunoassay (LFIA) is one of the conventional methods for coronaviruses-related diseases, which represents a paper-like membrane strip that contains a sample well, a conjugate pad (contains SARS-CoV-2 antigen-gold conjugates and rabbit antibody-gold conjugates), a test lines (coated with anti-human IgG and IgM antibodies correspondingly), a control line (coated with anti-rabbit IgG antibodies). After the sample addition, specific IgG and IgM antibodies flow by capillary action toward the lines going through the conjugate pad where specific immunoglobulins bind with SARS-CoV-2 gold conjugated antigens. The formed immune complexes bind with immobilized anti-human IgG and IgM antibodies at the test lines, whereas rabbit gold conjugated antibodies bind to the control line while interacting with immobilized anti-rabbit IgG antibodies. The presented serological method has the main advantage of being suitable to diagnose COVID-19 at the different infection stages due to the combined determination of IgG and IgM. Moreover, IgG-IgM LFIA was reported as an accurate assay with a sensitivity of 88.66% and specificity of 90.63% with test time less than 15 min [47]. One more conventional antibody-based test is the Enzyme-Linked Immunosorbent Assay (ELISA). For the analysis, the inner surface of multiwell polystyrene plates was coated with SARS-CoV-2 antigen [48], afterward, the patient sample was added and incubated for an hour. Furthermore, secondary antibodies conjugated with a reported enzyme were added. These secondary antibodies are bound to specific antibodies present in the immune complex with SARS-CoV-2 antigen [49]. After the addition of the ready-to-use substrate to the enzyme bound to the secondary antibody (with 3,3′,5,5′-tetramethylbenzidine as chromogen), the specific antibodies present on the surface were detected from the color alterations [50,51]. ELISA showed a sensitivity of 77.3% and specificity of 100% for IgM while those were 83.3% and 95% respectively for IgG on the fourth day after the disease onset [52]. However, this sensible approach requires 2–5 h for the test [53]. Conventional techniques also include chemiluminescence immunoassay (CLIA), which is a label-based method that uses chemiluminescent tags or enzymatic labels with subsequent addition of a luminol-based substrate that induces a chemiluminescence-based signal, the intensity of which can be registered by luminesce detecting system [54]. An example of CLIA assay, which is applied for COVID-19 diagnosis, is rather rapid (takes just 20 min) and in this test magnetic bead-conjugated recombinant N-proteins are used as the capture agents, alkaline phosphatase-labeled anti-immunoglobulin antibodies–as the detection probes and lumigen APS-5–as the chemiluminescent substrate. This method has revealed a sensitivity and specificity 60.76% and 92.25% for IgM and 82.28% and 97.5% for IgG [55]. It should be noted, that magnetic bead- conjugated recombinant S-protein or open reading frame 1a and 1b (ORF1a/b) proteins specific to SARS-CoV-2 might be used as the capture agents [56]. Common

advantages of serological assays are: suitability for clinical application because of low costs, short time-to-results, relative simplicity and ability to scale to very large throughput.

However, antibody tests have several drawbacks, including the individuality of immune response for each patient, and seroconversion delay, which prevents immediate testing of probable cases and increases the possibility of false results.

5.3. Methods for the Determination of SARS-CoV-2 Antigens

This type of diagnostic includes the properties of the above-mentioned molecular and antibody tests. Like the molecular assay, the antigen detection method allows defining the presence of a current viral infection, whereas the principle of the test procedure is similar to that of the antibody test and is based on the detection of specific antigen-antibody complexes. For the determination of SARS-CoV-2 N-proteins in nasopharyngeal secretions LFIA and fluorescent immunoassay (FIA) are applied. 'COVID-19 Ag Respi-Strip (CORIS)' assay refers to LFIA-based type and it is based on a nitrocellulose membrane technology with colloidal gold nanoparticles conjugated with monoclonal antibodies against SARS-CoV-2 N-protein. The method allows determining the antigen in the sample within 15 min with overall sensitivity of 30.2% and specificity of 100% [57]. In FIA, the evaluation of analytical signal performs using fluorescence microscopy. An example of FIA-based approach is 'standard F COVID-19 Ag FIA' test dedicated to the determination of SARS-CoV-2 N-proteins. It represents a test cassette on which a pre-extracted sample interacts with a monoclonal anti-SARS-CoV-2 antibody and, after incubation, fluorescence analyzer reads the intensity of fluorescence, which is induced by the antibody-antigen complex formation. Test time is 30 min with sensitivity around 47% [58]. For the determination of N-protein half-strip lateral flow assay (LFA) [59], fluorescence immunochromatography (FIC) [60] and CLIA [61] are also used.

To summarize, conventional molecular and serological methods have some limitations. In the case of molecular approaches, a long sample proceeding time is needed, which also requires sophisticated and expensive facilities. Although serological assays bypass these disadvantages, they are less sensitive and limited for the determination of COVID-19 infection. Biosensors have the potential to become a modern, portable and sensitive alternative to the existing cumbersome and complicated methods. In this review, we consider several types of affinity sensors, which are currently used or might be potentially used for SARS-CoV-2 detection.

6. Affinity Biosensors for COVID-19 Diagnosis

SARS-CoV-2 infection can be identified using affinity biosensors [62]. Several different types of signal transduction systems can be applied, which include electrochemical, optical, piezoelectric and some others. Electrochemical affinity biosensors are the most prevalent in biomedical applications due to their cheapness, ease and facility of mass manufacture [62].

6.1. Affinity Biosensors for the Determination of SARS-CoV-2 RNA

An electrochemical DNA/RNA biosensor employs the hybridization of single-stranded nucleic acid (NA) with the complementary strand as a source of the electrochemical signal [63]. The affinity biosensor includes a biorecognition element consisting of the capture NA specifically interacting with the target NA, and the signal transducer where the identification event is transformed into an electrical signal [64] (Figure 2). The detection of specific hybridization of two complementary strands of NA is the key of the affinity biosensor working principle [65,66]. Sometimes additional reporter probes, which are marked with signaling compounds, are used. The reaction of hybridization occurs on an electrode or in a solution [67].

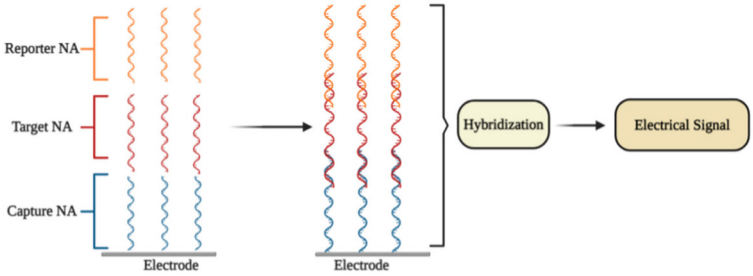

Figure 2. The general principle of electrochemical affinity biosensors for the detection of specific nucleic acid sequences.

In some electrochemical sensors, NA hybridization [63] includes an electrochemical reaction, which is further used for the quantitation of the detected NA fragment concentration and thus to the concentration of SARS-CoV-2 virus. Electrochemical NA biosensors are classified according to the types of reporter NA (label-free or labeled) and through the signal generation principle (reagent-free or reagent-dependent) [68].

The selective identification of a low amount of DNA and/or RNA copies in specimens is the most important task for electrochemical NA biosensors. The choice of the most efficient signal amplification method is the key aspect that is used to resolve this task. The molecular approaches are classified into (1) NA-based amplification methods (enzyme-mediated isothermal amplification of NA), (2) nanomaterials-based methods (large surface area for the loading of capture NA; nanomaterials as reporter probes), and (3) enzyme-mediated signal amplification (enzymes are connected with NA hybridization system) [68]. Different electrochemical methods are employed for the quantitation of amplified signals, namely, electrochemical impedance spectroscopy (EIS) [69,70], chronoamperometry [71], pulsed amperometric detection [63,72], square wave voltammetry [73], differential pulse voltammetry (DPV) [74], and cyclic voltammetry (CV) [75,76].

6.1.1. DPV-Based Affinity Biosensors

Some researchers presented ultrasensitive DPV-based detection technology using calixarene functionalized graphene oxide for targeting RNA of SARS-CoV-2 [77]. It was affirmed that the technology identifies RNA of SARS-CoV-2 avoiding amplification and reverse transcription stages by employing a portable electrochemical smartphone. The biosensor consists of a capture probe, target sequence, label probe, and an auxiliary probe [78]. The capture probe is complementary to the 5′-terminal of the target sequence, while the label probe is complementary to the 3′-terminal; two different label probe areas have complementary sequences to 5′- and 3′-regions of the auxiliary probe [78,79]. Commonly, each label probe was marked with only one signal compound that led to a low current signal. Hence, it is assumed that transferring the label probe of signaling molecules to other materials or compounds may help to increase the sensitivity [77]. The LOD in the clinical sample is 200 copies/mL, from which it follows that only two copies (10 µL) of all viral RNA copies are needed per analysis. The sensitivity for samples from confirmed COVID-19 patients was 85.5%. [77].

It is worth noting that there are some investigations concerning the potential use of G-quadruplex-based biosensors in COVID-19 diagnosis [80]. G-quadruplex (GQ) is a guanine-rich DNA/RNA sequence, which is folded into four-stranded secondary structures. These structures take part in crucial genome functions such as transcription, replication, and genome stability [81]. Recently, 25 putative G-quadruplex-forming sequences (PQSs) in the genome of SARS-CoV-2 virus were recognized [82]. The PQSs are situated in the ORF1ab, ORF3a, S-, M-, and N-genes of SARS-CoV-2 [80]. Some of the found PQSs are observed in a wide range of coronaviruses, while the main two PQSs, which generate RNA G-quadruplex structures, are strictly observed only in a limited range of viruses. Moreover, a straight

interaction between G-quadruplex of coronavirus and viral helicase (nsp13) was obtained by microscale thermophoresis. The results of molecular docking-based modeling suggest that nsp13 alters the G-quadruplex structure. The helicase allows the guanine bases to go out of the guanine quartet planes, therefore, simplifying their unfolding [82]. Thus, RNA G-quadruplex sequences of SARS-CoV-2 could be used for the design of affinity-sensors, which are based on the identification of the viral helicase protein, nsp13 [82].

Fluorescence quenching is a powerful technique for the design of affinity biosensors [83]. One type of biosensor for the determination of enzymes based on fluorescence quenching by G-quadruplex has been reported recently [84]. Guanine at a lower oxidation state can act as the electron donor, while the fluorescence able group acts as an acceptor, which further produces a signal [85].

6.1.2. Plasmonics-Based Affinity Biosensors

The primary concept of plasmonic biosensors is based on the distribution of surface plasmons lengthwise the interface of the thin metallic layer (usually noble metals), and dielectric [86]. This method consists of real-time monitoring changes of the refractive index of the medium surrounding the sensor surface during the interactions between the target biocompound and the immobilized biorecognition element [87–90]. Most plasmonic biosensors are built on the basics of surface plasmon resonance (SPR) [86,91]. Interactions occur on the surface that is suitable for observation SPR-based signals in two different modes: (1) bulk SPR signal and (2) localized SPR (LSPR) signal. Both effects rely on the refractive index of the ambient media to evoke spectral shifts. Nevertheless, the distinction between SPR and LSPR is defined by the dimensions of applied plasmonic nanomaterials [92].

It was reported that a dual-functional plasmonic biosensor incorporating the plasmonic photothermal (PPT) effect and LSPR sensing transmission enables the development of an alternative approach for SARS-CoV-2 virus detection, where the detection is provided through the hybridization of complementary NA with one NA immobilized on the surface of the gold nanoislands (AuNIs). The LSPR and PPT effects were utilized mutually to increase the signal. The LOD of this assay for the RdRp gene was 0.22 pM. The specificity, the discrimination between the RdRp gene of SARS-CoV and SARS-CoV-2, can be precisely established by onsite PPT improvement on gold AuNIs-based chips [93].

Plasmonic biosensing has technological benefits including the possibility of a combination of SPR with electrochemical, and electroassisted chemiluminescence methods [94]. Moreover, some nanomaterials were applied to establish the optical aperture and reach very sensitive virus identification by SPR method combined with colorimetric and fluorescence determination based approaches [86]. Kinds of plasmonic nanomaterials can alter from metallic nanoparticles and quantum dots to graphene nanostructures [95–98].

6.2. Immunosensors for Determination of SARS-CoV-2 Proteins

6.2.1. Field-Effect Transistor Based Immunosensors

It was reported that a Field-effect transistor (FET)-based biosensor enables the real-time detection of SARS-CoV-2 in clinical specimens. The device was manufactured by covering the graphene plates of the FET with an antibody produced as a response to the SARS-CoV-2 S-protein. The antibody was fixed on the surface of the biosensor by 1-pyrenebutyric acid N-hydroxysuccinimide ester (PBASE) (Figure 3). The cultured virus, antigen protein, and nasopharyngeal swab samples from an infected person have been utilized for the assessment of the efficiency of the immunosensor. It was determined that the FET immunosensor enables the detection of the S-protein at a concentration of 1 fg/mL in PBS and 100 fg/mL in the transport medium, whereas LOD for SARS-CoV-2 was 1.6×10^1 pfu/mL in culture medium and 2.42×10^2 copies/mL in clinical specimens [99].

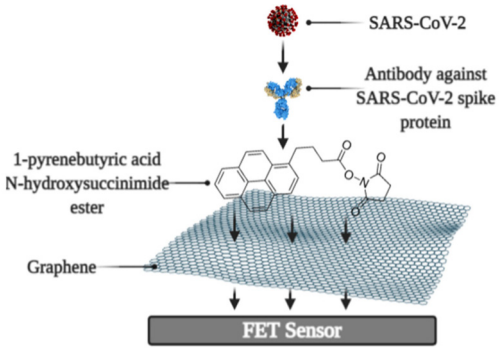

Figure 3. Schematic representation of field-effect transistor-based immunosensor for SARS-CoV-2 detection.

6.2.2. Quartz Crystal Microbalance Based Biosensors

The quartz crystal microbalance (QCM) can be successfully applied for the development of affinity biosensors [100]. In QCM-based approach, the binding with the viral S-protein occurs on the engineered quartz crystal surface covered by self-assembled monolayer (SAM), and the detection is carried out by QCM. A very simple approach for the determination of proteins is to exploit rather basic surface properties such as hydrophobicity, which is one of the key properties of the working surface of such an analytical system since the increasing the wettability of the surface leads to the increased surface concentration of proteins [101,102]. For this purpose, SAMs with a varied range of hydrophobicity, which is controlled by surface functional groups, were investigated and developed [103]. The SAMs, which have terminal –COOH and $–CH_3$ groups, have been shown as the most suitable for the specific and strong binding of SARS-CoV-2 S-protein [104]. The main working principle of the QCM is altering (decreasing) the frequency of the vibrating quartz crystal with the increasing the adsorbed mass [105]. Therefore, QCM-based techniques enable performing sensitive, rapid, and label-free tests [105,106].

One more type of affinity biosensor, which is very promising for the determination of virus-induced diseases, is the ultrasound transducer-based immunosensors, e.g.: capacitive micromachined ultrasound transducer (cMUT) was applied in immunosensors for the detection of specific antibodies against some virus proteins [107]. Moreover, the ultrasound-based test allows performing the SARS-CoV-2 virus detection in the gas phase (ultrasonator-produced viral aerosol) [108], while the vast majority of the assays are designed for the solution.

6.2.3. Molecularly Imprinted Polymer Based Electrochemical Affinity Sensors

In affinity sensors, the target protein is detected on the surface of the device, thus the design of the surface with appropriate protein recognition properties is required for the development of such sensors. For this purpose, molecularly imprinted polymers (MIPs) can be very efficiently applied [70,109–112]. The advantage of molecularly imprinted sensors is that they are cheaper and more stable, and can be based on protein-imprinted polymers such as polypyrrole [113] and some other electrochemically deposited polymers [114–116]. Various signal determination methods can be applied in the design of MIP-based sensors, but mostly potentiodynamic electrochemical techniques [113] or QCM-based [100,117] approaches are used for this purpose.

Development and application of MIPs in sensor design is reasonable because MIPs can be developed for small and low molecular weight molecules [75,118]. The efficiency of MIPs for the determination of some virus proteins was also demonstrated [113] and this technology recently was applied for the development of a molecularly imprinted poly-m-

phenylenediamine based electrochemical sensors for the detection of SARS-CoV-2 proteins, namely, N-protein [119]. The sensor represented a disposable MIP-modified thin film electrode possessing selectivity to N-protein. Electrochemical signal was observed by DPV and a linear response to N-protein was up to 111 fM with a detection and quantification limit of 15 fM and 50 fM [119].

It should be noted that even some short DNA-based oligomers can be determined by MIP-based sensors [110], which makes MIP-based sensors attractive for DNA and probably for RNA fragment determination. Due to the rather low price of MIPs in comparison to that of antibodies, MIP-related research area is of particular interest and, therefore, MIPs potentially can replace antibodies during the design of various bioanalytical systems and immunosensors.

6.3. Ellipsometry and SPR Based Immunosensors

Optical ellipsometry-based techniques have great potential to be applied in the design of various immunosensors [120]. Comparing with other existing methods (ELISA, RT-PCR, indirect fluorescent, western blot) of SARS-CoV detection, the imaging ellipsometry-based approach has established itself as a direct, nondestructive, quick, label-free, simple, and low-cost technique [121].

Recently, spectroscopic ellipsometry (SE) in total internal reflection mode (TIRE) was applied for the monitoring the kinetic of interactions between on SAM-modified gold disk immobilized SARS-CoV-2 N-protein and antibodies against it [122]. TIRE allowed detecting biomolecules mass changes at solid-liquid interface by phase shift measurement. The high sensitivity of SE TIRE was attained with the support of SPR, what enabled the registration of two kinetic curves $\Psi(t)$ and $\Delta(t)$ simultaneously [123,124]. It was reported, that antigen-antibody complex is strongly bound and the complex formation has very strict orientation requirements, which was established by meaning of mathematical model building [122]. The main working element of the sensor is the piezoelectric resonator, on which an antigen or antibody is immobilized using SAM-based technology. Incidentally, the application of antibody fragments seems to be a very promising approach for the development of sensors for the determination of virus proteins because it enables increasing the surface concertation of sites that are selective to virus proteins [125,126]

There are some other researches dedicated to the development of biosensors with the potential application for the determination of SARS-CoV-2 infection, based on the antigen-antibody interactions. In order to exploit such interactions, an electrochemical biosensor based on electrode covered with a SAM and specific-antibodies against SARS-CoV-2 proteins, was designed [127].

6.4. Photoluminescence-Based Immunosensors

Photoluminescence is a very sensitive technique that can be applied in the design of various affinity biosensors for the determination of pathological cells [128] and virus-induced diseases [129–131]. Some researchers designed a split luciferase (spLUC) based antibody test that is showing itself as simple (not need 'washing', two-stage of reagent addition, rapid (less than 5 min), reliable ($\geq$98%), low-volume specimen (1 µL for 1 reaction), inexpensive and solution-based quantitative approach to identify antibodies against S- and N- proteins of SARS-CoV-2 [132]. The biosensor was designed by merging small BiT (SmBiT) and large BiT (LgBiT) fragments [133] of Nanoluciferase (NanoLuc) to viral protein antigens. The immunoglobulin has two antigen-binding sites, thus the outcome of incubating 1:1 mixture of SmBiT and LgBiT with serum will be the coupling of one antigen-binding site with LgBiT and another site with SmBiT. The fixing of LgBiT and SmBiT fragments leads to the reduction of NanoLuc enzyme for the following luminescence-based identification (Figure 4).

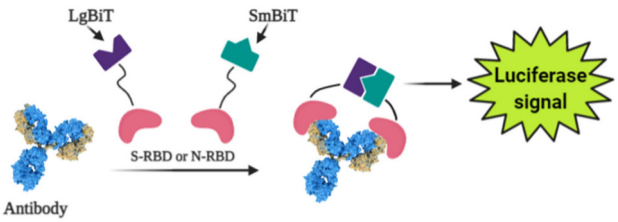

Figure 4. Scheme of the general working principle of split luciferase based immunosensor.

Sensors based on S- and N-proteins of the SARS-CoV-2 were designed because SARS-CoV-2 infected patients contain antibodies, which are primarily addressed to S- and N-protein epitopes [134,135]. The sensor-based on genetically engineered S-protein containing merged RBD with NanoLuc fragments, whereas for the creation of N-protein-based sensor N-terminal sequence was utilized. The ordinary differential equation modeling was executed to describe the ratio between signal intensity and immunoglobulin concentration and it was shown that there was a linear correlation between the specific antibody concentration and luciferase signal. The sensor showed sensitivity of 89% towards S-protein and 98% towards N-protein [132].

While the existing ELISA-based analysis possesses such disadvantages as laboriousness with numerous washing stages, which complicates point-of-care diagnostics and implementation in regions with limited analytical hardware and reagent sources, the spLUC approach has critical properties that are compliant with all these usages [126]. The reagents used for the spLUC assay were demonstrated to be quite stable to lyophilization for storage and simple transport and rapidly identify immunoglobulins straight from the clinical specimens. The kit containing common pipettes and a portable luminometer is enough for readily setting of the spLUC assay at any care centers despite the infrastructure. The modularity is another benefit of the assay, which can allow accommodating the test to the immune response against almost any infection with known antigens [132].

6.5. Determination of Reactive Oxygen Species

It was reported that coronaviruses induce mitochondrial reactive oxygen species (ROS) promotes viral replications in lung host cells [136]. ROS concentrations were significantly enlarged in SARS-CoV^{3L} proexpressing cells [137]. This phenomenon can be explained by the high level of ROS for the activation of SARS-CoV 3a-induced NLRP3 inflammasome [138] because virus infection activates nod-like pyrin domain-containing 3 (NLRP3) family, which is activating the release of ROS from damaged mitochondria [139].

The detector of reactive oxygen species stimulated by COVID-19 is an electrochemical ROS/H_2O_2 system [140]. This device includes an integrated portable automatic real-time electrochemical readout board and a sensor, which was made from the multiwall carbon nanotube (MWCNT) on the tip of steel needles. The basic operating principle is the immersion of the electrode into sputum and the latching signals of reactive oxygen species. The intensity of ROS levels, which were released from viral-infected epithelium, were determined by CV.

Unlike other ROS detection approaches, the electrochemical method is rapid (less than 30 s) and can be performed in vivo, without any additional specimen preparation. Electrochemical ROS detection assay was shown as the system operating with lower than 500 μL volumes of aliquots with a rather high accuracy of over 97% [139].

7. Conclusions

To date, the scientific community has done a great deal of work studying the properties of the SARS-CoV-2 virus, its spreading, and the effects of the infection on the human body. The most hazardous feature of the virus is the probability of asymptomatic disease, which leads to difficulties in monitoring the spread of the infection as well as an

increased probability of fatality due to the late detection of the already developed severe respiratory syndrome. Hence, it is important to have the capacity to diagnose such diseases rapidly to help reduce the distribution of destructive pathogens. Inaccuracies in the time-consuming process of sample preparation and analysis. At the same time, affinity biosensors with similar operating principles can negotiate some of the shortcomings of common approaches.

In this review, we have considered some affinity biosensors used for COVID-19 diagnosis (Table 2). As an analytical signal source, NA hybridization, antigen-antibody interactions, monitoring surface alterations, and changes of ROS levels are employed. The biosensors based on NA hybridization as the signal source were shown as precise, but they still have limitations based on the demand of amplification step and application of specific labels. Among the overviewed sensors, the lowest detection limit is determined for MIP based electrochemical sensor (15 fM). Moreover, MIP-based sensors are more stable in comparison to protein based sensors. ROS detection method is another promising label-free diagnostic method and it is characterized by high sensitivity despite rather low sample volume. Regardless of the unidentified sensitivity, the SE/SPR based technique made it possible to draw important conclusions about the structure of the antigen-antibody complex, as well as to study the kinetics of its formation, which is valuable for the design of new immunosensors. Photoluminescence-based immunosensor is shown as the most sensitive (98% for N-sensor), however it still requires labeling reagents and additional sample preparation steps. The main advantage of QCM and FET based techniques is the ability of real-time tracking of bio-interactions on the working surface.

The commonly used signal registration methods are electrochemical and optical. The examples of affinity sensors reviewed show a clear tendency to design analytical systems that are simple to use due to the elimination of additional steps in probe preparation and the use of auxiliary labeling reagents. These conditions are best met by electrochemical sensors, which detect the interaction of target biomolecules with complementary compounds immobilized on the working surface. Besides, electrochemical biosensors are the most widely used for biomedical purposes due to their cheapness, simplicity, and mass production capability.

It is important to note that, while much work has been done to study the properties of the SARS-CoV-2 and its detection techniques, there is a need to continue to develop and refine diagnostic methods avoiding the shortcomings of these methods, which are already in place, and by exploiting the most significant advantages, which already were achieved by these methods.

Table 2. Summary table of biosensors used for the diagnosis of COVID-19.

#	Biosensor	Biorecognition Element	Signal Source	Registration Methods	Label Need	Immobilization Method	LOD	Sensitivity
6.1 Affinity biosensors for the determination of SARS-CoV-2 RNA								
6.1.1	Electrochemical	Capture NA	RNA hybrid.	DPV-signal	Label NA	Au/Fe_3O_4 NPs	200 copies/mL	85.5%
6.1.2	Plasmonics based			PPT+LSPR	Label-free	Au NPs	0.22 pM	-
6.2 Immunosensors for determination of SARS-CoV-2 proteins								
6.2.1	FET based	Surface properties alterations	Antibody-antigen affinity	FET current response	Label-free	PBASE	242 copies/mL	-
6.2.2	QCM based	Surface properties alterations	S-protein binding	Change of QCM resonance frequency	Label-free	SAM	-	-
6.2.3	MIP based electrochemical	MIP-modified electrode selective to N-protein	N-protein binding	DPV	Label-free	MIP	15 fM	-
6.3	Spectroscopic Ellipsometry	N-protein	Antibody-antigen affinity	TIRE + SPR signals	Label-free	SAM	-	-
6.4	Optical	S- or N-protein	Antigen-Antibody affinity	Photoluminescence	SmBiT and LgBiT	-	-	89% (S-sensor) and 98% (N-sensor)
6.5	Reactive oxygen species detection	MWCNT electrode	ROS level	CV	Label-free	-	Sputum sample vol. <500 µL	>97%

Author Contributions: M.D. performed literature research, analysis, and drafted the paper. A.R. (Almira Ramanaviciene) performed literature research, analysis, and drafted the paper. A.R. (Arunas Ramanavicius) initiated and supervised the work and provided insights and drafted some parts of the paper. R.V. performed literature analysis, and drafted some parts of the paper. All authors have read and agreed to the published version of the manuscript.

Funding: This project has received funding from Research Council of Lithuania (LMTLT) grant No. S-LLT-21-3 and performed in cooperation with the University of Latvia Project No FP-21106-ZF-N-109.

Acknowledgments: This project has received funding from Research Council of Lithuania (LMTLT) grant No. S-LLT-21-3 and performed in cooperation with the University of Latvia Project No FP-21106-ZF-N-109. Schematic illustrations were created with BioRender (https://biorender.com/ (accessed on 28 February 2021)).

Conflicts of Interest: There are no conflict of interest to be declared.

References

1. Neuman, B.W.; Adair, B.D.; Yoshioka, C.; Quispe, J.D.; Orca, G.; Kuhn, P.; Milligan, R.A.; Yeager, M.; Buchmeier, M.J. Supramolecular architecture of severe acute respiratory syndrome coronavirus revealed by electron cryomicroscopy. *J. Virol.* **2006**, *80*, 7918–7928. [CrossRef]
2. Barcena, M.; Oostergetel, G.T.; Bartelink, W.; Faas, F.G.; Verkleij, A.; Rottier, P.J.; Koster, A.J.; Bosch, B.J. Cryo-electron tomography of mouse hepatitis virus: Insights into the structure of the coronavirion. *Proc. Natl. Acad. Sci. USA* **2009**, *106*, 582–587. [CrossRef] [PubMed]
3. Ren, L.L.; Wang, Y.M.; Wu, Z.Q.; Xiang, Z.C.; Guo, L.; Xu, T.; Jiang, Y.Z.; Xiong, Y.; Li, Y.J.; Li, X.W.; et al. Identification of a novel coronavirus causing severe pneumonia in human: A descriptive study. *Chin. Med. J.* **2020**, *133*, 1015–1024. [CrossRef]
4. Malik, Y.A. Properties of Coronavirus and SARS-CoV-2. *Malays. J. Pathol.* **2020**, *42*, 3–11. [PubMed]
5. Ou, X.; Liu, Y.; Lei, X.; Li, P.; Mi, D.; Ren, L.; Guo, L.; Guo, R.; Chen, T.; Hu, J.; et al. Characterization of spike glycoprotein of SARS-CoV-2 on virus entry and its immune cross-reactivity with SARS-CoV. *Nat. Commun.* **2020**, *11*, 1620. [CrossRef]
6. Wrapp, D.; Wang, N.; Corbett, K.S.; Goldsmith, J.A.; Hsieh, C.L.; Abiona, O.; Graham, B.S.; McLellan, J.S. Cryo-EM structure of the 2019-nCoV spike in the prefusion conformation. *Science* **2020**, *367*, 1260–1263. [CrossRef] [PubMed]
7. Song, H.C.; Seo, M.Y.; Stadler, K.; Yoo, B.J.; Choo, Q.L.; Coates, S.R.; Uematsu, Y.; Harada, T.; Greer, C.E.; Polo, J.M.; et al. Synthesis and characterization of a native, oligomeric form of recombinant severe acute respiratory syndrome coronavirus spike glycoprotein. *J. Virol.* **2004**, *78*, 10328–10335. [CrossRef]
8. Kirchdoerfer, R.N.; Cottrell, C.A.; Wang, N.; Pallesen, J.; Yassine, H.M.; Turner, H.L.; Corbett, K.S.; Graham, B.S.; McLellan, J.S.; Ward, A.B. Pre-fusion structure of a human coronavirus spike protein. *Nature* **2016**, *531*, 118–121. [CrossRef]
9. Liu, S.; Xiao, G.; Chen, Y.; He, Y.; Niu, J.; Escalante, C.R.; Xiong, H.; Farmar, J.; Debnath, A.K.; Tien, P.; et al. Interaction between heptad repeat 1 and 2 regions in spike protein of SARS-associated coronavirus: Implications for virus fusogenic mechanism and identification of fusion inhibitors. *Lancet* **2004**, *363*, 938–947. [CrossRef]
10. Li, F.; Li, W.; Farzan, M.; Harrison, S.C. Structure of SARS coronavirus spike receptor-binding domain complexed with receptor. *Science* **2005**, *309*, 1864–1868. [CrossRef]
11. Lu, G.; Hu, Y.; Wang, Q.; Qi, J.; Gao, F.; Li, Y.; Zhang, Y.; Zhang, W.; Yuan, Y.; Bao, J.; et al. Molecular basis of binding between novel human coronavirus MERS-CoV and its receptor CD26. *Nature* **2013**, *500*, 227–231. [CrossRef]
12. Walls, A.C.; Park, Y.J.; Tortorici, M.A.; Wall, A.; McGuire, A.T.; Veesler, D. Structure, Function, and Antigenicity of the SARS-CoV-2 Spike Glycoprotein. *Cell* **2020**, *181*, 281–292. [CrossRef]
13. Nieto-Torres, J.L.; Dediego, M.L.; Alvarez, E.; Jimenez-Guardeno, J.M.; Regla-Nava, J.A.; Llorente, M.; Kremer, L.; Shuo, S.; Enjuanes, L. Subcellular location and topology of severe acute respiratory syndrome coronavirus envelope protein. *Virology* **2011**, *415*, 69–82. [CrossRef] [PubMed]
14. Venkatagopalan, P.; Daskalova, S.M.; Lopez, L.A.; Dolezal, K.A.; Hogue, B.G. Coronavirus envelope (E) protein remains at the site of assembly. *Virology* **2015**, *478*, 75–85. [CrossRef] [PubMed]
15. De Haan, C.A.; Rottier, P.J. Molecular interactions in the assembly of coronaviruses. *Adv. Virus Res.* **2005**, *64*, 165–230. [CrossRef] [PubMed]
16. Chang, C.K.; Sue, S.C.; Yu, T.H.; Hsieh, C.M.; Tsai, C.K.; Chiang, Y.C.; Lee, S.J.; Hsiao, H.H.; Wu, W.J.; Chang, W.L.; et al. Modular organization of SARS coronavirus nucleocapsid protein. *J. Biomed. Sci.* **2006**, *13*, 59–72. [CrossRef] [PubMed]
17. Peng, Y.; Du, N.; Lei, Y.; Dorje, S.; Qi, J.; Luo, T.; Gao, G.F.; Song, H. Structures of the SARS-CoV-2 nucleocapsid and their perspectives for drug design. *EMBO J.* **2020**, *39*, e105938. [CrossRef] [PubMed]
18. Neuman, B.W.; Kiss, G.; Kunding, A.H.; Bhella, D.; Baksh, M.F.; Connelly, S.; Droese, B.; Klaus, J.P.; Makino, S.; Sawicki, S.G.; et al. A structural analysis of M protein in coronavirus assembly and morphology. *J. Struct. Biol.* **2011**, *174*, 11–22. [CrossRef]
19. Fehr, A.R.; Perlman, S. Coronaviruses: An overview of their replication and pathogenesis. *Methods Mol. Biol.* **2015**, *1282*, 1–23. [CrossRef] [PubMed]

20. Escors, D.; Ortego, J.; Laude, H.; Enjuanes, L. The membrane M protein carboxy terminus binds to transmissible gastroenteritis coronavirus core and contributes to core stability. *J. Virol.* **2001**, *75*, 1312–1324. [CrossRef]
21. Vennema, H.; Godeke, G.J.; Rossen, J.W.; Voorhout, W.F.; Horzinek, M.C.; Opstelten, D.J.; Rottier, P.J. Nucleocapsid-independent assembly of coronavirus-like particles by co-expression of viral envelope protein genes. *EMBO J.* **1996**, *15*, 2020–2028. [CrossRef]
22. Chen, W.; Lan, Y.; Yuan, X.; Deng, X.; Li, Y.; Cai, X.; Li, L.; He, R.; Tan, Y.; Deng, X.; et al. Detectable 2019-nCoV viral RNA in blood is a strong indicator for the further clinical severity. *Emerg. Microbes Infect.* **2020**, *9*, 469–473. [CrossRef] [PubMed]
23. Zhang, H.; Kang, Z.; Gong, H.; Xu, D.; Wang, J.; Li, Z.; Li, Z.; Cui, X.; Xiao, J.; Zhan, J.; et al. Digestive system is a potential route of COVID-19: An analysis of single-cell coexpression pattern of key proteins in viral entry process. *Gut* **2020**, *69*, 1010–1018. [CrossRef]
24. Chai, X.; Hu, L.; Zhang, Y.; Han, W.; Lu, Z.; Ke, A.; Zhou, J.; Shi, G.; Fang, N.; Fan, J.; et al. Specific ACE2 Expression in Cholangiocytes May Cause Liver Damage After 2019-nCoV Infection. *bioRxiv* **2020**, preprint. [CrossRef]
25. Zou, X.; Chen, K.; Zou, J.; Han, P.; Hao, J.; Han, Z. Single-cell RNA-seq data analysis on the receptor ACE2 expression reveals the potential risk of different human organs vulnerable to 2019-nCoV infection. *Front. Med.* **2020**, *14*, 185–192. [CrossRef]
26. Chen, Y.; Guo, Y.; Pan, Y.; Zhao, Z.J. Structure analysis of the receptor binding of 2019-nCoV. *Biochem. Biophys. Res. Commun.* **2020**, *525*, 135–140. [CrossRef]
27. Tooze, J.; Tooze, S.; Warren, G. Replication of coronavirus MHV-A59 in sac- cells: Determination of the first site of budding of progeny virions. *Eur. J. Cell Biol.* **1984**, *33*, 281–293.
28. Krijnse-Locker, J.; Ericsson, M.; Rottier, P.J.; Griffiths, G. Characterization of the budding compartment of mouse hepatitis virus: Evidence that transport from the RER to the Golgi complex requires only one vesicular transport step. *J. Cell Biol.* **1994**, *124*, 55–70. [CrossRef]
29. Li, G.; Fan, Y.; Lai, Y.; Han, T.; Li, Z.; Zhou, P.; Pan, P.; Wang, W.; Hu, D.; Liu, X.; et al. Coronavirus infections and immune responses. *J. Med. Virol.* **2020**, *92*, 424–432. [CrossRef]
30. Li, X.; Geng, M.; Peng, Y.; Meng, L.; Lu, S. Molecular immune pathogenesis and diagnosis of COVID-19. *J. Pharm. Anal.* **2020**, *10*, 102–108. [CrossRef]
31. Post, N.; Eddy, D.; Huntley, C.; van Schalkwyk, M.C.I.; Shrotri, M.; Leeman, D.; Rigby, S.; Williams, S.V.; Bermingham, W.H.; Kellam, P.; et al. Antibody response to SARS-CoV-2 infection in humans: A systematic review. *PLoS ONE* **2020**, *15*, e0244126. [CrossRef]
32. Isho, B.; Abe, K.T.; Zuo, M.; Jamal, A.J.; Rathod, B.; Wang, J.H.; Li, Z.; Chao, G.; Rojas, O.L.; Bang, Y.M.; et al. Persistence of serum and saliva antibody responses to SARS-CoV-2 spike antigens in COVID-19 patients. *Sci. Immunol.* **2020**, *5*, eabe5511. [CrossRef]
33. Pecora, N.D.; Zand, M.S. Measuring the Serologic Response to Severe Acute Respiratory Syndrome Coronavirus 2: Methods and Meaning. *Clin. Lab. Med.* **2020**, *40*, 603–614. [CrossRef]
34. Mayer, L.M.; Kahlert, C.; Rassouli, F.; Vernazza, P.; Albrich, W.C. Impact of viral multiplex real-time PCR on management of respiratory tract infection: A retrospective cohort study. *Pneumonia* **2017**, *9*, 4. [CrossRef] [PubMed]
35. Smithgall, M.C.; Dowlatshahi, M.; Spitalnik, S.L.; Hod, E.A.; Rai, A.J. Types of Assays for SARS-CoV-2 Testing: A Review. *Lab. Med.* **2020**, *51*, e59–e65. [CrossRef]
36. Pfefferle, S.; Reucher, S.; Nörz, D.; Lütgehetmann, M. Evaluation of a quantitative RT-PCR assay for the detection of the emerging coronavirus SARS-CoV-2 using a high throughput system. *Eurosurveillance* **2020**, *25*. [CrossRef]
37. Khan, P.; Aufdembrink, L.M.; Engelhart, A.E. Isothermal SARS-CoV-2 Diagnostics: Tools for Enabling Distributed Pandemic Testing as a Means of Supporting Safe Reopenings. *ACS Synth. Biol.* **2020**, *9*, 2861–2880. [CrossRef] [PubMed]
38. Notomi, T.; Okayama, H.; Masubuchi, H.; Yonekawa, T.; Watanabe, K.; Amino, N.; Hase, T. Loop-mediated isothermal amplification of DNA. *Nucleic Acids Res.* **2000**, *28*, E63. [CrossRef] [PubMed]
39. Baek, Y.H.; Um, J.; Antigua, K.J.C.; Park, J.H.; Kim, Y.; Oh, S.; Kim, Y.I.; Choi, W.S.; Kim, S.G.; Jeong, J.H.; et al. Development of a reverse transcription-loop-mediated isothermal amplification as a rapid early-detection method for novel SARS-CoV-2. *Emerg. Microb. Infect.* **2020**, *9*, 998–1007. [CrossRef] [PubMed]
40. Piepenburg, O.; Williams, C.H.; Stemple, D.L.; Armes, N.A. DNA detection using recombination proteins. *PLoS Biol.* **2006**, *4*, 1115–1121. [CrossRef] [PubMed]
41. Lau, Y.L.; Ismail, I.B.; Mustapa, N.I.B.; Lai, M.Y.; Tuan Soh, T.S.; Haji Hassan, A.; Peariasamy, K.M.; Lee, Y.L.; Abdul Kahar, M.K.B.; Chong, J.; et al. Development of a reverse transcription recombinase polymerase amplification assay for rapid and direct visual detection of Severe Acute Respiratory Syndrome Coronavirus 2 (SARS-CoV-2). *PLoS ONE* **2021**, *16*, e0245164. [CrossRef]
42. Gootenberg, J.S.; Abudayyeh, O.O.; Kellner, M.J.; Joung, J.; Collins, J.J.; Zhang, F. Multiplexed and portable nucleic acid detection platform with Cas13, Cas12a, and Csm6. *Science* **2018**, *360*, 439–444. [CrossRef]
43. Broughton, J.P.; Deng, X.; Yu, G.; Fasching, C.L.; Servellita, V.; Singh, J.; Miao, X.; Streithorst, J.A.; Granados, A.; Sotomayor-Gonzalez, A.; et al. CRISPR-Cas12-based detection of SARS-CoV-2. *Nat. Biotechnol.* **2020**, *38*, 870–874. [CrossRef] [PubMed]
44. Broughton, J.; Deng, X.; Yu, G.; Fasching, C.; Singh, J.; Streithorst, J.; Granados, A.; Sotomayor-Gonzalez, A.; Zorn, K.; Gopez, A.; et al. Rapid Detection of 2019 Novel Coronavirus SARS-CoV-2 Using a CRISPR-based DETECTR Lateral Flow Assay. *medRxiv* **2020**, *preprint*, 1–28. [CrossRef]
45. Joung, J.; Ladha, A.; Saito, M.; Segel, M.; Bruneau, R.; Huang, M.W.; Kim, N.G.; Yu, X.; Li, J.; Walker, B.D.; et al. Point-of-care testing for COVID-19 using SHERLOCK diagnostics. *medRxiv* **2020**, preprint. [CrossRef]

46. Dronina, J.; Bubniene, U.S.; Ramanavicius, A. The application of DNA polymerases and Cas9 as representative of DNA-modifying enzymes group in DNA sensor design (review). *Biosens. Bioelectron.* **2021**, *175*, 112867. [CrossRef]
47. Li, Z.; Yi, Y.; Luo, X.; Xiong, N.; Liu, Y.; Li, S.; Sun, R.; Wang, Y.; Hu, B.; Chen, W.; et al. Development and clinical application of a rapid IgM-IgG combined antibody test for SARS-CoV-2 infection diagnosis. *J. Med. Virol.* **2020**, *92*, 1518–1524. [CrossRef] [PubMed]
48. Gao, X.; Zhou, H.; Wu, C.; Xiao, Y.; Ren, L.; Paranhos-Baccala, G.; Guo, L.; Wang, J. Antibody against nucleocapsid protein predicts susceptibility to human coronavirus infection. *J. Infect.* **2015**, *71*, 599–602. [CrossRef]
49. Dhamad, A.E.; Abdal Rhida, M.A. COVID-19: Molecular and serological detection methods. *PeerJ* **2020**, *8*, e10180. [CrossRef]
50. Lee, M.; Harrison, B.A.; Lewis, G.E., Jr. A rapid sporozoite ELISA using 3,3′,5,5′-tetramethylbenzidine as the substrate chromogen. *Am. J. Trop Med. Hyg.* **1990**, *42*, 314–319. [CrossRef]
51. Madersbacher, S.; Berger, P. Double wavelength measurement of 3,3′,5,5′-tetramethylbenzidine (TMB) provides a three-fold enhancement of the ELISA measuring range. *J. Immunol. Methods* **1991**, *138*, 121–124. [CrossRef]
52. Xiang, F.; Wang, X.; He, X.; Peng, Z.; Yang, B.; Zhang, J.; Zhou, Q.; Ye, H.; Ma, Y.; Li, H.; et al. Antibody Detection and Dynamic Characteristics in Patients with Coronavirus Disease 2019. *Clin. Infect. Dis.* **2020**, *71*, 1930–1934. [CrossRef] [PubMed]
53. Zhang, W.; Du, R.H.; Li, B.; Zheng, X.S.; Yang, X.L.; Hu, B.; Wang, Y.Y.; Xiao, G.F.; Yan, B.; Shi, Z.L.; et al. Molecular and serological investigation of 2019-nCoV infected patients: Implication of multiple shedding routes. *Emerg. Microbes Infect.* **2020**, *9*, 386–389. [CrossRef]
54. Zhao, L.; Sun, L.; Chu, X. Chemiluminescence immunoassay. *TrAC Trends Anal. Chem.* **2009**, *28*, 404–415. [CrossRef]
55. Lin, D.; Liu, L.; Zhang, M.; Hu, Y.; Yang, Q.; Guo, J.; Dai, Y.; Xu, Y.; Cai, Y.; Chen, X.; et al. Evaluations of the serological test in the diagnosis of 2019 novel coronavirus (SARS-CoV-2) infections during the COVID-19 outbreak. *Eur. J. Clin. Microbiol. Infect. Dis.* **2020**, *39*, 2271–2277. [CrossRef] [PubMed]
56. Cai, X.; Chen, J.; Hu, J.; Long, Q.; Deng, H.; Fan, K.; Liao, P.; Liu, B.; Wu, G.; Chen, Y.; et al. A Peptide-based Magnetic Chemiluminescence Enzyme Immunoassay for Serological Diagnosis of Corona Virus Disease 2019 (COVID-19). *medRxiv* **2020**, preprint. [CrossRef]
57. Scohy, A.; Anantharajah, A.; Bodeus, M.; Kabamba-Mukadi, B.; Verroken, A.; Rodriguez-Villalobos, H. Low performance of rapid antigen detection test as frontline testing for COVID-19 diagnosis. *J. Clin. Virol.* **2020**, *129*, 104455. [CrossRef] [PubMed]
58. Liotti, F.M.; Menchinelli, G.; Lalle, E.; Palucci, I.; Marchetti, S.; Colavita, F.; La Sorda, M.; Sberna, G.; Bordi, L.; Sanguinetti, M.; et al. Performance of a novel diagnostic assay for rapid SARS-CoV-2 antigen detection in nasopharynx samples. *Clin. Microbiol. Infect.* **2021**, *27*, 487–488. [CrossRef]
59. Grant, B.D.; Anderson, C.E.; Williford, J.R.; Alonzo, L.F.; Glukhova, V.A.; Boyle, D.S.; Weigl, B.H.; Nichols, K.P. SARS-CoV-2 Coronavirus Nucleocapsid Antigen-Detecting Half-Strip Lateral Flow Assay Toward the Development of Point of Care Tests Using Commercially Available Reagents. *Anal. Chem.* **2020**, *92*, 11305–11309. [CrossRef]
60. Porte, L.; Legarraga, P.; Vollrath, V.; Aguilera, X.; Munita, J.M.; Araos, R.; Pizarro, G.; Vial, P.; Iruretagoyena, M.; Dittrich, S.; et al. Evaluation of a novel antigen-based rapid detection test for the diagnosis of SARS-CoV-2 in respiratory samples. *Int. J. Infect. Dis.* **2020**, *99*, 328–333. [CrossRef]
61. Hirotsu, Y.; Maejima, M.; Shibusawa, M.; Nagakubo, Y.; Hosaka, K.; Amemiya, K.; Sueki, H.; Hayakawa, M.; Mochizuki, H.; Tsutsui, T.; et al. Comparison of automated SARS-CoV-2 antigen test for COVID-19 infection with quantitative RT-PCR using 313 nasopharyngeal swabs, including from seven serially followed patients. *Int. J. Infect. Dis.* **2020**, *99*, 397–402. [CrossRef] [PubMed]
62. Cui, F.; Zhou, H.S. Diagnostic methods and potential portable biosensors for coronavirus disease 2019. *Biosens. Bioelectron.* **2020**, *165*, 112349. [CrossRef]
63. Ramanaviciene, A.; Ramanavicius, A. Pulsed amperometric detection of DNA with an ssDNA/polypyrrole-modified electrode. *Anal. Bioanal. Chem.* **2004**, *379*, 287–293. [CrossRef]
64. Drummond, T.G.; Hill, M.G.; Barton, J.K. Electrochemical DNA sensors. *Nat. Biotechnol.* **2003**, *21*, 1192–1199. [CrossRef] [PubMed]
65. Zhang, D.Y.; Chen, S.X.; Yin, P. Optimizing the specificity of nucleic acid hybridization. *Nat. Chem.* **2012**, *4*, 208–214. [CrossRef] [PubMed]
66. Pellitero, M.A.; Shaver, A.; Arroyo-Currás, N. Critical Review—Approaches for the Electrochemical Interrogation of DNA-Based Sensors: A Critical Review. *J. Electrochem. Soc.* **2020**, *167*, 037529. [CrossRef]
67. Trotter, M.; Borst, N.; Thewes, R.; von Stetten, F. Review: Electrochemical DNA sensing—Principles, commercial systems, and applications. *Biosens. Bioelectron.* **2020**, *154*, 112069. [CrossRef] [PubMed]
68. Santhanam, M.; Algov, I.; Alfonta, L. DNA/RNA Electrochemical Biosensing Devices a Future Replacement of PCR Methods for a Fast Epidemic Containment. *Sensors* **2020**, *20*, 4648. [CrossRef]
69. Ramanavicius, A.; Finkelsteinas, A.; Cesiulis, H.; Ramanaviciene, A. Electrochemical impedance spectroscopy of polypyrrole based electrochemical immunosensor. *Bioelectrochemistry* **2010**, *79*, 11–16. [CrossRef] [PubMed]
70. Ratautaite, V.; Janssens, S.D.; Haenen, K.; Nesládek, M.; Ramanaviciene, A.; Baleviciute, I.; Ramanavicius, A. Molecularly Imprinted Polypyrrole Based Impedimentric Sensor for Theophylline Determination. *Electrochim. Acta* **2014**, *130*, 361–367. [CrossRef]
71. German, N.; Ramanavicius, A.; Ramanaviciene, A. Electrochemical deposition of gold nanoparticles on graphite rod for glucose biosensing. *Sens. Actuators B Chem.* **2014**, *203*, 25–34. [CrossRef]

72. Ramanavicius, A.; Oztekin, Y.; Ramanaviciene, A. Electrochemical formation of polypyrrole-based layer for immunosensor design. *Sens. Actuators B Chem.* **2014**, *197*, 237–243. [CrossRef]
73. Oztekin, Y.; Yazicigil, Z.; Ramanaviciene, A.; Ramanavicius, A. Square wave voltammetry based on determination of copper (II) ions by polyluteolin- and polykaempferol-modified electrodes. *Talanta* **2011**, *85*, 1020–1027. [CrossRef] [PubMed]
74. Deshmukh, M.A.; Patil, H.K.; Bodkhe, G.A.; Yasuzawa, M.; Koinkar, P.; Ramanaviciene, A.; Shirsat, M.D.; Ramanavicius, A. EDTA-modified PANI/SWNTs nanocomposite for differential pulse voltammetry based determination of Cu(II) ions. *Sens. Actuators B Chem.* **2018**, *260*, 331–338. [CrossRef]
75. Ramanavicius, S.; Ramanavicius, A. Conducting Polymers in the Design of Biosensors and Biofuel Cells. *Polymers* **2020**, *13*, 49. [CrossRef]
76. Samukaite-Bubniene, U.; Valiuniene, A.; Bucinskas, V.; Genys, P.; Ratautaite, V.; Ramanaviciene, A.; Aksun, E.; Tereshchenko, A.; Zeybek, B.; Ramanavicius, A. Towards supercapacitors: Cyclic voltammetry and fast Fourier transform electrochemical impedance spectroscopy based evaluation of polypyrrole electrochemically deposited on the pencil graphite electrode. *Colloid Surf. A Physicochem. Eng. Asp.* **2021**, *610*. [CrossRef]
77. Zhao, H.; Liu, F.; Xie, W.; Zhou, T.C.; OuYang, J.; Jin, L.; Li, H.; Zhao, C.Y.; Zhang, L.; Wei, J.; et al. Ultrasensitive supersandwich-type electrochemical sensor for SARS-CoV-2 from the infected COVID-19 patients using a smartphone. *Sens. Actuators B Chem.* **2021**, *327*, 128899. [CrossRef]
78. Chen, X.; Lin, Y.H.; Li, J.; Lin, L.S.; Chen, G.N.; Yang, H.H. A simple and ultrasensitive electrochemical DNA biosensor based on DNA concatamers. *Chem. Commun.* **2011**, *47*, 12116–12118. [CrossRef]
79. Wang, J.; Shi, A.; Fang, X.; Han, X.; Zhang, Y. An ultrasensitive supersandwich electrochemical DNA biosensor based on gold nanoparticles decorated reduced graphene oxide. *Anal. Biochem.* **2015**, *469*, 71–75. [CrossRef]
80. Xi, H.; Juhas, M.; Zhang, Y. G-quadruplex based biosensor: A potential tool for SARS-CoV-2 detection. *Biosens. Bioelectron.* **2020**, *167*, 112494. [CrossRef]
81. Spiegel, J.; Adhikari, S.; Balasubramanian, S. The Structure and Function of DNA G-Quadruplexes. *Trends Chem.* **2020**, *2*, 123–136. [CrossRef]
82. Ji, D.; Juhas, M.; Tsang, C.M.; Kwok, C.K.; Li, Y.; Zhang, Y. Discovery of G-quadruplex-forming sequences in SARS-CoV-2. *Brief. Bioinf.* **2020**. [CrossRef] [PubMed]
83. Ramanavicius, A.; Kurilcik, N.; Jursenas, S.; Finkelsteinas, A.; Ramanaviciene, A. Conducting polymer based fluorescence quenching as a new approach to increase the selectivity of immunosensors. *Biosens. Bioelectron.* **2007**, *23*, 499–505. [CrossRef]
84. Wu, K.; Ma, C.; Deng, Z.; Fang, N.; Tang, Z.; Zhu, X.; Wang, K. Label-free and nicking enzyme-assisted fluorescence signal amplification for RNase H determination based on a G-quadruplexe/thioflavin T complex. *Talanta* **2018**, *182*, 142–147. [CrossRef]
85. Ying, L.; Green, J.J.; Li, H.; Klenerman, D.; Balasubramanian, S. Studies on the structure and dynamics of the human telomeric G quadruplex by single-molecule fluorescence resonance energy transfer. *Proc. Natl. Acad. Sci. USA* **2003**, *100*, 14629–14634. [CrossRef] [PubMed]
86. Mauriz, E. Recent Progress in Plasmonic Biosensing Schemes for Virus Detection. *Sensors* **2020**, *20*, 4745. [CrossRef]
87. Homola, J. Surface plasmon resonance sensors for detection of chemical and biological species. *Chem. Rev.* **2008**, *108*, 462–493. [CrossRef]
88. Brolo, A.G. Plasmonics for future biosensors. *Nat. Photonics* **2012**, *6*, 709–713. [CrossRef]
89. Sipova, H.; Homola, J. Surface plasmon resonance sensing of nucleic acids: A review. *Anal. Chim. Acta* **2013**, *773*, 9–23. [CrossRef]
90. Li, Z.; Leustean, L.; Inci, F.; Zheng, M.; Demirci, U.; Wang, S. Plasmonic-based platforms for diagnosis of infectious diseases at the point-of-care. *Biotechnol. Adv.* **2019**, *37*, 107440. [CrossRef]
91. Kausaite-Minkstimiene, A.; Ramanavicius, A.; Ruksnaite, J.; Ramanaviciene, A. A surface plasmon resonance immunosensor for human growth hormone based on fragmented antibodies. *Anal. Methods* **2013**, *5*, 4757–4763. [CrossRef]
92. Li, M.; Cushing, S.K.; Wu, N. Plasmon-enhanced optical sensors: A review. *Analyst* **2015**, *140*, 386–406. [CrossRef]
93. Qiu, G.; Gai, Z.; Tao, Y.; Schmitt, J.; Kullak-Ublick, G.A.; Wang, J. Dual-Functional Plasmonic Photothermal Biosensors for Highly Accurate Severe Acute Respiratory Syndrome Coronavirus 2 Detection. *ACS Nano* **2020**, *14*, 5268–5277. [CrossRef]
94. Ramanaviciene, A.; German, N.; Kausaite-Minkstimiene, A.; Voronovic, J.; Kirlyte, J.; Ramanavicius, A. Comparative study of surface plasmon resonance, electrochemical and electroassisted chemiluminescence methods based immunosensor for the determination of antibodies against human growth hormone. *Biosens. Bioelectron.* **2012**, *36*, 48–55. [CrossRef] [PubMed]
95. Tran, V.T.; Zhou, H.; Kim, S.; Lee, J.; Kim, J.; Zou, F.; Kim, J.; Park, J.Y. Self-assembled magnetoplasmonic nanochain for DNA sensing. *Sens. Actuators B Chem.* **2014**, *203*, 817–823. [CrossRef]
96. Adegoke, O.; Park, E.Y. Gold Nanoparticle-Quantum Dot Fluorescent Nanohybrid: Application for Localized Surface Plasmon Resonance-induced Molecular Beacon Ultrasensitive DNA Detection. *Nanoscale Res. Lett.* **2016**, *11*, 523. [CrossRef] [PubMed]
97. Lee, J.; Takemura, K.; Park, E.Y. Plasmonic Nanomaterial-Based Optical Biosensing Platforms for Virus Detection. *Sensors* **2017**, *17*. [CrossRef] [PubMed]
98. Farzin, L.; Shamsipur, M.; Samandari, L.; Sheibani, S. HIV biosensors for early diagnosis of infection: The intertwine of nanotechnology with sensing strategies. *Talanta* **2020**, *206*, 120201. [CrossRef]
99. Seo, G.; Lee, G.; Kim, M.J.; Baek, S.H.; Choi, M.; Ku, K.B.; Lee, C.S.; Jun, S.; Park, D.; Kim, H.G.; et al. Rapid Detection of COVID-19 Causative Virus (SARS-CoV-2) in Human Nasopharyngeal Swab Specimens Using Field-Effect Transistor-Based Biosensor. *ACS Nano* **2020**, *14*, 5135–5142. [CrossRef]

100. Plausinaitis, D.; Sinkevicius, L.; Samukaite-Bubniene, U.; Ratautaite, V.; Ramanavicius, A. Evaluation of electrochemical quartz crystal microbalance based sensor modified by uric acid-imprinted polypyrrole. *Talanta* **2020**, *220*, 121414. [CrossRef]
101. Disley, D.M.; Cullen, D.C.; You, H.-X.; Lowe, C.R. Covalent coupling of immunoglobulin G to self-assembled monolayers as a method for immobilizing the interfacial-recognition layer of a surface plasmon resonance immunosensor. *Biosens. Bioelectron.* **1998**, *13*, 1213–1225. [CrossRef]
102. Hasan, A.; Pattanayek, S.K.; Pandey, L.M. Effect of Functional Groups of Self-Assembled Monolayers on Protein Adsorption and Initial Cell Adhesion. *ACS Biomater. Sci. Eng.* **2018**, *4*, 3224–3233. [CrossRef]
103. Pandey, L.M.; Pattanayek, S.K. Relation between the Wetting Effect and the Adsorbed Amount of Water-Soluble Polymers or Proteins at Various Interfaces. *J. Chem. Eng. Data* **2013**, *58*, 3440–3446. [CrossRef]
104. Pandey, L.M. Design of engineered surfaces for prospective detection of SARS-CoV-2 using quartz crystal microbalance-based techniques. *Expert Rev. Proteomics* **2020**, *17*, 425–432. [CrossRef]
105. Pandey, L.M.; Pattanayek, S.K. Hybrid surface from self-assembled layer and its effect on protein adsorption. *Appl. Surface Sci.* **2011**, *257*, 4731–4737. [CrossRef]
106. Deng, T.; Li, J.S.; Huan, S.Y.; Yang, H.F.; Wang, H.; Shen, G.L.; Yu, R.Q. Quartz crystal microbalance bioaffinity sensor for biotin based on mixed self-assembled monolayers and metastable molecular complex receptor. *Biosens. Bioelectron.* **2006**, *21*, 1545–1552. [CrossRef] [PubMed]
107. Ramaniviciene, A.; Virzonis, D.; Vanagas, G.; Ramanavicius, A. Capacitive micromachined ultrasound transducer (cMUT) for immunosensor design. *Analyst* **2010**, *135*, 1531–1534. [CrossRef]
108. Zuo, B.; Li, S.; Guo, Z.; Zhang, J.; Chen, C. Piezoelectric immunosensor for SARS-associated coronavirus in sputum. *Anal. Chem.* **2004**, *76*, 3536–3540. [CrossRef]
109. Ramanaviciene, A.; Ramanavicius, A.; Finkelsteinas, A. Basic Electrochemistry Meets Nanotechnology: Electrochemical Preparation of Artificial Receptors Based on Nanostructured Conducting Polymer, Polypyrrole. *J. Chem. Educ.* **2006**, *83*, 1212–1214. [CrossRef]
110. Ratautaite, V.; Topkaya, S.N.; Mikoliunaite, L.; Ozsoz, M.; Oztekin, Y.; Ramaniviciene, A.; Ramanavicius, A. Molecularly Imprinted Polypyrrole for DNA Determination. *Electroanalysis* **2013**, *25*, 1169–1177. [CrossRef]
111. Viter, R.; Kunene, K.; Genys, P.; Jevdokimovs, D.; Erts, D.; Sutka, A.; Bisetty, K.; Viksna, A.; Ramaniviciene, A.; Ramanavicius, A. Photoelectrochemical Bisphenol S Sensor Based on ZnO-Nanoroads Modified by Molecularly Imprinted Polypyrrole. *Macromol. Chem. Phys.* **2019**, *221*. [CrossRef]
112. Syritski, V.; Reut, J.; Menaker, A.; Gyurcsányi, R.E.; Öpik, A. Electrosynthesized molecularly imprinted polypyrrole films for enantioselective recognition of l-aspartic acid. *Electrochim. Acta* **2008**, *53*, 2729–2736. [CrossRef]
113. Ramanaviciene, A.; Ramanavicius, A. Molecularly imprinted polypyrrole-based synthetic receptor for direct detection of bovine leukemia virus glycoproteins. *Biosens. Bioelectron.* **2004**, *20*, 1076–1082. [CrossRef] [PubMed]
114. Boroznjak, R.; Reut, J.; Tretjakov, A.; Lomaka, A.; Opik, A.; Syritski, V. A computational approach to study functional monomer-protein molecular interactions to optimize protein molecular imprinting. *J. Mol. Recognit.* **2017**, *30*. [CrossRef] [PubMed]
115. Menaker, A.; Syritski, V.; Reut, J.; Öpik, A.; Horváth, V.; Gyurcsányi, R.E. Electrosynthesized Surface-Imprinted Conducting Polymer Microrods for Selective Protein Recognition. *Adv. Mater.* **2009**, *21*, 2271–2275. [CrossRef]
116. Tretjakov, A.; Syritski, V.; Reut, J.; Boroznjak, R.; Volobujeva, O.; Öpik, A. Surface molecularly imprinted polydopamine films for recognition of immunoglobulin G. *Microchim. Acta* **2013**, *180*, 1433–1442. [CrossRef]
117. Syritski, V.; Reut, J.; Öpik, A.; Idla, K. Environmental QCM sensors coated with polypyrrole. *Synth. Metals* **1999**, *102*, 1326–1327. [CrossRef]
118. Ramanavicius, S.; Ramanavicius, A. Charge Transfer and Biocompatibility Aspects in Conducting Polymer-Based Enzymatic Biosensors and Biofuel Cells. *Nanomaterials* **2021**, *11*, 371. [CrossRef]
119. Raziq, A.; Kidakova, A.; Boroznjak, R.; Reut, J.; Opik, A.; Syritski, V. Development of a portable MIP-based electrochemical sensor for detection of SARS-CoV-2 antigen. *Biosens. Bioelectron.* **2021**, *178*, 113029. [CrossRef]
120. Balevicius, Z.; Paulauskas, A.; Plikusiene, I.; Mikoliunaite, L.; Bechelany, M.; Popov, A.; Ramanavicius, A.; Ramaniviciene, A. Towards the application of Al2O3/ZnO nanolaminates in immunosensors: Total internal reflection spectroscopic ellipsometry based evaluation of BSA immobilization. *J. Mater. Chem. C* **2018**, *6*, 8778–8783. [CrossRef]
121. Qi, C.; Duan, J.Z.; Wang, Z.H.; Chen, Y.Y.; Zhang, P.H.; Zhan, L.; Yan, X.Y.; Cao, W.C.; Jin, G. Investigation of interaction between two neutralizing monoclonal antibodies and SARS virus using biosensor based on imaging ellipsometry. *Biomed. Microdevices* **2006**, *8*, 247–253. [CrossRef]
122. Plikusiene, I.; Maciulis, V.; Ramanaviciene, A.; Balevicius, Z.; Buzavaite-Verteliene, E.; Ciplys, E.; Slibinskas, R.; Simanavicius, M.; Zvirbliene, A.; Ramanavicius, A. Evaluation of Kinetics and Thermodynamics of Interaction between Immobilized SARS-CoV-2 Nucleoprotein and Specific Antibodies by Total Internal Reflection Ellipsometry. *J. Colloid Interface Sci.* **2021**. [CrossRef] [PubMed]
123. Baleviciute, I.; Balevicius, Z.; Makaraviciute, A.; Ramanaviciene, A.; Ramanavicius, A. Study of antibody/antigen binding kinetics by total internal reflection ellipsometry. *Biosens. Bioelectron.* **2013**, *39*, 170–176. [CrossRef] [PubMed]
124. Arwin, H.; Poksinski, M.; Johansen, K. Total internal reflection ellipsometry: Principles and applications. *Appl. Opt.* **2004**, *43*, 3028–3036. [CrossRef]
125. Kausaite-Minkstimiene, A.; Ramanaviciene, A.; Kirlyte, J.; Ramanavicius, A. Comparative study of random and oriented antibody immobilization techniques on the binding capacity of immunosensor. *Anal. Chem.* **2010**, *82*, 6401–6408. [CrossRef]

126. Balevicius, Z.; Ramanaviciene, A.; Baleviciute, I.; Makaraviciute, A.; Mikoliunaite, L.; Ramanavicius, A. Evaluation of intact- and fragmented-antibody based immunosensors by total internal reflection ellipsometry. *Sens. Actuators B Chem.* **2011**, *160*, 555–562. [CrossRef]
127. Mayall, R.M.; Smith, C.A.; Hyla, A.S.; Lee, D.S.; Crudden, C.M.; Birss, V.I. Ultrasensitive and Label-Free Detection of the Measles Virus Using an N-Heterocyclic Carbene-Based Electrochemical Biosensor. *ACS Sens.* **2020**, *5*, 2747–2752. [CrossRef]
128. Tamashevski, A.; Harmaza, Y.; Viter, R.; Jevdokimovs, D.; Poplausks, R.; Slobozhanina, E.; Mikoliunaite, L.; Erts, D.; Ramanaviciene, A.; Ramanavicius, A. Zinc oxide nanorod based immunosensing platform for the determination of human leukemic cells. *Talanta* **2019**, *200*, 378–386. [CrossRef] [PubMed]
129. Tereshchenko, A.; Smyntyna, V.; Ramanavicius, A. Interaction mechanism between TiO_2 nanostructures and bovine leukemia virus proteins in photoluminescence-based immunosensors. *RSC Adv.* **2018**, *8*, 37740–37748. [CrossRef]
130. Viter, R.; Savchuk, M.; Iatsunskyi, I.; Pietralik, Z.; Starodub, N.; Shpyrka, N.; Ramanaviciene, A.; Ramanavicius, A. Analytical, thermodynamical and kinetic characteristics of photoluminescence immunosensor for the determination of Ochratoxin A. *Biosens. Bioelectron.* **2018**, *99*, 237–243. [CrossRef] [PubMed]
131. Viter, R.; Savchuk, M.; Starodub, N.; Balevicius, Z.; Tumenas, S.; Ramanaviciene, A.; Jevdokimovs, D.; Erts, D.; Iatsunskyi, I.; Ramanavicius, A. Photoluminescence immunosensor based on bovine leukemia virus proteins immobilized on the ZnO nanorods. *Sens. Actuators B Chem.* **2019**, *285*, 601–606. [CrossRef]
132. Elledge, S.K.; Zhou, X.X.; Byrnes, J.R.; Martinko, A.J.; Lui, I.; Pance, K.; Lim, S.A.; Glasgow, J.E.; Glasgow, A.A.; Turcios, K.; et al. Engineering luminescent biosensors for point-of-care SARS-CoV-2 antibody detection. *medRxiv* **2020**, preprint. [CrossRef]
133. Dixon, A.S.; Schwinn, M.K.; Hall, M.P.; Zimmerman, K.; Otto, P.; Lubben, T.H.; Butler, B.L.; Binkowski, B.F.; Machleidt, T.; Kirkland, T.A.; et al. NanoLuc Complementation Reporter Optimized for Accurate Measurement of Protein Interactions in Cells. *ACS Chem. Biol.* **2016**, *11*, 400–408. [CrossRef] [PubMed]
134. Kang, S.; Yang, M.; Hong, Z.; Zhang, L.; Huang, Z.; Chen, X.; He, S.; Zhou, Z.; Zhou, Z.; Chen, Q.; et al. Crystal structure of SARS-CoV-2 nucleocapsid protein RNA binding domain reveals potential unique drug targeting sites. *Acta Pharm. Sin. B* **2020**, *10*, 1228–1238. [CrossRef]
135. Letko, M.; Marzi, A.; Munster, V. Functional assessment of cell entry and receptor usage for SARS-CoV-2 and other lineage B betacoronaviruses. *Nat. Microbiol.* **2020**, *5*, 562–569. [CrossRef] [PubMed]
136. Cheng, M.L.; Weng, S.F.; Kuo, C.H.; Ho, H.Y. Enterovirus 71 induces mitochondrial reactive oxygen species generation that is required for efficient replication. *PLoS ONE* **2014**, *9*, e113234. [CrossRef]
137. Lin, C.W.; Lin, K.H.; Hsieh, T.H.; Shiu, S.Y.; Li, J.Y. Severe acute respiratory syndrome coronavirus 3C-like protease-induced apoptosis. *FEMS Immunol. Med. Microbiol.* **2006**, *46*, 375–380. [CrossRef] [PubMed]
138. Chen, I.Y.; Moriyama, M.; Chang, M.F.; Ichinohe, T. Severe Acute Respiratory Syndrome Coronavirus Viroporin 3a Activates the NLRP3 Inflammasome. *Front. Microbiol.* **2019**, *10*, 50. [CrossRef] [PubMed]
139. Miripour, Z.S.; Sarrami-Forooshani, R.; Sanati, H.; Makarem, J.; Taheri, M.S.; Shojaeian, F.; Eskafi, A.H.; Abbasvandi, F.; Namdar, N.; Ghafari, H.; et al. Real-time diagnosis of reactive oxygen species (ROS) in fresh sputum by electrochemical tracing; correlation between COVID-19 and viral-induced ROS in lung/respiratory epithelium during this pandemic. *Biosens. Bioelectron.* **2020**, *165*, 112435. [CrossRef] [PubMed]
140. Abdolahad, M.; Miripour, Z.S.; NajafiKhoshnoo, S. Real-Time and Label Free Analyzer for In-Vitro and In-Vivo Detection of Cancer. U.S. Patent 10786188, 29 September 2020.

biosensors

MDPI

Article

Determination of rSpike Protein by Specific Antibodies with Screen-Printed Carbon Electrode Modified by Electrodeposited Gold Nanostructures

Maryia Drobysh [1,2,†], Viktorija Liustrovaite [2,†], Ausra Baradoke [1], Roman Viter [3,4], Chien-Fu Chen [5], Arunas Ramanavicius [1,2,*] and Almira Ramanaviciene [2]

[1] State Research Institute Center for Physical and Technological Sciences, Sauletekio Ave. 3, LT-10257 Vilnius, Lithuania; maryia.drobysh@ftmc.lt (M.D.); ausra.baradoke@ftmc.lt (A.B.)
[2] NanoTechnas—Center of Nanotechnology and Materials Science, Faculty of Chemistry and Geosciences, Vilnius University, Naugarduko Str. 24, LT-03225 Vilnius, Lithuania; viktorija.liustrovaite@chgf.stud.vu.lt (V.L.); almira.ramanaviciene@chf.vu.lt (A.R.)
[3] Institute of Atomic Physics and Spectroscopy, University of Latvia, Jelgavas Street 3, LV-1004 Riga, Latvia; roman.viter@lu.lv
[4] Center for Collective Use of Research Equipment, Sumy State University, 31 Sanatorna Street, 40000 Sumy, Ukraine
[5] Institute of Applied Mechanics, National Taiwan University, 1 Sec. 4, Roosevelt Rd., Da'an Dist., Taipei City 106, Taiwan; stevechen@iam.ntu.edu.tw
* Correspondence: arunas.ramanavicius@chf.vu.lt; Tel.: +370-600-32332
† These authors contributed equally to this work.

Abstract: In this research, we assessed the applicability of electrochemical sensing techniques for detecting specific antibodies against severe acute respiratory syndrome coronavirus 2 (SARS-CoV-2) spike proteins in the blood serum of patient samples following coronavirus disease 2019 (COVID-19). Herein, screen-printed carbon electrodes (SPCE) with electrodeposited gold nanostructures (AuNS) were modified with L-Cysteine for further covalent immobilization of recombinant SARS-CoV-2 spike proteins (rSpike). The affinity interactions of the rSpike protein with specific antibodies against this protein (anti-rSpike) were assessed using cyclic voltammetry (CV) and differential pulse voltammetry (DPV) methods. It was revealed that the SPCE electroactive surface area increased from 1.49 ± 0.02 cm^2 to 1.82 ± 0.01 cm^2 when AuNS were electrodeposited, and the value of the heterogeneous electron transfer rate constant (k^0) changed from 6.30×10^{-5} to 14.56×10^{-5}. The performance of the developed electrochemical immunosensor was evaluated by calculating the limit of detection and limit of quantification, giving values of 0.27 nM and 0.81 nM for CV and 0.14 nM and 0.42 nM for DPV. Furthermore, a specificity test was performed with a solution of antibodies against bovine serum albumin as the control aliquot, which was used to assess nonspecific binding, and this evaluation revealed that the developed rSpike-based sensor exhibits low nonspecific binding towards anti-rSpike antibodies.

Keywords: COVID-19; SARS-CoV-2 virus; electrochemical immunosensor; differential pulse voltammetry (DPV); cyclic voltammetry (CV); electrochemical impedance spectroscopy (EIS); self-assembled monolayer (SAM); antigen–antibody complex; spike protein (Spike); gold nanostructures (AuNS)

Citation: Drobysh, M.; Liustrovaite, V.; Baradoke, A.; Viter, R.; Chen, C.-F.; Ramanavicius, A.; Ramanaviciene, A. Determination of rSpike Protein by Specific Antibodies with Screen-Printed Carbon Electrode Modified by Electrodeposited Gold Nanostructures. *Biosensors* **2022**, *12*, 593. https://doi.org/10.3390/bios12080593

Received: 1 July 2022
Accepted: 27 July 2022
Published: 3 August 2022

1. Introduction

Severe acute respiratory syndrome coronavirus 2 (SARS-CoV-2) is a highly transmissible and pathogenic coronavirus that first appeared in late 2019 and has since created a pandemic of acute respiratory sickness known as 'coronavirus disease 2019' (COVID-19), which poses a threat to human health since human-to-human transmission has grown significantly [1]. The progression of the COVID-19 pandemic has shown that there is a crucial need to develop quick and accurate tests to better control the spread of the disease

and monitor illness progression. Immunosensors are the most suitable type of sensors for this purpose since they can be used to detect the SARS-CoV-2 virus, confirming the presence of the disease in the individual, or to monitor antibodies against the virus to check for past illness or immunity [2].

The application of electrochemical immunosensors [3,4] and other affinity sensors [5,6] has additional advantages such as cost-effectiveness, ease of use, point-of-care detection, and reduced sample analysis time, which can significantly help in the early diagnosis of COVID-19 disease [7]. The electrochemical transducer element may be directly coupled to an electrochemical biosensor to provide analytical information about the target species via the biochemical or chemical receptor [8]. Several novel systems for the detection of SARS-CoV-2 spike protein have been proposed. Although most of the sensors have been proven to be successful in detecting SARS-CoV-2, several of them lack sensitivity and/or selectivity, have a low sampling rate, and are designed to use a complicated electrode manufacturing technique [9]. In this regard, nanoparticles may offer a viable solution to the sensitivity and selectivity issues [10,11]. Furthermore, some qualitative SARS-CoV-2 antibodies against spike protein methods have been created, allowing for confirmation of antibodies present in the blood; however, immunosensors for quantitative detection of antibodies have been less reported [12].

Carbon is an excellent platform for antibody immobilization features such as large surface area, good conductivity, and high stability [13]. Nonetheless, covalently attaching biomolecules to carbon remains difficult, whereas physisorption does not typically generate permanent coatings and does not allow for control of antibody orientation. The linkage of biomolecules through self-assembled monolayers (SAMs) on a gold substrate has been widely reported in the biosensorics-related literature [14]. However, gold electrodes (or gold screen-printed electrodes (SPCE)) have scarcely been used, due to high cost of gold [15]. Nanostructured metals such as Au nanostructures (AuNS) result in stronger, more defined binding, e.g., amine/carboxy terminated alkanethiols for N-hydroxysuccinimide/N-(3-dimethylaminopropyl)-N′-ethyl-carbodiimide hydrochloride (NHS/EDC) coupling. Furthermore, AuNS can boost the rate of heterogeneous electron transfer, resulting in increased detection sensitivity [16].

For the development of electrochemical immunosensors for the determination of proteins, the surface of the working electrode must be modified by the protein-recognizing antibodies, receptors, or some artificial structures [5,9]. A SAM is often employed for electrode surface modification purposes, and SAMs terminated by –COOH groups are the most suitable for selective and stable rSpike protein immobilization [17]. In this work, L-Cysteine was used for the presence of functional groups such as thiol (–SH), which has a high affinity towards metallic gold and attaches strongly to the gold surface due to the gold–sulphur interaction. This is useful for well-oriented protein immobilization on gold-based transducers [18].

Total internal reflection ellipsometry [7], scanning electrochemical microscopy, surface plasmon resonance [19], quartz crystal microbalance methods, colorimetry [20], electrochemiluminescence [21–24], electrochemical techniques [25], and other methods [26] are among those that can be used to determine analytical signals generated by affinity sensors. When using the techniques of differential pulse voltammetry (DPV) and cyclic voltammetry (CV), the current response is proportional to the analyte concentration [27]. In our previous work [21], the affinity interaction of recombinant spike protein (rSpike) with antibodies against rSpike (anti-rSpike) was detected using two electrochemical methods: CV and electrochemical impedance spectroscopy (EIS). EIS is frequently used to analyse films produced on electrodes because the EIS method is able to discriminate between various conductivity-/capacitance-related processes that occur on the electrode/solution interface. EIS results are frequently assessed using the corresponding electrical circuit, in which factors such as electrolyte resistance, ionic conductivity, electrical double-layer capacitance, and electron transfer resistance may be distinguished and calculated. Regardless of the fact that EIS is rarely used for analytical purposes, the redox

process or analyte-related CV features can be utilized for quantitative findings; however, due to its limitations, EIS is more typically used for exploratory purposes such as assessing the redox process for diverse analytes [28]. In general, pulse techniques such as DPV are more sensitive than linear-sweep-based methods, since CV is the technique most frequently employed for exploratory purposes. Thus, it is rather common in sensor development to employ both these techniques, because CV provides critical information on aspects such as process reversibility and the types of redox processes occurring during the analysis at the interface between the electrode and the solution, whereas potential-pulse-based techniques sometimes enable simplification of the quantification of the analyte [29]. The miniaturization of electrochemical systems enables the determination of protein-based analytes in rather small volumes of aliquots [30].

Therefore, in our present work we compare the applicability of both these two voltametric sensing methods (namely, DPV and CV), taking into account the advantages of their durability and low detection limits in small volumes of aliquots.

To achieve this goal, a label-free electrochemical immunosensor based on SPCE modified with AuNS (SPCE/AuNS) and rSpike protein was designed. The functionalization of SPCE by rSpike was accomplished by the formation of a SAM, L-cysteine (SPCE/AuNS/SAM/rSpike). The affinity reaction was monitored by measuring the decrease in the DPV and CV responses of an $[Fe(CN)_6]^{3-/4-}$ redox probe recorded upon the addition of an anti-rSpike-containing sample (SPCE/AuNS/SAM/rSpike/anti-rSpike). The created immunoplatform met the sensitivity, selectivity, and repeatability criteria and was successfully used to detect anti-rSpike.

2. Experimental

2.1. Materials

Tetrachloroauric acid trihydrate ($HAuCl_4 \cdot 3H_2O$) (99%, CAS# 16961-25-4), KNO_3 (≥99.0%, CAS# 7757-79-1), ethanol (EtOH) (99.9%, CAS# 64-17-5), L-Cysteine (97%, CAS# 52-90-4), N-(3-dimethylaminopropyl)-N′-ethyl-carbodiimide hydrochloride (EDC) (≥99.0%, CAS# 25952-53-8), ethanolamine (EA) (≥98%, CAS# 141-43-5), $K_3Fe(CN)_6$ (≥99.0%, CAS# 13746-66-2), $K_4Fe(CN)_6$ (≥99.0%, CAS# 14459-95-1), and phosphate-buffered saline (PBS) tablets, pH 7.4, were obtained from Sigma–Aldrich (Steinheim, Germany). N-hydroxysuccinimide (NHS) (98.0%, CAS# 6066-82-6) was purchased from Alfa Aesar (Karlsruhe, Germany). Anti-bovine albumin (BSA) antibodies (anti-BSA) were obtained from Biotecha, Lithuania. All reagents were analytical grade and were used without additional purification. All aqueous solutions were prepared in deionized water.

The SARS-CoV-2 recombinant spike protein of SARS-CoV-2 (rSpike) was produced by Baltymas (Vilnius, Lithuania) [31]. Serum samples containing antibodies (anti-rSpike) of volunteers vaccinated with a single dose of the Vaxzevria vaccine who had COVID-19 after two weeks were collected [10] according to Lithuanian ethics law. The ethics committee's permission was not required for this project (as confirmed by the Vilnius Regional Biomedical Research Ethics Committee).

2.2. Electrochemical Measurements

Electrochemical characterization of the working surface was performed using a potentiostat controlled by the DStat interface software from Wheeler Microfluidics Lab (University of Toronto, Toronto, ON, Canada). DRP-110 screen-printed carbon electrode systems (SPCEs), which are based on a working electrode (geometric area of 0.126 cm^2), a carbon counter, and Ag/AgCl reference electrodes, were purchased from Metrohm DropSens (Oviedo, Spain). SPCEs were connected through a specialized 'box-connector' for screen-printed electrodes (DRP-DSC, DropSens, Oviedo, Spain).

All electrochemical measurements were performed in 0.1 M PBS, pH 7.4 solution, adding 2 mM $K_3Fe(CN)_6/K_4Fe(CN)_6$ ($[Fe(CN_6)]^{3-/4-}$) solution as a redox probe. Electrochemical characterization of the working electrode at different modification stages was carried out using DPV and CV. DPV experiments were measured in the potential range from

−0.4 to +0.6 V vs. Ag/AgCl, with a step size of 0.004 V. CV was registered in the potential window from −0.4 to +0.6 V vs. Ag/AgCl, at a scan rate of 0.05 V/s. All experiments were performed at room temperature (20 °C).

Scanning electron microscope (SEM) images were acquired with a scanning electron microscope (Hitachi-70 S3400 N VP-SEM).

2.3. Au Deposition on SPCE

The SPCE was covered with 100 µL of the solution containing 0.1 M KNO_3 and 5 mM $HAuCl_4$. Electrodeposition was performed at a potential of -0.4 V for 60 s. Then, after AuNS deposition on the SPCE (SPCE/AuNS), the electrode was rinsed with deionized water and dried under a N_2 (%) flow (Figure 1, step 1).

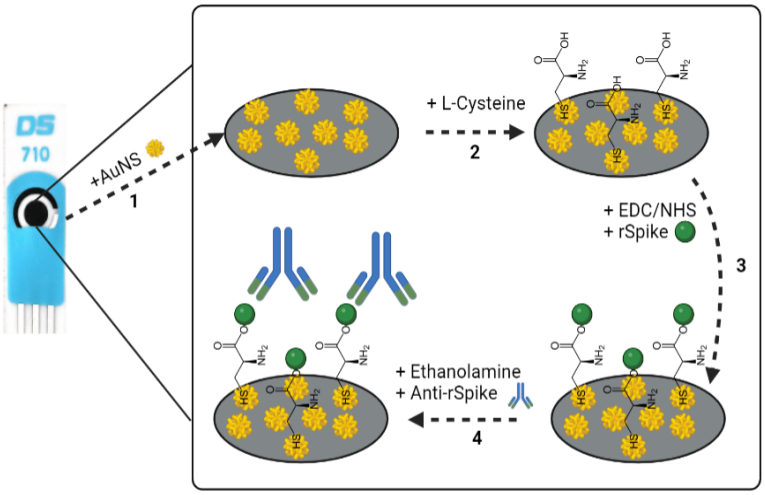

Figure 1. Schematic representation of experimental stages occurring on the SPCE. (**1**): The formation of SPCE/AuNS by electrodeposition; (**2**): SPCE/AuNS/SAM formation; (**3**): the activation of the SPCE/AuNS/SAM by EDC-NHS mixture following SPCE/AuNS/SAM/rSpike formation; (**4**): ethanolamine blocking of remaining active functional groups and SPCE/AuNS/SAM/rSpike/anti-rSpike immunocomplex formation via the interaction between immobilized rSpike protein and the anti-rSpike antibodies present in the aliquot.

2.4. Immobilisation of rSpike and Anti-rSpike

The SPCE/AuNS were incubated at 20 °C for 4 h in 5 mM L-Cysteine ethanolic solution to form a self-assembled monolayer (SAM) on the working surface (SPCE/AuNS/SAM) (Figure 1, step 2). After incubation, the SPCE/AuNS/SAM electrode was rinsed with deionized water and then dried under a N_2 flow. SPCE/AuNS/SAM was activated with 10 µL of a mixture of 0.02 M EDC and 0.005 M NHS in PBS, pH 7.4, for 10 min. After the activation, the electrode was incubated with 10 µL of 50 µg/mL rSpike in PBS, pH 7.4, at 20 °C for 20 min. Immobilization of rSpike was performed through covalent coupling of the protein's primary amine functional groups and the activated carboxylic groups of the SAM (SPCE/AuNS/SAM/rSpike) (Figure 1, step 3). The remaining reactive esters were deactivated by incubating with a 1 mM water solution of ethanolamine for 10 min. Afterwards, SPCE/AuNS/SAM/rSpike was incubated with 10 µL of anti-rSpike in PBS, pH 7.4, with a concentration range from 0.5 to 3.5 nM, at 20 °C for 10 min (SPCE/AuNS/SAM/rSpike/anti-rSpike) (Figure 1, step 4). After each stage of incubation, the system was rinsed with deionized water and used for further electrochemical measurements.

2.5. Calibration of Anti-rSpike

The initial number of binding antibody units (BAU) per mL against the spike protein of SARS-CoV-2 in the serum sample was 5860 BAU/mL. The concentration was defined by a chemiluminescent microparticle immunoassay performed in the laboratory of Tavo Klinika, Ltd. (Vilnius, Lithuania). The target antibodies in the sample were recalculated from BAU/mL to nM using the ratio 1 BAU/mL: 20 ng/mL (considering the molecular weight of immunoglobulin G as ~150 kDa) [32–34].

Calibration curves were obtained by the incubation of SPCE/AuNS/SAM/rSpike in serum samples containing 0.5, 1.0, 1.5, 2.5, and 3.5 nM of anti-rSpike, for 10 min for each concentration. DPV and CV data were used to plot the calibration curves. The relative response (RR%) used for the evaluation of the method specificity was calculated using the equation $RR\% = ((X_i - \mu X_{blank})/(X_{blank})) \times 100\%$, where X_i is the response for concentration i and X_{blank} is the response for a blank.

3. Results and Discussion

3.1. Electrochemical Characterisation of SPCE and SPCE/AuNS

In order to improve the surface area for rSpike immobilization and to facilitate better electron transfer kinetics, electrochemical deposition of AuNS was performed on the SPCE working electrode. The CV and DPV results are provided in Figure 2. In addition, the electroactive surface area for SPCE/AuNS was determined using CV in 10 mM H_2SO_4 (Figure 3). The characteristic gold reduction and oxidation peaks are present in the potential window from 0 to +1.0 V [35], while the measurements for the unmodified SPCE surface reveal no oxidation or reduction peaks (Figure 3, inset).

With the aim of evaluating the electrochemical performance of the sensor, it is critical to quantify the electrochemically active surface area of the substrate material [36], as well as to define the heterogeneous electron transfer rate constant (k^0) [37]. For this purpose, CV at a range of scan rates from 0.01 to 0.15 V/s was performed in PBS, pH 7.4, containing 2 mM $[Fe(CN_6)]^{3-/4-}$ for both SPCE and SPCE/AuNS (Figure 4, Table 1).

Table 1. Experimental data obtained from CV at different scan rates for SPCE and SPCE/AuNS. Error bars were calculated as a percentage of standard error.

Scan Rate, V/s	SPCE		SPCE/AuNS	
	Ip, A	ΔE, V	Ip, A	ΔE, V
0.01	$2.24 \times 10^{-5} \pm 0.73\%$	$0.14 \pm 0.91\%$	$2.63 \times 10^{-5} \pm 1.05\%$	$0.10 \pm 0.44\%$
0.025	$3.38 \times 10^{-5} \pm 0.65\%$	$0.17 \pm 0.15\%$	$4.13 \times 10^{-5} \pm 0.56\%$	$0.12 \pm 0.80\%$
0.05	$4.59 \times 10^{-5} \pm 0.17\%$	$0.21 \pm 0.31\%$	$5.78 \times 10^{-5} \pm 0.10\%$	$0.14 \pm 0.21\%$
0.075	$5.55 \times 10^{-5} \pm 0.01\%$	$0.24 \pm 0.45\%$	$7.10 \times 10^{-5} \pm 0.00\%$	$0.16 \pm 0.66\%$
0.10	$6.34 \times 10^{-5} \pm 0.20\%$	$0.25 \pm 0.66\%$	$8.09 \times 10^{-5} \pm 0.28\%$	$0.17 \pm 0.37\%$
0.15	$7.57 \times 10^{-5} \pm 0.33\%$	$0.29 \pm 0.16\%$	$9.69 \times 10^{-5} \pm 0.38\%$	$0.20 \pm 0.25\%$

Using the Randles–Sevcik equation, the electrochemically active surface areas were calculated as 1.49 ± 0.02 cm^2 for SPCE and 1.82 ± 0.01 cm^2 for SPCE/AuNS (Figure 5A). The difference between the values can be explained by the increase in the surface roughness (Figure 6), thus improving the working substrate properties for the subsequent immobilization of the biorecognition element. Furthermore, the data obtained from CV at different scan rates allowed us to assess k^0 by means of the improved Nicholson's approach for the quasi-reversible electrochemical reaction [38,39]. The value for SPCE was $6.30 \pm 0.13 \times 10^{-5}$, while that for SPCE/AuNS was $14.56 \pm 0.20 \times 10^{-5}$ (Figure 5B), which is more than twice as high. Thus, it can be concluded that the electrodeposition of AuNS contributes not only to an increase in the electrode active area but also to the rate of heterogeneous electron transfer.

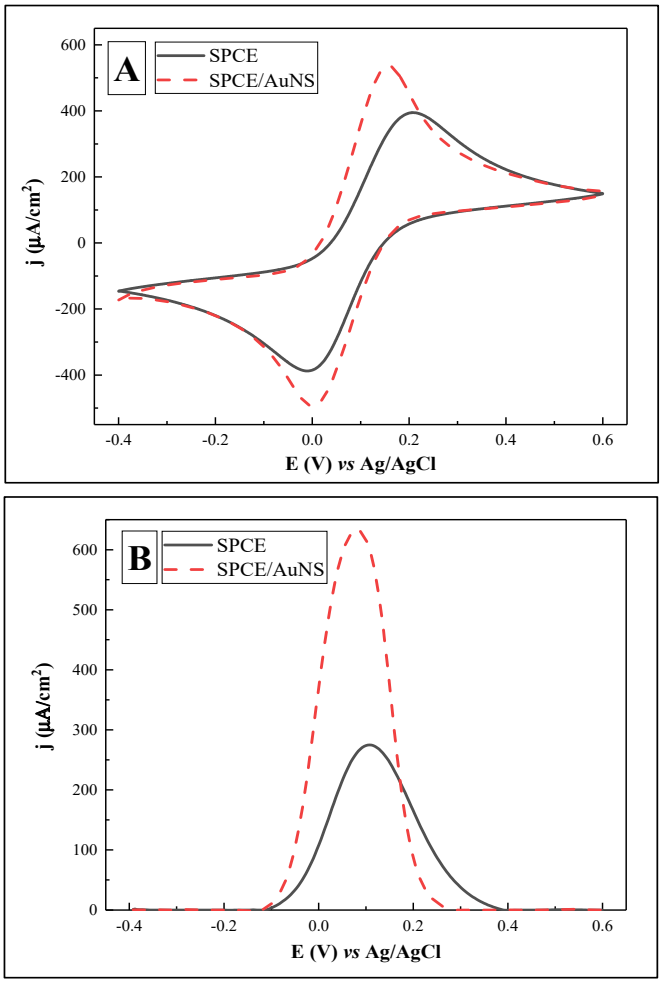

Figure 2. Cyclic voltammograms (**A**) and differential pulse voltammograms (**B**) for SPCE (—) and SPCE/AuNS (- - -). Potential range was from −0.4 to +0.6 V, with a CV scan rate of 0.05 V/s, DPV step size of 0.004 V, pulse height of 0.05 V, pulse period of 100 ms, and pulse width of 50 ms, in 10 mM PBS, pH 7.4, containing 2 mM $[Fe(CN_6)]^{3-/4-}$. Signal normalized to the geometrical area of the working electrode (0.126 cm^2).

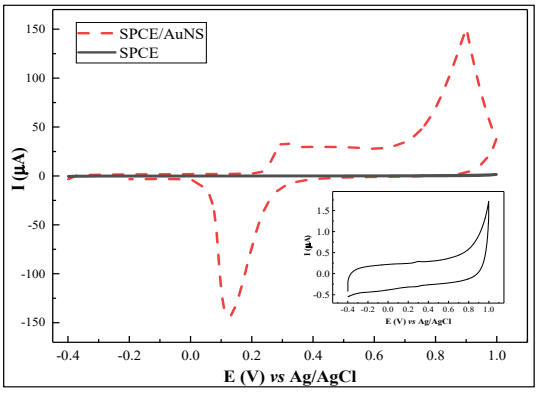

Figure 3. Cyclic voltammogram of SPCE/AuNS in 10 mM H_2SO_4. Inset: cyclic voltammogram of SPCE. Potential scan range was from −0.4 to +1.0 V vs. Ag/AgCl, at a scan rate of 0.1 V/s.

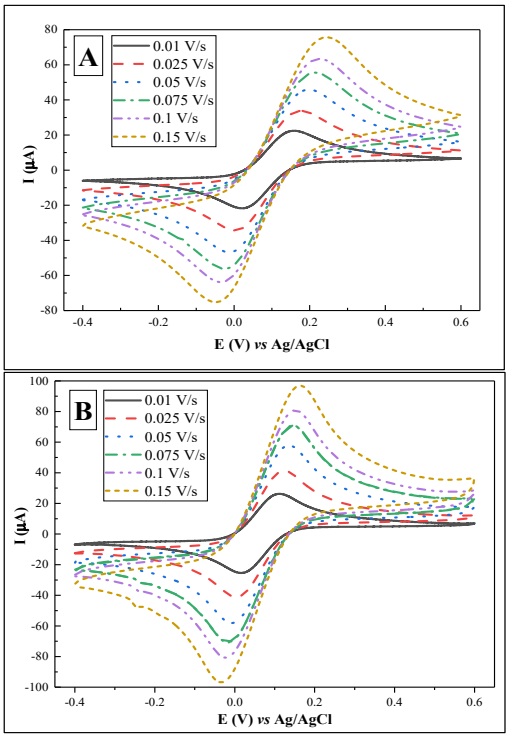

Figure 4. Cyclic voltammograms for SPCE (**A**) and SPCE/AuNS (**B**) at scan rates of 0.01, 0.025, 0.05, 0.075, 0.1, and 0.15 V/s in PBS, pH 7.4, containing 2 mM $[Fe(CN_6)]^{3-/4-}$.

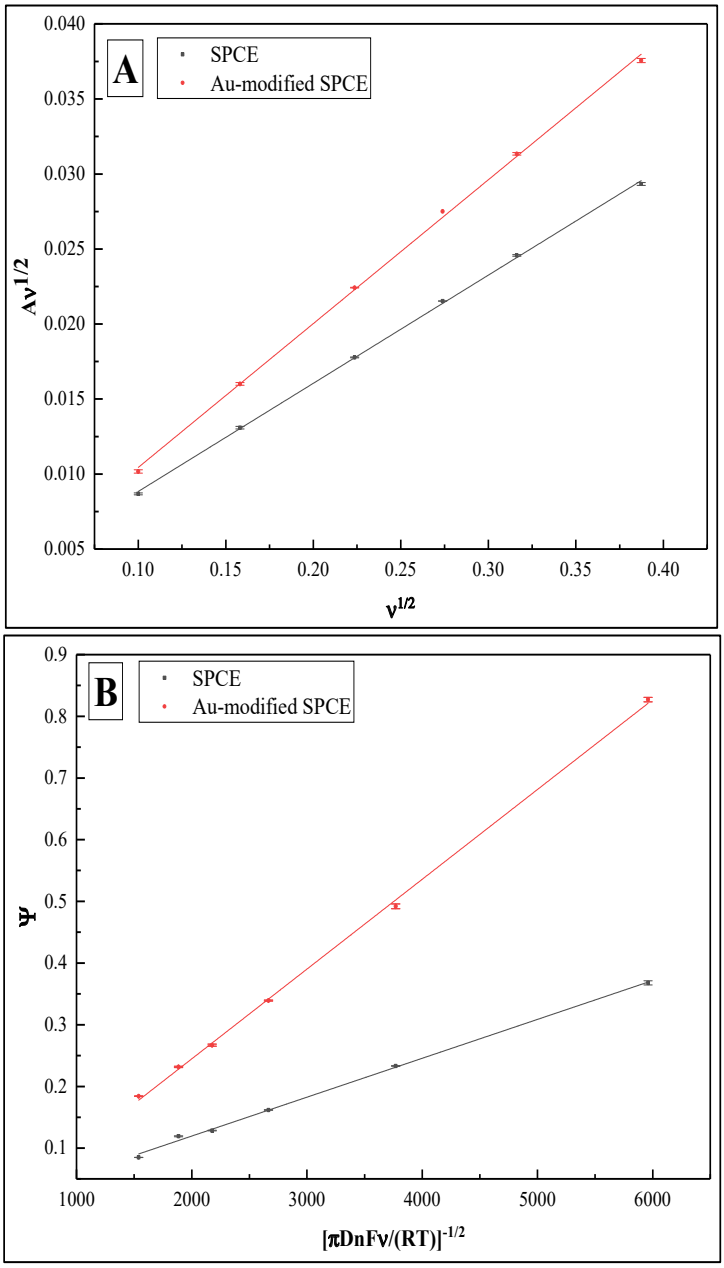

Figure 5. (**A**) Plot of $A\nu^{1/2}$ vs. $\nu^{1/2}$ showing calculated electrochemically active surface areas of SPCE and SPCE/AuNS as slopes. (**B**) Plot of Ψ vs. $[\pi DnF\nu/(RT)]^{-1/2}$ showing calculated k^0 values of SPCE and SPCE/AuNS as slopes.

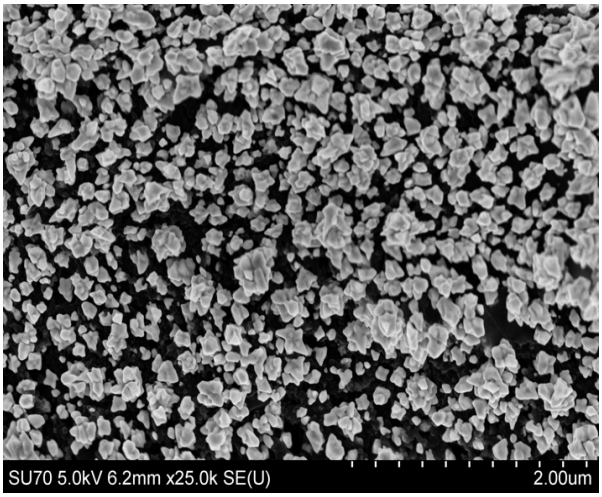

Figure 6. SEM micrograph of SPCE/AuNS.

For further investigations of the electrochemical surface properties, CV and DPV measurements in 10 mM PBS, pH 7.4, containing 2 mM $[Fe(CN_6)]^{3-/4-}$ were performed for SPCE and SPCE/AuNS in the potential range from −0.4 to +0.6 V (Figure 2).

DPV is known to be a potentiostatic method, suggesting some advantages over conventional methods such as CV. In the waveform, DPV is a series of pulses, while for CV the potential is ramped linearly with time. Due to the minimization of the capacitive current, pulse methods, including DPV, are considered to be more sensitive than linear sweep methods. On the other hand, CV is the method most frequently used for research purposes. Hence, it is quite a common practice in sensor development to use both types of electrochemical methods. While CV reveals key electrochemical characteristics such as process reversibility and reflects the redox processes that occur in the system, DPV is employed for quantitative analysis [40].

Since the obtained cyclic voltammograms were quasi-reversible [41], the character of the correlation between the current peak intensity and the surface modification step was not the same for cathodic and anodic peaks. For instance, in Figure 2, the resolution of the current density signals in the anodic region was higher than in cathodic region. This trend increased with further surface modification, leading to the overlapping of the cathodic peaks (Figure 7). Hence, to facilitate quantitative data analysis, we used the values of the anodic current density (j_{pa}) as the analytical parameter gained from the CV experiments.

As shown in Figure 2, cyclic and differential pulse voltammograms revealed the same trend of increasing current densities after the working surface modification. Specifically, the values increased from 394.71 ± 0.69 to 536.30 ± 0.42 and from 274.89 ± 0.17 to 632.53 ± 0.83 μA/cm^2 for CV and DPV, respectively. Potential values were also changed, moving left along the axis. This indicates a substrate material change with increasing the conductivity.

3.2. Electrochemical Characterisation of the Biosensing Element

CV and DPV in 10 mM PBS, pH 7.4, with 2 mM $[Fe(CN_6)]^{3-/4-}$ as a redox probe were performed and evaluated for SPCE/AuNS, SPCE/AuNS/SAM, and SPCE/AuNS/SAM/rSpike (Figure 7, Table 2). The CV oxidation peaks were compared after each of the abovementioned stages of the biosensing element formation.

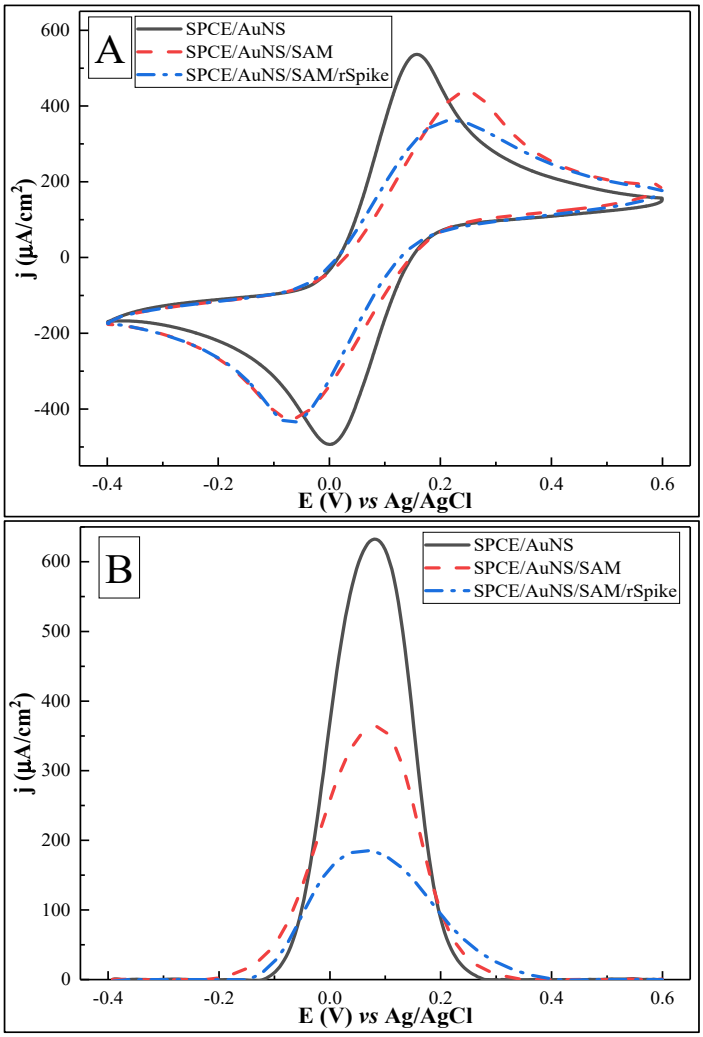

Figure 7. Cyclic voltammograms (**A**) and differential pulse voltammograms (**B**) of SPCE/AuNS (—), after SPCE/AuNS/SAM formation (- - -), and for SPCE/AuNS/SAM/rSpike protein immobilization (-·-). Potential range was from −0.4 to +0.6 V, with a CV scan rate of 0.05 V/s, DPV step size of 0.004 V, pulse height of 0.05 V, pulse period of 100 ms, and pulse width of 50 ms, in 10 mM PBS, pH 7.4, containing 2 mM $[Fe(CN_6)]^{3-/4-}$. Signal normalized to the geometrical area of the working electrode (0.126 cm^2).

Table 2. Analytical parameters obtained from CV and DPV. Error bars are calculated as a percentage standard error.

	CV	DPV	RR for CV	RR for DPV
	j_{pa}, μA/cm^2	j_p, μA/cm^2	%	%
Au-modified SPCE	536.30 ± 0.42%	632.53 ± 0.83%		
SAM	436.96 ± 0.18%	363.52 ± 0.28%		
rSpike (blank)	361.83 ± 0.28%	185.26 ± 1.17%	0	0
Anti-rSpike 0.5 nM	323.11 ± 0.13%	148.86 ± 1.02%	10.70 ± 0.13	19.65 ± 1.02
Anti-rSpike 1.0 nM	303.18 ± 0.10%	124.25 ± 0.32%	16.21 ± 0.10	32.93 ± 0.32
Anti-rSpike 1.5 nM	297.42 ± 0.07%	105.86 ± 0.32%	17.80 ± 0.07	42.86 ± 0.32
Anti-rSpike 2.5 nM	276.91 ± 0.49%	82.23 ± 0.59%	23.47 ± 0.49	55.61 ± 0.59
Anti-rSpike 3.5 nM	270.04 ± 0.63%	66.93 ± 0.20%	25,370.63	63.87 ± 0.20

As considered in the previous section, CV for SPCE/AuNS was characterized by a voltammogram with sharp oxidative/reductive peaks and with a j_{pa} value of 536.30 ± 0.42 μA/cm^2. After SPCE/AuNS/SAM formation, a decrease in j_{pa} to 436.96 ± 0.18 μA/cm^2 was observed. Then, the activation of the terminal –COOH group of the L-Cysteine took place without accompanying electrochemical measurements, to ensure subsequent effective rSpike immobilization. Afterwards, the remainder of the activated functional groups of the SAM were blocked by 1 mM ethanol amine, to avoid nonspecific interactions during the anti-rSpike coupling stages. CV after antigen immobilization with SPCE/AuNS/SAM/rSpike formation and blocking revealed a further current density decrease to 361.83 ± 0.28 μA/cm^2.

DPV measurements for the above-mentioned stages of biosensing element formation showed the same tendency toward a stepwise decrease in the current density to 632.53 ± 0.83, 363.52 ± 0.28, and 185.26 ± 1.17 μA/cm^2 for SPCE/AuNS, SPCE/AuNS/SAM, and SPCE/AuNS/SAM/rSpike. These results are summarized in Table 1.

The decrease in current density according to both CV and DPV methods can be explained by the increasing layer thickness on the working electrode surface, thus hampering electron transfer. The stepwise broadening of the DPV peaks could be related to a reduced electron exchange rate.

For CV measurements, the potential values for j_{pa} moved within the 0.1–0.2 V window. Again, this could be related to alterations in the electron transfer process and/or to changes in the reference Ag/AgCl electrode, which is quite sensitive to experimental conditions such as the presence of Cl^- in PBS, pH 7.4, during AuNS electrodeposition. At the same time, the DPV is characterized by rather stable potential value, changing only slightly in the range of 0.0 to 0.1 V, which is observed due to different nature of the electrochemical signal recording/assessment principles in the CV and DPV techniques.

3.3. Electrochemical Characterisation of the Anti-rSpike Detection

The next step of the experiment was to test the ability of the biosensor to detect anti-rSpike. For this purpose, SPCE/AuNS/SAM/rSpike was sequentially incubated with 10 μL of anti-rSpike in a concentration range from 0.5 to 3.5 nM. Each subsequent incubation was accompanied by CV and DPV measurements (Figure 8) in 10 mM PBS, pH 7.4, containing 2 mM $[Fe(CN_6)]^{3-/4-}$.

CV measurements (Figure 8A) illustrate that stepwise 'flattening' of the voltammograms in the anodic region is observed, with a corresponding decrease in j_{pa} values, starting from 361.83 ± 0.28 for the solution containing 0 nM of anti-Spike antibodies and decreasing to 270.04 ± 0.63 for the solution with 3.5 nM of anti-Spike antibodies, in the potential window of 0.2 to 0.4 V. The 'flattening' of the voltammograms and the potential shifts indicate increasing insulation of the working surface, further hindering access for electrons and changing the value of the redox reaction potential.

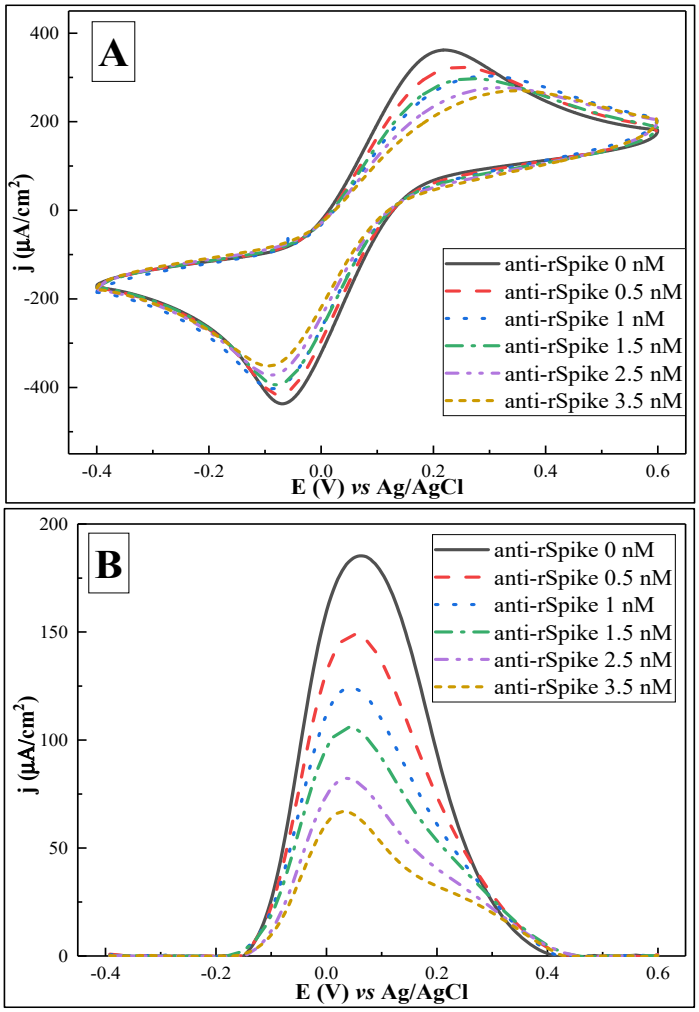

Figure 8. Cyclic voltammograms (**A**) and differential pulse voltammograms (**B**) after interaction with anti-rSpike antibodies of different concentrations (0–3.5 nM). Potential range was from −0.4 to +0.6 V, with a CV scan rate of 0.05 V/s, DPV step size of 0.004 V, pulse height of 0.05 V, pulse period of 100 ms, and pulse width of 50 ms, in 10 mM PBS, pH 7.4, containing 2 mM $[Fe(CN_6)]^{3-/4-}$. Signal normalised to the geometrical area of the working electrode (0.126 cm^2). Data are represented as means of three independent experiments.

DPV experiments revealed the same effect, with a sequential decrease in j_p, i.e., 185.26 ± 1.17, 148.86 ± 1.02, 124.25 ± 0.32, 105.86 ± 0.32, 82.23 ± 0.59, and 66.93 ± 0.2 μA/cm^2 for 0, 0.5, 1.0, 1.5, 2.5, and 3.5 nM, respectively. In contrast to CV-based experiments, the peaks of the differential pulse voltammograms for solutions with different concentrations of anti-Spike antibodies are characterized by higher resolution and more stable potential values, which correspond to particular concentrations of anti-Spike antibodies.

3.4. Limit of Detection and Limit of Quantification

Data gained from the performed electrochemical measurements were used to evaluate the limit of detection (LOD) and limit of quantification (LOQ) for the developed immunosensor, using both the CV and DPV methods. The j_{pa} and j_p values were used as analytical signals for CV and DPV, respectively. Figure 9 shows the calibration curves.

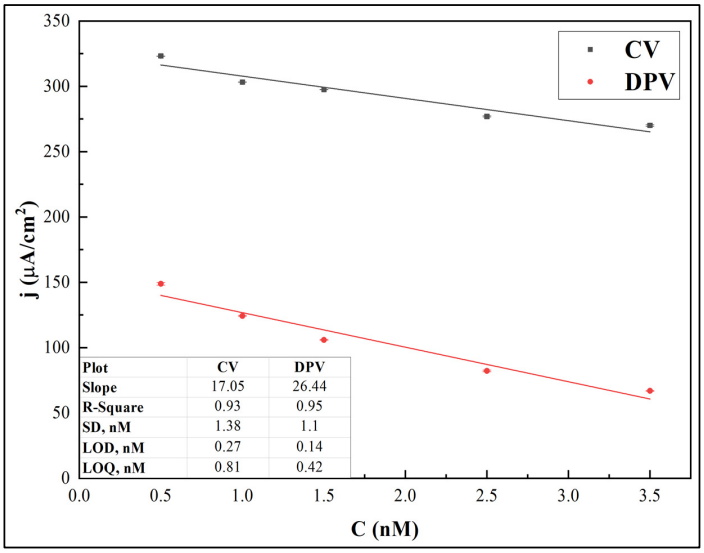

Figure 9. Calibration curves for j_{pa} and j_p obtained from CV and DPV peak values, respectively, vs. anti-rSpike antibody concentration. Error bars are calculated as a percentage of standard error.

The LOD was calculated as 3.33σ/s and LOQ was calculated as 10σ/s, where σ is the standard deviation for the blank response and s is the slope of the calibration curve [42]. It was revealed that the LOD and LOQ values for the CV-based method were 0.27 nM and 0.81 nM, respectively, while the values calculated from DPV data were 0.14 nM and 0.42 nM, respectively.

3.5. Specificity Test

The experiment for nonspecific binding on SPCE/AuNS/SAM/rSpike was performed by comparison of the relative electrochemical signal responses (initial values from Table 2) after incubation of the electrode in 10 mM PBS, pH 7.4, with solutions of 1.5 nM anti-rSpike and 15 nM anti-BSA, (Figure 10). The comparison of the relative responses revealed that for CV, the RR(%) values were 17.80 ± 0.07% and 3.24 ± 0.46% for anti-rSpike and anti-BSA, respectively. Similarly, the RR(%) values for the DPV method were 42.86 ± 0.32% for anti-rSpike and 7.57 ± 0.09% for anti-BSA.

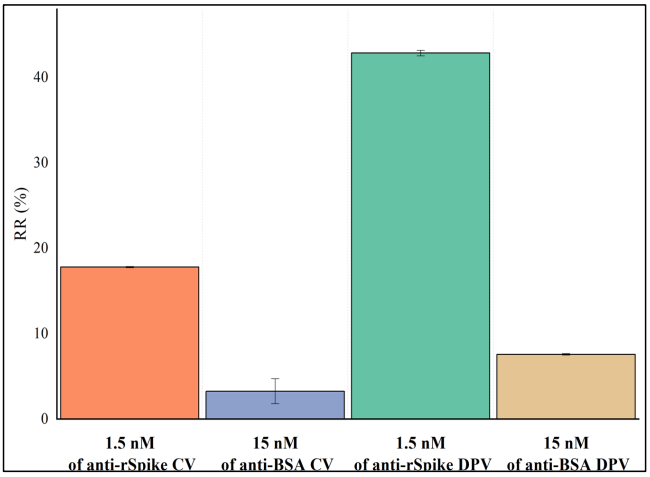

Figure 10. Comparison of the relative responses after 10 min of incubation with 1.5 nM anti-rSpike and 15 nM anti-BSA, for DPV and CV methods. Error bars are calculated as a percentage standard error.

4. Conclusions

In this work, electrochemical characterization of SPCE/rSpike and SPCE/AuNS/SAM/rSpike was performed. The electroactive surface area and the heterogeneous electron transfer rate constants were determined and were 22% and 131% higher for SPCE with electrodeposited AuNS, making the SPCE/AuNS surface more suitable for electrochemical measurements. The formation of the SPCE/AuNS/SAM/rSpike biosensing element, as well as the interaction between immobilized rSpike and anti-rSpike, were accompanied by CV and DPV measurements after key stages. For both detection methods, a stepwise decrease in current density was measured after each modification stage, including that applied for the detection of anti-rSpike occurring due to increasingly prohibited access of the $[Fe(CN)_6]^{3-/4-}$ redox probe to the working electrode. The DPV method was more reliable and more sensitive compared to CV, resulting in 48% lower LOD and LOQ values, making the DPV method more suitable for quantitative analysis. Specificity tests with anti-BSA showed low nonspecific binding for this antibody type. In conclusion, it is expected that the electrochemical immunosensor designed in this research will prove suitable for the diagnosis of the immunological response generated during the course of COVID-19 disease or after vaccination.

Author Contributions: Conceptualization, A.B. and A.R. (Almira Ramanaviciene); methodology, V.L., A.B., A.R. (Arunas Ramanavicius) and A.R. (Almira Ramanaviciene); validation, M.D., A.B. and A.R. (Arunas Ramanavicius); formal analysis, M.D. and V.L.; investigation, M.D., V.L. and A.B.; resources, R.V. and A.R. (Arunas Ramanavicius); data curation, M.D., V.L. and A.B.; writing—original draft preparation, M.D. and V.L.; writing—review and editing, C.-F.C., A.R. (Arunas Ramanavicius) and A.R. (Almira Ramanaviciene); visualization, M.D. and R.V.; project administration, A.R. (Arunas Ramanavicius); funding acquisition, R.V. and C.-F.C. All authors have read and agreed to the published version of the manuscript.

Funding: This research was funded by Lietuvos Mokslo Taryba and grant number is S-LLT-21-3.

Institutional Review Board Statement: Not applicable.

Informed Consent Statement: Not applicable.

Acknowledgments: This research was conducted under the Lithuania–Latvia–China (Taiwan) project, and it has received funding according to agreement No S-LLT-21-3 with the Research Council of Lithuania (LMTLT) (No. 110-2923-E-002-004-MY3 for Taiwan). Schematic illustrations were created with BioRender (https://biorender.com, accessed on 30 June 2022).

Conflicts of Interest: The authors declare no conflict of interest.

References

1. Hu, B.; Guo, H.; Zhou, P.; Shi, Z.-L. Characteristics of SARS-CoV-2 and COVID-19. *Nat. Rev. Microbiol.* **2021**, *19*, 141–154. [CrossRef] [PubMed]
2. Yadav, A.; Verma, D.; Kumar, A.; Kumar, P.; Solanki, P. The perspectives of biomarker-based electrochemical immunosensors, artificial intelligence and the Internet of Medical Things toward COVID-19 diagnosis and management. *Mater. Today Chem.* **2021**, *20*, 100443. [CrossRef] [PubMed]
3. Ramanavicius, S.; Ramanavicius, A. Progress and Insights in the Application of MXenes as New 2D Nano-Materials Suitable for Biosensors and Biofuel Cell Design. *Int. J. Mol. Sci.* **2020**, *21*, 9224. [CrossRef] [PubMed]
4. Ramanavicius, S.; Ramanavicius, A. Conducting Polymers in the Design of Biosensors and Biofuel Cells. *Polymers* **2021**, *13*, 49. [CrossRef] [PubMed]
5. Ramanavicius, S.; Jagminas, A.; Ramanavicius, A. Advances in Molecularly Imprinted Polymers Based Affinity Sensors (Review). *Polymers* **2021**, *13*, 974. [CrossRef] [PubMed]
6. Ratautaite, V.; Boguzaite, R.; Brazys, E.; Ramanaviciene, A.; Ciplys, E.; Juozapaitis, M.; Slibinskas, R.; Bechelany, M.; Ramanavicius, A. Molecularly imprinted polypyrrole based sensor for the detection of SARS-CoV-2 spike glycoprotein. *Electrochim. Acta* **2022**, *403*, 139581. [CrossRef] [PubMed]
7. Plikusiene, I.; Maciulis, V.; Ramanaviciene, A.; Balevicius, Z.; Buzavaite-Verteliene, E.; Ciplys, E.; Slibinskas, R.; Simanavicius, M.; Zvirbliene, A.; Ramanavicius, A. Evaluation of kinetics and thermodynamics of interaction between immobilized SARS-CoV-2 nucleoprotein and specific antibodies by total internal reflection ellipsometry. *J. Colloid Interface Sci.* **2021**, *594*, 195–203. [CrossRef] [PubMed]
8. Thévenot, D.R.; Toth, K.; Durst, R.A.; Wilson, G.S. Electrochemical biosensors: Recommended definitions and classification. *Biosens. Bioelectron.* **2001**, *16*, 121–131. [CrossRef]
9. Drobysh, M.; Ramanaviciene, A.; Viter, R.; Ramanavicius, A. Affinity Sensors for the Diagnosis of COVID-19. *Micromachines* **2021**, *12*, 390. [CrossRef] [PubMed]
10. Lim, R.R.X.; Bonanni, A. The potential of electrochemistry for the detection of coronavirus-induced infections. *TrAC Trends Anal. Chem.* **2020**, *133*, 116081. [CrossRef] [PubMed]
11. Abid, S.A.; Muneer, A.A.; Al-Kadmy, I.M.; Sattar, A.A.; Beshbishy, A.M.; Batiha, G.E.-S.; Hetta, H.F. Biosensors as a future diagnostic approach for COVID-19. *Life Sci.* **2021**, *273*, 119117. [CrossRef] [PubMed]
12. Drobysh, M.; Ramanaviciene, A.; Viter, R.; Chen, C.-F.; Samukaite-Bubniene, U.; Ratautaite, V.; Ramanavicius, A. Biosensors for the Determination of SARS-CoV-2 Virus and Diagnosis of COVID-19 Infection. *Int. J. Mol. Sci.* **2022**, *23*, 666. [CrossRef] [PubMed]
13. Hill, E.W.; Vijayaragahvan, A.; Novoselov, K. Graphene Sensors. *IEEE Sens. J.* **2011**, *11*, 3161–3170. [CrossRef]
14. Makaraviciute, A.; Ramanavicius, A.; Ramanaviciene, A. Development of a reusable protein G based SPR immunosensor for direct human growth hormone detection in real samples. *Anal. Methods* **2015**, *7*, 9875–9884. [CrossRef]
15. Alonso-Lomillo, M.; Yardimci, C.; Domínguez-Renedo, O.; Arcos-Martínez, M. CYP450 2B4 covalently attached to carbon and gold screen printed electrodes by diazonium salt and thiols monolayers. *Anal. Chim. Acta* **2009**, *633*, 51–56. [CrossRef] [PubMed]
16. Baradoke, A.; Jose, B.; Pauliukaite, R.; Forster, R.J. Properties of Anti-CA125 antibody layers on screen-printed carbon electrodes modified by gold and platinum nanostructures. *Electrochim. Acta* **2019**, *306*, 299–306. [CrossRef]
17. Pandey, L.M. Design of engineered surfaces for prospective detection of SARS-CoV-2 using quartz crystal microbalance-based techniques. *Expert Rev. Proteom.* **2020**, *17*, 425–432. [CrossRef] [PubMed]
18. Lee, J.M.; Park, H.K.; Jung, Y.; Kim, J.K.; Jung, S.O.; Chung, B.H. Direct Immobilization of Protein G Variants with Various Numbers of Cysteine Residues on a Gold Surface. *Anal. Chem.* **2007**, *79*, 2680–2687. [CrossRef] [PubMed]
19. Kausaite, A.; van Dijk, M.; Castrop, J.; Ramanaviciene, A.; Baltrus, J.P.; Acaite, J.; Ramanavicius, A. Surface plasmon resonance label-free monitoring of antibody antigen interactions in real time. *Biochem. Mol. Biol. Educ.* **2007**, *35*, 57–63. [CrossRef] [PubMed]
20. Yan, B.; Wang, F.; He, S.; Liu, W.; Zhang, C.; Chen, C.; Lu, Y. Peroxidase-like activity of Ru–N–C nanozymes in colorimetric assay of acetylcholinesterase activity. *Anal. Chim. Acta* **2021**, *1191*, 339362. [CrossRef]
21. Zhang, W.; Song, Y.; Wang, Y.; He, S.; Shang, L.; Ma, R.-N.; Jia, L.; Wang, H. A perylenetetracarboxylic dianhydride and aniline-assembled supramolecular nanomaterial with multi-color electrochemiluminescence for a highly sensitive label-free immunoassay. *J. Mater. Chem. B* **2020**, *8*, 3676–3682. [CrossRef] [PubMed]
22. Zhang, W.; Song, Y.; Wang, Y.; Gong, Y.; Shang, L.; Ma, R.; Jia, L.; Xue, Q.; Du, Y.; He, S.; et al. Perylene Dianhydride and Perylene Diimide Luminophores Integrated with Gold Nanoparticles for Dual-Potential Electrochemiluminescence Ratiometric Immunosensors. *ACS Appl. Nano Mater.* **2020**, *4*, 683–690. [CrossRef]

23. Song, Y.; Zhang, W.; He, S.; Shang, L.; Ma, R.; Jia, L.; Wang, H. Perylene Diimide and Luminol as Potential-Resolved Electrochemiluminescence Nanoprobes for Dual Targets Immunoassay at Low Potential. *ACS Appl. Mater. Interfaces* **2019**, *11*, 33676–33683. [CrossRef] [PubMed]
24. Zhang, C.; Hu, F.; Hao, X.; Rao, Q.; Hu, T.; Sun, W.; Guo, C.; Li, C.M. Sandwiching Phosphorene with Iron Porphyrin Monolayer for High Stability and Its Biomimetic Sensor to Sensitively Detect Living Cell Released NO. *Adv. Sci.* **2022**, *9*, 2104066. [CrossRef] [PubMed]
25. Baradoke, A.; Hein, R.; Li, X.; Davis, J.J. Reagentless Redox Capacitive Assaying of C-Reactive Protein at a Polyaniline Interface. *Anal. Chem.* **2020**, *92*, 3508–3511. [CrossRef] [PubMed]
26. Saeb, M.R.; Rabiee, N.; Seidi, F.; Far, B.F.; Bagherzadeh, M.; Lima, E.C.; Rabiee, M. Green CoNi2S4/porphyrin decorated carbon-based nanocomposites for genetic materials detection. *J. Bioresour. Bioprod.* **2021**, *6*, 215–222. [CrossRef]
27. Grieshaber, D.; MacKenzie, R.; Vörös, J.; Reimhult, E.; Grieshaber, D.; MacKenzie, R.; Vörös, J.; Reimhult, E. Electrochemical Biosensors-Sensor Principles and Architectures. *Sensors* **2008**, *8*, 1400–1458. [CrossRef] [PubMed]
28. Brett, C.M.; Brett, O.; Electrochemistry, A.M. *Electrochemistry: Principles, Methods, and Applications*; Oxford University Press: New York, NY, USA, 1993.
29. Ramanavicius, A.; Oztekin, Y.; Ramanaviciene, A. Electrochemical formation of polypyrrole-based layer for immunosensor design. *Sens. Actuators B Chem.* **2014**, *197*, 237–243. [CrossRef]
30. Zhao, H.; Liu, F.; Xie, W.; Zhou, T.-C.; OuYang, J.; Jin, L.; Li, H.; Zhao, C.-Y.; Zhang, L.; Wei, J.; et al. Ultrasensitive supersandwich-type electrochemical sensor for SARS-CoV-2 from the infected COVID-19 patients using a smartphone. *Sens. Actuators B Chem.* **2020**, *327*, 128899. [CrossRef] [PubMed]
31. Liustrovaite, V.; Drobysh, M.; Rucinskiene, A.; Baradoke, A.; Ramanaviciene, A.; Plikusiene, I.; Samukaite-Bubniene, U.; Viter, R.; Chen, C.-F.; Ramanavicius, A. Towards an Electrochemical Immunosensor for the Detection of Antibodies against SARS-CoV-2 Spike Protein. *J. Electrochem. Soc.* **2022**, *169*, 037523. [CrossRef]
32. *NIBSC 20/136*; First WHO International Standard for Anti-SARS-CoV-2 Immunoglobulin (Human). National Institute for Biological Standards and Control: London, UK, 2020.
33. Immundiagnostik AG. *IDK Anti-SARS-CoV-2 IgG ELISA (Manual)*; Immundiagnostik AG: Bensheim, Germany, 2021.
34. Dietzen, D.J. Amino acids, peptides, and proteins. In *Principles and Applications of Molecular Diagnostics*; Rifai, N., Horvath, A.R., Wittwer, C.T., Eds.; Elsevier: Amsterdam, The Netherlands, 2018; pp. 345–380.
35. Park, I.-S.; Lee, K.-S.; Jung, D.-S.; Park, H.-Y.; Sung, Y.-E. Electrocatalytic activity of carbon-supported Pt–Au nanoparticles for methanol electro-oxidation. *Electrochim. Acta* **2007**, *52*, 5599–5605. [CrossRef]
36. Trasatti, S.; Petrii, O. Real surface area measurements in electrochemistry. *J. Electroanal. Chem.* **1992**, *327*, 353–376. [CrossRef]
37. Randviir, E.P. A cross examination of electron transfer rate constants for carbon screen-printed electrodes using Electrochemical Impedance Spectroscopy and cyclic voltammetry. *Electrochim. Acta* **2018**, *286*, 179–186. [CrossRef]
38. Nicholson, R.S. Theory and Application of Cyclic Voltammetry for Measurement of Electrode Reaction Kinetics. *Anal. Chem.* **1965**, *37*, 1351–1355. [CrossRef]
39. Lavagnini, I.; Antiochia, R.; Magno, F. An Extended Method for the Practical Evaluation of the Standard Rate Constant from Cyclic Voltammetric Data. *Electroanalysis* **2004**, *16*, 505–506. [CrossRef]
40. Islam, M.N.; Channon, R.B. Electrochemical sensors. In *Bioengineering Innovative Solutions for Cancer*; Academic Press: Cambridge, MA, USA, 2020; pp. 47–71. [CrossRef]
41. Savéant, J.M. *Elements of Molecular and Biomolecular Electrochemistry: An Electrochemical Approach to Electron Transfer Chemistry*; John Wiley & Sons: Hoboken, NJ, USA, 2006.
42. Shrivastava, A.; Gupta, V.B. Methods for the determination of limit of detection and limit of quantitation of the analytical methods. *Chron. Young Sci.* **2011**, *2*, 21–25. [CrossRef]

NOTES

NOTES

Vilniaus universiteto leidykla
Saulėtekio al. 9, III rūmai, LT-10222 Vilnius
El. p. info@leidykla.vu.lt, www.leidykla.vu.lt
bookshop.vu.lt, journals.vu.lt
Tiražas 20 egz.